LOCAL L 1 SUB-FINSLER GEOMETRY IN DIMENSION 3: NON-GENERIC CASES

Fazia Harrache, Francesca Chittaro, Mohamed Aidene

Local L^1 sub-Finsler geometry in dimension 3: non-generic cases

F. Harrache[1,2] F. C. Chittaro[2] M. Aidène[1]

[1] Laboratoire de Conception et Conduite des Systémes de Production, Université Mouloud Mammeri, Tizi-Ouzou, Algeria
[2]LIS, UMR CNRS 7020, Université de Toulon, Aix Marseille University, France

Abstract

We study the local geometry of the sub-Finsler structure induced by a sub-Riemannian metric on a 3-dimensional manifold. We provide a description of the upper part of the cut locus of short geodesics, in some non generic cases.

1 Introduction

Consider a pair of smooth vector fields f, g on $\mathbb{R}^3$, such that f, g and their Lie brackets $[f, g]$ are linearly independent at every point of $\mathbb{R}^3$. For every $\boldsymbol{q} \in \mathbb{R}^3$, define on $\text{span}\{f(\boldsymbol{q}), g(\boldsymbol{q})\}$ some norm $h_{\boldsymbol{q}}$, smoothly depending on $\boldsymbol{q}$. This norm endows the whole $\mathbb{R}^3$ with a distance function, defined in the following way: given two points $\boldsymbol{q}_0, \boldsymbol{q}_1 \in \mathbb{R}^3$, their distance is defined as

$$d(\boldsymbol{q}_0, \boldsymbol{q}_1) = \inf \left\{ \int_0^1 h_{\gamma(t)}(\dot\gamma(t))dt \ : \ \left\{ \begin{array}{c} \gamma \in AC([0,1], \mathbb{R}^3) \\ \dot\gamma(t) \in \text{span}\{f(\gamma(t)), g(\gamma(t))\} \text{ a.e. } t \\ \gamma(0) = \boldsymbol{q}_0, \ \gamma(1) = \boldsymbol{q}_1. \end{array} \right. \right\}. \quad (1)$$

If the norm $h_{\boldsymbol{q}}$ is the restriction to $\text{span}\{f(\boldsymbol{q}), g(\boldsymbol{q})\}$ of some Riemannian norm on $\mathbb{R}^3$, the variational problem (1) is the well known sub-Riemannian problem (see for instance the books [4, 20] and references therein). If instead $h_{\boldsymbol{q}}$ is not related to a scalar product on the span of f and g, we are in the more general case of sub-Finsler geometry. In sub-Riemannian and sub-Finsler geometry, very natural questions concern, for instance, the characterization of the shortest-path curves between two endpoints, the localization of the points where they cease to be length-minimizing (*cut points* and *conjugate points*), the shape of the spheres and the regularity of the distance function.

Differently from sub-Riemannian geometry, which is a very active research field since the nineties, sub-Finsler geometry is a rather new research field, and, comparatively, few publications are currently available. We mention the paper [11], in which the authors study the unit sphere of left-invariant sub-Finsler metrics on Lie groups, and the papers [13, 14], where $h_{\boldsymbol{q}}$ is a positive homogeneous function on the distribution $\text{span}\{f, g\}$, smooth outside the zero section; the generic three dimensional case and the Engel group in dimension four are studied.

In the papers [6, 7, 8, 9, 19], the sub-Finsler problem is approached from the viewpoint of geometric control; in particular, thanks to a suitable time reparametrization, the problem of finding the shortest path between two endpoints can be reformulated as a minimum time problem associated with a control system, linear in the control, in which the control functions are allowed to take values in a compact set, that is determined by $h_{\boldsymbol{q}}$. In particular, in [9] the time-optimal synthesis (from the origin) is provided for three celebrated distributions in dimension 2 and 3, that is, the Grushin, Heisenberg and Martinet distribution. In [8], the Pontryagin extremals for a free nilpotent distribution of rank 2 and step 3 in $\mathbb{R}^5$ are analyzed.

The papers [6, 7] deal with generic distributions in dimension 2 and 3. In particular, in [7] the authors consider a generic distribution of rank at most 2 in $\mathbb{R}^3$, endowed with a maximum (i.e., L^∞) norm, and study the associated minimum time problem; in particular, they are

interested in the local time-optimal synthesis, that is, in understanding the local synthesis for small times (or small distances), near generic points (where the distribution is of rank 2 and step 2); we remark that the Heisenberg system studied in [9] corresponds to a special non-generic distribution. As the authors are interested only in the local problem, the analysis can be carried out by means of a perturbative expansion in terms of a small parameter, linked to the final time, in the spirit of the results obtained in [2, 10, 12] for the conjugate locus of the contact sub-Riemannian case in dimension 3 (see also [23] for an analogous result in dimension 5). In [7], the authors identify two invariants of the distribution (called respectively C_1 and C_2) that appear in the expansion of the Jacobian of the exponential map; if they are both nonzero, their signs completely determine the conjugate locus of the short geodesics. In addition, the authors provide a complete characterization of the cut locus of short geodesics, under the generic assumptions that $C_1 C_2 \neq 0$.

In this paper, we carry over the analysis of [7], by investigating the local time-optimal synthesis in the less generic case in which the invariant C_1 is zero, while we still assume that $C_2 \neq 0$. We are interested in the local problem, that is, we are studying the optimality of short geodesics; following the cited papers [2, 7, 12], we develop the geodesics of the minimum time problem in a power series of a small parameter (linked to the final time), and provide a detailed description of the upper part of the cut locus of the jets of the geodesics.

Though, we are not considering exactly the same system of [7], but some difference are present. First of all, we are concerned with the sub-Finsler L^1 problem, that is, we assume that the norm of any vector $X \in \mathrm{span}\{f(\boldsymbol{q}), g(\boldsymbol{q})\}$ is defined by $h_{\boldsymbol{q}}(X) = |\alpha| + |\beta|$, where $X = \alpha f(\boldsymbol{q}) + \beta g(\boldsymbol{q})$. The induced metric structure is called a sub-Finsler L^1 metric. Nevertheless, as already remarked in [7, 9], the sub-Finsler L^1 and the sub-Finsler L^∞ problems are completely equivalent, up to a change of variable. We are moreover restricting ourselves to a special class of L^1 sub-Finsler structures, that is, L^1 sub-Finsler structures *compatible with a sub-Riemannian metric* (according to Definition 6); loosely speaking, we require that the manifold is endowed with a Riemannian structure, and that the vector fields f and g are obtained from an orthonormal frame by applying a *constant* non-singular linear transformation. As it has been proved in [16], even restricting to the class of L^1 sub-Finsler structures compatible with a sub-Riemannian metric, in the generic case $C_1 C_2 \neq 0$ we still can recover the results of [7] (at least, for what concerns the part of the sphere satisfying $z \geq |xy|/2$).

Thanks to the choice of studying sub-Finsler structures that are compatible with a sub-Riemannian metric, we can take advantage of the Agrachev-Gauthier normal form of the vector fields f and g (see [5, 12]), which permits us to considerably simplify the computations. The choice of focusing on such structures has also other advantages: first of all, thanks to the symmetries of the vector fields, it is sufficient to compute the analytic expression of a rather reduced number of trajectories, and recover the other ones by applying suitable coordinate changes and permutations in the invariants; the same can be done for several other computations (such as the computation of the switching times, the Maxwell points and of wavefronts). Moreover, we will be able to single out six main invariants of the distribution (called A, C_1, C_2, D_1, E_1, where C_1 and C_2 are equivalent to their homonyms in [7]) that describe the local conjugate locus, and provide a complete characterization, based on the values of these invariants, for sub-Finsler structures such that $C_1 = 0$ and $A C_2 D_1 E_1 \neq 0$, of the upper part of the cut locus.

Adapting the same techniques of [12], it is possible to prove that the condition $C_1 \neq 0$ is generically true (in the sense specified in Section 2.5.1); in particular, for a generic L^1 sub-Finsler structure compatible with a sub-Riemannian structure, the set of points $\boldsymbol{q} \in M$ such that $C_1 = 0$ has codimension 1 in M. We can also prove that the subset characterized by $D_1 = E_1 = 0$ has codimension 2 in the set of points for which $C_1 = 0$. The assumption $D_1 E_1 \neq 0$ is thus generically true in the subset of non-generic cases.

The structure of the paper is the following: in Section 2 we state the problem under concern, we provide the normal form of the vector fields f and g and we start the investigation of the time-optimal synthesis, by applying the Pontryagin Maximum Principle (PMP); finally, we recall the structure of the optimal trajectories of the nilpotent case, already studied in [9]. In Section 3 we compute the jets of the bang-bang extremals and of the switching times; we also briefly discuss the notions of local and global optimality, and we give a definition for the cut and the conjugate locus. In Theorem 2, we provide the expression of the the conjugate times of bang-bang geodesics with large positive $p_z(0)$.

The main results, that is, the computation of the description of the upper part of the cut loci in non-generic cases, are briefly presented in Section 4. More precisely, we classify 60 cases (according to the different values of the invariants of the metric), that can be reduced to 30 by symmetry properties. In this section, we illustrate the suspensions of the cut locus of these 30 cases, highlighting the main novelties with respect to the generic case studied in [7], and we provide some hints on the methods we used to determine the cut points of each geodesic. A detailed analysis of all 30 subcases is provided in Appendix C. We conclude with Section 5, where we discuss the problems which are still left to analyze.

The Appendices contain the results of some useful computations and collect the results of the analysis of the intersections of the fronts.

2 Preliminaries

2.1 Notations

In this paper, we deal with several coordinates frames and time reparametrization; to improve the readability of the paper, we try to use different fonts for every coordinate setting. In particular

- points on a smooth manifold are denoted with $\boldsymbol{q}$, and their expressions in some coordinates frame with $\mathbf{x}$. Moreover, the special font $(\mathscr{x}, \mathscr{y}, \mathscr{z})$ is reserved to the normal coordinates associated with a sub-Riemannian structure, as defined in [12, Theorem 3.1]; they will be adopted only in Section 2. On the other hand, the coordinates (x, y, z) are those defined in Proposition 1, issued from $(\mathscr{x}, \mathscr{y}, \mathscr{z})$ by means of the linear transformation (10).
- Analogously, elements in the cotangent bundle T^*M are denoted with $\boldsymbol{\ell}$, and the coordinates on T^*M are denoted with $(\boldsymbol{p}, \mathbf{x})$. π denotes the canonical projection from the cotangent (or the tangent) bundle to the manifold M.
- $f, g, \mathscr{f}, \mathscr{g}$ denote vector fields on M (more precisely, they all belong to the distribution $\mathcal{D}$). In particular, f and g are the vector fields defining the sub-Finsler distance (see Definition 2 and Remark 1), while $(\mathscr{f}, \mathscr{g})$ are two orthonormal vector fields associated with the sub-Riemannian structure on M (see Section 2.5). The two pairs of vector fields are related to each other by equation (8).
- trajectories on M are denoted with $\boldsymbol{\xi}$ (as a shortcut for $t \mapsto \boldsymbol{\xi}(t)$ or $\boldsymbol{\xi}(\cdot)$); analogously, trajectories on the cotangent bundle are denoted with $\boldsymbol{\lambda} = (\boldsymbol{\mu}, \boldsymbol{\xi})$

We moreover denote with F and G the Hamiltonian lifts of the vector fields f and g (that is, $F(\boldsymbol{\ell}) = \langle \boldsymbol{\ell}, f(\pi\boldsymbol{\ell})\rangle$), and with $\vec{F}$ and $\vec{G}$ the Hamiltonian vector fields associated with the Hamiltonian functions F and G, respectively.

The expression $\exp(t_1 f)(\boldsymbol{q})$, where f is a vector field on M (or T^*M) and $t_1 \in \mathbb{R}$, denotes the solution at time t_1 of the Cauchy problem on M (or T^*M)

$$\begin{cases} \dot\gamma(t) = f(\gamma(t)) \\ \gamma(0) = \boldsymbol{q}. \end{cases}$$

2.2 Statement of the problem and preliminary analysis

To provide a rigorous definition of a sub-Finsler structure on a smooth manifold, we adopt the one given in [9], slightly adapted to our context.

Definition 1 *Let M be a connected smooth manifold of dimension 3. A sub-Finsler structure (trivialized and of constant-type norm) of rank at most 2 on M is a pair $(\varphi, \|\cdot\|)$ where*

- *$\varphi : M \times \mathbb{R}^2 \to TM$ is a smooth morphism of vector bundles such that $\varphi(\{\boldsymbol{q}\} \times \mathbb{R}^2) \subseteq T_{\boldsymbol{q}}M$ for every $\boldsymbol{q} \in M$*
- *$\|\cdot\|$ is a norm defined on $\mathbb{R}^2$*

The triple $(M, \varphi, \|\cdot\|)$ is called a sub-Finsler manifold.

The morphism φ identifies a vector distribution $\mathcal{D} \subset TM$ of rank at most 2, defined as the image of φ. Given a sub-Finsler structure as in Definition 1, it is possible to endow M with the distance function defined in the Introduction (equation (1)), where the function $h_{\boldsymbol{q}}$ is defined as

$$h_{\boldsymbol{q}}(X) = \inf\{\|\mathrm{v}\| : \varphi(\boldsymbol{q}, \mathrm{v}) = X\}$$

and the curves γ are assumed to be tangent to the vector distribution $\mathcal{D}$.

Choosing the norm $\|\cdot\|$ as the L^1 norm on $\mathbb{R}^2$, we obtain a sub-Finsler L^1 metric, accordingly to the following definition:

Definition 2 *Let M be a connected smooth manifold of dimension 3. A L^1 sub-Finsler metric on M is a sub-Finsler structure $(\varphi, \|\cdot\|)$ on M such that $\|\cdot\|$ is the L^1 norm on $\mathbb{R}^2$, that is $\forall (v_1, v_2) \in \mathbb{R}^2$ we have that $\|(v_1, v_2)\| = |v_1| + |v_2|$.*

Remark 1 *Let $(\varphi, \|\cdot\|_1)$ be a sub-Finsler L^1 structure on M as in Definition 2. Thanks to the morphism φ, we can identify the two vector fields $f(\cdot) = \varphi(\cdot, e_1)$ and $g(\cdot) = \varphi(\cdot, e_2)$, where $\{e_1, e_2\}$ is the canonical basis of $\mathbb{R}^2$; we remark that*

$$h_{\boldsymbol{q}}(f(\boldsymbol{q})) = h_{\boldsymbol{q}}(g(\boldsymbol{q})) = 1 \quad \forall \boldsymbol{q} \in M$$
$$h_{\boldsymbol{q}}(X) = |\alpha| + |\beta| \qquad \text{for } X = \alpha f(\boldsymbol{q}) + \beta g(\boldsymbol{q}).$$

As for the sub-Riemannian problem, the variational problem (1) can be written as an optimal control one: indeed, given two points $\boldsymbol{q}_0$ and $\boldsymbol{q}_1 \in M$, their distance can be defined as the infimum of the functional

$$J(\boldsymbol{u}) = \int_0^1 |u_1(t)| + |u_2(t)| \, dt$$

over all measurable L^1 functions $\boldsymbol{u} = (u_1, u_2) : [0, 1] \to \mathbb{R}^2$ such that the trajectories of the control system

$$\dot{\boldsymbol{\xi}}(t) = \big(u_1(t) f + u_2(t) g\big) \circ \boldsymbol{\xi}(t)$$

satisfy $\boldsymbol{\xi}(0) = \boldsymbol{q}_0$ and $\boldsymbol{\xi}(1) = \boldsymbol{q}_1$ (if the minimum is not attained, the distance is set to $+\infty$). Applying a suitable time reparametrization, this optimal control problem can be rewritten as the following minimum time problem:

$$\text{minimize } T \text{ subject to} \tag{2a}$$
$$\dot{\boldsymbol{\xi}}(t) = \big(u_1(t) f + u_2(t) g\big) \circ \boldsymbol{\xi}(t), \tag{2b}$$
$$\boldsymbol{\xi}(0) = \boldsymbol{q}_0, \quad \boldsymbol{\xi}(T) = \boldsymbol{q}_1, \tag{2c}$$
$$\boldsymbol{u} : [0, T] \to Q \quad \text{measurable}, \tag{2d}$$

where $Q = \{(u_1, u_2) \in \mathbb{R}^2 : |u_1| + |u_2| \leq 1\}$ and the final time T is free.

Before going on with the analysis of the problem (2), we make a hypothesis on the vector fields f, g, that will be assumed to hold true in Sections 2.3-2.4. As we will remark afterwards, this hypothesis is automatically satisfied under Assumption 1.

Assumption 0 *For every $\boldsymbol{q} \in M$, the vector fields f, g and $[f, g]$ are linearly independent.*

Under Assumption 0, $\mathcal{D}$ is a rank 2 step 2 distribution on M (see [18]) and the control system (2b) is small-time locally controllable (see for instance [25]).

2.3 Pontryagin Maximum Principle

As already said in the Introduction, in this paper we are interested in the local sub-Finsler problem, that is, we fix some $\boldsymbol{q}_0$, we restrict ourselves to a (small enough) open neighborhood $U \subset M$ of $\boldsymbol{q}_0$ and we study the sub-Finsler distance from $\boldsymbol{q}_0$ to points in U. A straightforward application of Filippov's theorem (see for instance [3]) guarantees that, for U small enough, the minimum time (2a) is attained for every pair $(\boldsymbol{q}_0, \boldsymbol{q}_1)$ belonging to U.

Pontryagin Maximum Principle (PMP) is a celebrated first-order necessary optimality condition for optimal control problems. Here below, we recall it in a formulation adapted to problem (2); for more references, see for instance [3, 4]. We define the control-dependent Hamiltonian

$$h(\boldsymbol{\ell}, \boldsymbol{u}) = u_1 F(\boldsymbol{\ell}) + u_2 G(\boldsymbol{\ell}), \qquad \boldsymbol{\ell} \in T^*M, \boldsymbol{u} \in Q$$

with $F(\boldsymbol{\ell}) = \langle \boldsymbol{\ell}, f(\pi\boldsymbol{\ell})\rangle$ and $G(\boldsymbol{\ell}) = \langle \boldsymbol{\ell}, g(\pi\boldsymbol{\ell})\rangle$. Pontryagin Maximum Principle states that, if $\widehat{\boldsymbol{\xi}} : [0,T] \to M$ is an optimal solution for the minimum time problem (2), and $\widehat{\boldsymbol{u}}$ is its associated control function, then there exist a Lipschitz curve $\widehat{\boldsymbol{\lambda}}(t) = (\widehat{\boldsymbol{\mu}}(t), \widehat{\boldsymbol{\xi}}(t)) \in T^*M$ and a constant $\nu \in \{0,1\}$ such that

$$\widehat{\boldsymbol{\mu}}(t) \neq 0 \qquad \forall t \tag{3a}$$

$$\dot{\widehat{\boldsymbol{\mu}}}(t) = -\frac{\partial h}{\partial \mathbf{x}}(\widehat{\boldsymbol{\lambda}}(t), \widehat{\boldsymbol{u}}(t)) \quad \dot{\widehat{\boldsymbol{\xi}}}(t) = \frac{\partial h}{\partial \boldsymbol{p}}(\widehat{\boldsymbol{\lambda}}(t), \widehat{\boldsymbol{u}}(t)) \qquad \text{a.e. } t \tag{3b}$$

$$h(\widehat{\boldsymbol{\lambda}}(t), \widehat{\boldsymbol{u}}(t)) = \max_{\boldsymbol{v}\in Q} h(\widehat{\boldsymbol{\lambda}}(t), \boldsymbol{v}) \qquad \text{a.e. } t \tag{3c}$$

$$h(\widehat{\boldsymbol{\lambda}}(t), \widehat{\boldsymbol{u}}(t)) \equiv \nu \qquad \forall t. \tag{3d}$$

Any curve $\boldsymbol{\lambda} : [0,T] \to T^*M$ satisfying equations (3) for some admissible control $\boldsymbol{u}$ is called an *extremal* of the optimal control problem (2). If the constant ν is equal to 1, we say that the extremal is *normal*; otherwise, it is said to be *abnormal*. The projections of extremals are called *geodesics*.

Under Assumption 0, equations (3a)-(3c)-(3d) imply that there is no abnormal extremals and that the control associated with an extremal takes values on the boundary of Q, i.e., internal control are not optimal. The value of the control is determined by the relative values of F and G along the extremal: let $I \subset [0,T]$ be some interval, and $\boldsymbol{\lambda} : I \to T^*M$ an extremal of (2); then

- if $|F(\boldsymbol{\lambda}(t))| \neq |G(\boldsymbol{\lambda}(t))|$ $\forall t \in I$, then, on I, the control takes value on one of the vertices of Q. In this case, $\boldsymbol{\lambda}|_I$ is said to be a *regular bang arc*.
- if $|F(\boldsymbol{\lambda}(t)| = |G(\boldsymbol{\lambda}(t))|$ $\forall t \in I$, then the control takes values on one of the sides of Q, and, in particular, it is not uniquely determined by the PMP. In this case, $\boldsymbol{\lambda}|_I$ is a *singular arc*.

When an extremal crosses transversely one of the subsets (of T^*M) $\{F = G\}$ or $\{F = -G\}$, the control *switches*, that is, its value jumps from one vertex of Q to another one; in particular, by continuity of the extremals and from the fact that F and G cannot be both zero along an extremal, a control associated with an extremal can switch only from one vertex of Q to a neighboring one. For these reasons, F and G are called the *switching functions*, and the subsets $\{F = G\}$ and $\{F = -G\}$ are called *switching surfaces*. The derivatives of the switching functions along an extremal are given by

$$\frac{d}{dt}F(\boldsymbol{\lambda}(t)) = -u_2(t)\Theta(\boldsymbol{\lambda}(t)), \quad \frac{d}{dt}G(\boldsymbol{\lambda}(t)) = u_1(t)\Theta(\boldsymbol{\lambda}(t)),$$

where $\Theta(\boldsymbol{\ell}) = \langle \boldsymbol{\ell}, [f,g](\pi\boldsymbol{\ell})\rangle$.

2.4 Optimality of geodesics

It is rather obvious that, if an admissible trajectory is time-minimizing between its two endpoints, it is time-minimizing also between any two intermediate points of its. On the contrary, in general a geodesic is not time-minimizing on its whole length, but at some point it ceases to be optimal; the point where a geodesics loses its optimality is called a *cut point*. More precisely, following [4, 7], we can define the cut time and the cut point as follows:

Definition 3 *Let $\boldsymbol{\xi}$ be a geodesic of the control system* (2b)*. Define*

$$t_{\text{cut}}(\boldsymbol{\xi}) = \sup\left\{t > 0 : \boldsymbol{\xi}|_{[0,t]} \text{ is time-minimizing}\right\}.$$

If $t_{\text{cut}}(\boldsymbol{\xi}) < +\infty$, we say that $\boldsymbol{\xi}(t_{\text{cut}})$ is the cut point to $\boldsymbol{\xi}(0)$ along $\boldsymbol{\xi}$.

Moreover, we call the cut locus *(to $\boldsymbol{q}_0$) the set of all cut points of geodesics starting from a point $\boldsymbol{q}_0 \in M$.*

Definition 4 *Using Arnold's terminology, the points reached in the same time by more than one geodesic (with same initial point) are called Maxwell points.*

The set of all Maxwell points of geodesics starting from a point $\boldsymbol{q}_0 \in M$ is called the Maxwell set to $\boldsymbol{q}_0$.

In optimal control, it is worth investigating also the *local* optimality of geodesics, with respect to some suitable topology; in this paper we are interested in optimality in the strong (i.e. C^0) topology: we say that an admissible trajectory $\boldsymbol{\xi}$ is locally optimal if there exists a neighborhood $\mathcal{U}$ of its graph in $\mathbb{R}\times M$ such that $\boldsymbol{\xi}$ is time minimizing among all trajectories with graph contained in $\mathcal{U}$, sharing the same endpoints.

In some optimal control problems such as, for instance, those issued from sub-Riemannian geometry, a usual method to detect the loss of local optimality is to look for the points of non invertibility of the exponential map (see for instance [3, 4]). Yet, for the problem under concern, the exponential map is well-defined only locally around regular bang-bang extremals, and it is only piecewise smooth. Nevertheless, under some regularity assumptions, it is still possible to extract from the Jacobian of the exponential map some information about the loss of local optimality (of bang-bang extremals): consider indeed some $\boldsymbol{\ell}_0 = (\boldsymbol{p}_0, \boldsymbol{q}_0) \in T^*_{\boldsymbol{q}_0}M$ and $T > 0$, such that the solution of the Hamilton equation (3b) with initial condition $\boldsymbol{\ell}_0$ crosses the switching surfaces only a finite number of times in the interval $[0,T]$, and that all these intersections are transversal: more precisely, we assume that there exist m times $0 < t_1 < \cdots < t_m < T$ such that the extremal $\boldsymbol{\lambda}$ with $\boldsymbol{\lambda}(0) = \boldsymbol{\ell}_0$ satisfies $|F(\boldsymbol{\lambda}(t))| \neq |G(\boldsymbol{\lambda}(t))|$ $\forall t \in [0,T]\setminus\{t_1,\dots,t_m\}$, $|F(\boldsymbol{\lambda}(t_k))| = |G(\boldsymbol{\lambda}(t_k))|$ for every k, and $\frac{d}{dt}(F-G)(\boldsymbol{\lambda}(t_k)) \neq 0$ whenever $F(\boldsymbol{\lambda}(t_k)) = G(\boldsymbol{\lambda}(t_k))$ (respectively, $\frac{d}{dt}(F+G)(\boldsymbol{\lambda}(t_k)) \neq 0$ whenever $F(\boldsymbol{\lambda}(t_k)) = -G(\boldsymbol{\lambda}(t_k))$). We denote with $\boldsymbol{u}^1,\dots,\boldsymbol{u}^{m+1}$ the controls associated with the extremal $\boldsymbol{\lambda}$ on the subintervals $(0,t_1),\dots,(t_m,T)$. Thanks to the structure of the extremal, we have that the controls $\boldsymbol{u}^1,\dots,\boldsymbol{u}^{m+1}$ take value in the set $\{(1,0),(0,1),(-1,0),(0,-1)\}$. A straight application of the implicit function theorem yields the following result; the proof uses the same arguments of [1, Section 4], and is thus omitted.

Lemma 1 *There exist a neighborhood $\mathcal{U}$ of $\boldsymbol{\ell}_0$ in $T^*_{\boldsymbol{q}_0}M$ and m smooth functions $\mathfrak{t}_k : \mathcal{U} \to \mathbb{R}$, $k = 1,\dots,m$, such that $\mathfrak{t}_k(\boldsymbol{\ell}_0) = t_k$ and, for every $\boldsymbol{\ell} \in \mathcal{U}$, there exists a regular bang-bang extremal $\boldsymbol{\lambda}_{\boldsymbol{\ell}}$ satisfying $\boldsymbol{\lambda}_{\boldsymbol{\ell}}(0) = \boldsymbol{\ell}$ and such that the control associated with $\boldsymbol{\lambda}_{\boldsymbol{\ell}}|_{(\mathfrak{t}_{k-1}(\boldsymbol{\ell}),\mathfrak{t}_k(\boldsymbol{\ell}))}$ is $\boldsymbol{u}^k$.*

Possibly further shrinking $\mathcal{U}$, we can define the exponential map on $\mathcal{U}\times[0,T]$ as follows

$$\mathrm{Exp}(\boldsymbol{\ell},t) = \begin{cases} \exp((u_1^1 f + u_2^1 g)t)(\boldsymbol{q}_0) & \text{if } t \in [0,\mathfrak{t}_1(\boldsymbol{\ell})] \\ \exp((u_1^k f + u_2^k g)(t-\mathfrak{t}_{k-1}(\boldsymbol{\ell}))) & \text{if } t \in [\mathfrak{t}_{k-1}(\boldsymbol{\ell}),\mathfrak{t}_k(\boldsymbol{\ell})], \\ \quad \circ \mathrm{Exp}(\boldsymbol{\ell},\mathfrak{t}_{k-1}(\boldsymbol{\ell}))(\boldsymbol{q}_0) & 2 \le k \le m. \end{cases} \tag{4}$$

The exponential map (4) is smooth on $\mathcal{U}\times[0,T]$, except at the points of the form $(\boldsymbol{\ell},\mathfrak{t}_k(\boldsymbol{\ell}))$, $k = 1,\dots,m$. Indeed, the differential of Exp evaluated at such points is a piecewise-defined linear map; more precisely, at these points, the hyperplane $\{\delta t = \langle d\mathfrak{t}_k(\boldsymbol{\ell}), \delta\boldsymbol{p}\rangle\}$ separates the linear space $\{(\delta\boldsymbol{p},\delta t) \in T_{\boldsymbol{\ell}}(T^*_{\boldsymbol{q}_0}M)\times\mathbb{R}\}$ into two half-spaces, on which of each one $\mathrm{DExp}(\boldsymbol{\ell},\mathfrak{t}_k(\boldsymbol{\ell}))$ has a different analytic expressions.

We finally observe that the exponential map depends only on three free parameters: indeed, thanks to (3d) and the fact that there is no abnormal extremals, we can consider only those $\boldsymbol{\ell} \in \mathcal{U}$ on which $\max_{v\in Q} h(\boldsymbol{\ell},\boldsymbol{v}) = 1$. Let us assume, without loss of generality, that $F(\boldsymbol{\ell}_0) = 1$. Further shrinking $\mathcal{U}$, we can assume that $|G(\boldsymbol{\ell})| \neq 1$ for every $\boldsymbol{\ell} \in \mathcal{U}$; then we can consider only the $\boldsymbol{\ell}$ belonging to $\mathcal{U}' = \mathcal{U} \cap \{\boldsymbol{\ell} \in T^*M : F(\boldsymbol{\ell}) = 1\}$, that is, we restrict the exponential map to the set $\mathcal{U}'\times[0,T]$, which is a three-dimensional submanifold of $T^*_{\boldsymbol{q}_0}M\times\mathbb{R}$. We can repeat the same procedure for $\boldsymbol{\ell}_0$ such that $F(\boldsymbol{\ell}_0) = -1$ or $|G(\boldsymbol{\ell}_0)| = 1$.

When computing $\mathrm{DExp}(\boldsymbol{\ell},t)$, we obtain the following result.

Lemma 2 *For every $(\boldsymbol{\ell},t) \in \mathcal{U}'\times[0,T]$ such that $t < \mathfrak{t}_2(\boldsymbol{\ell})$, $\mathrm{DExp}(\boldsymbol{\ell},t)$ is singular.*

Proof. First of all, for $\boldsymbol{\ell} \in \mathcal{U}'$, we define $\Pi_{\boldsymbol{\ell}} = T_{\boldsymbol{\ell}}\mathcal{H}_1 \cap T_{\boldsymbol{\ell}}(T^*_{\boldsymbol{q}_0}M)$, where $\mathcal{H}_1 = \{\boldsymbol{\ell} \in T^*M : |F(\boldsymbol{\ell})| = 1\} \cup \{\boldsymbol{\ell} \in T^*M : |G(\boldsymbol{\ell})| = 1\}$, and we notice that

$$\Pi_{\boldsymbol{\ell}} = \{\delta\boldsymbol{p} \in T_{\boldsymbol{\ell}}(T^*_{\boldsymbol{q}_0}M) : \langle dF(\boldsymbol{\ell}), \delta\boldsymbol{p}\rangle = 0\}.$$

We remark that $\mathrm{DExp}(\boldsymbol{\ell},t)$ is a linear map from $\Pi_{\boldsymbol{\ell}}\times\mathbb{R}$ to $\mathbb{R}^3$. As $\mathrm{Exp}(\boldsymbol{\ell},t)$ does not depend on $\boldsymbol{\ell}$ for every $t < \mathfrak{t}_1(\boldsymbol{\ell})$, then $\mathrm{DExp}(\boldsymbol{\ell},t)$ is singular for such times.

Let us now consider $t \in [\mathfrak{t}_1(\boldsymbol{\ell}),\mathfrak{t}_2(\boldsymbol{\ell}))$; we have that

$$\begin{aligned}\mathrm{DExp}_{(\boldsymbol{\ell},t)}[(\delta\boldsymbol{p},\delta t)] &= g(\mathrm{Exp}(\boldsymbol{\ell},t))\delta t \\ &\quad + \langle d\mathfrak{t}_1(\boldsymbol{\ell}), \delta\boldsymbol{p}\rangle\Big(- g(\mathrm{Exp}(\boldsymbol{\ell},t)) + \exp\big((t-\mathfrak{t}_1(\boldsymbol{\ell}))g\big)_* f(\exp(\mathfrak{t}_1(\boldsymbol{\ell})))(\boldsymbol{q}_0)\Big).\end{aligned}$$

Consider $\delta\boldsymbol{p} \in \Pi_{\boldsymbol{\ell}}$, $\delta\boldsymbol{p} \neq 0$, such that $\langle d\mathfrak{t}_1(\boldsymbol{\ell}), \delta\boldsymbol{p}\rangle = 0$; then $\delta\boldsymbol{\ell} = (\delta\boldsymbol{p}, 0)$ belongs to the kernel of $\mathrm{DExp}_{(\boldsymbol{\ell},t)}$. □

Yet, the singularity of $\mathrm{DExp}_{(\boldsymbol{\ell},t)}$ for $t < \mathfrak{t}_2(\boldsymbol{\ell})$ does not reflect a proper loss of optimality of the geodesics associated with the extremals issued from $\mathcal{U}'$; indeed, differentiating the function φ_1 defined in the proof of Lemma 1, we obtain that

$$\langle d\mathfrak{t}_1(\boldsymbol{\ell}_0), \delta\boldsymbol{p}\rangle = -\frac{\langle dG(\boldsymbol{\lambda}(t_1)), \delta\boldsymbol{p}\rangle}{\Theta(\boldsymbol{\lambda}(t_1))} \qquad \forall \delta\boldsymbol{p} \in \Pi_{\boldsymbol{\ell}_0}.$$

Assumption 0 implies that $dF \neq dG$, so that $d\mathfrak{t}_1(\boldsymbol{\ell}_0)$ is not identically null on $\Pi_{\boldsymbol{\ell}_0}$. We can then choose local coordinates (s_1, s_2) on $\mathcal{U}'$ and, applying the implicit function theorem, prove that there exists a locally defined smooth function $\eta : (-\delta, \delta) \to \mathbb{R}$ such that $\mathfrak{t}_1(\boldsymbol{\ell})$ is constant for all $\boldsymbol{\ell}$, belonging to a neighborhood of $\boldsymbol{\ell}_0$ in $\mathcal{U}'$, such that, in the local coordinates defined above, $\boldsymbol{\ell} = (1, s_1, \eta(s_1), \boldsymbol{q}_0)$. In other words, the set $\mathcal{U}'$ is foliated by level curves of $\mathfrak{t}_1$. Then, all geodesics associated with the extremals emanating from covectors belonging to each of these curves coincide, up to the second switching point. In other words, several extremals are associated with the same geodesic: the singularity of the exponential map does not reveal a loss of local optimality of the geodesics.

However, the differential of the exponential map, evaluated at points $(\boldsymbol{\ell}, t)$ such that $t > \mathfrak{t}_2(\boldsymbol{\ell})$, is useful to get information on the points where the geodesics cease to be locally optimal. Since local optimality cannot be lost along a bang arc (see [21]), we concentrate on what happens at the switching times. We recall the following fact.

Lemma 3 *Le $\boldsymbol{v} \in \mathbb{R}^n$, $\boldsymbol{v} \neq 0$, and consider two matrices A_+, A_- such that $A_+\boldsymbol{w} = A_-\boldsymbol{w}$ for every $\boldsymbol{w}$ such that $\boldsymbol{w} \cdot \boldsymbol{v} = 0$.*

Define the piecewise linear map $A : \mathbb{R}^n \to \mathbb{R}^n$ as

$$A\boldsymbol{w} = \begin{cases} A_+\boldsymbol{w} & \text{if } \boldsymbol{w} \cdot \boldsymbol{v} \geq 0 \\ A_-\boldsymbol{w} & \text{if } \boldsymbol{w} \cdot \boldsymbol{v} \leq 0. \end{cases}$$

Then A is invertible if and only if $(\det A_+)(\det A_-) > 0$.

Motivated by this Lemma, we adopt the following definition of conjugate time (we remark that it is the same proposed in [7]).

Definition 5 *Let $\boldsymbol{\lambda}$ be a regular bang-bang extremal for the optimal control problem (2). The first conjugate time along $\boldsymbol{\lambda}$ is defined as*

$$t_{\mathrm{conj}}(\boldsymbol{\lambda}) = \inf\left\{t > 0 : \exists\ t_1 < t < t_2 \text{ such that } \mathrm{JExp}(\boldsymbol{\ell}_0, t_1)\mathrm{JExp}(\boldsymbol{\ell}_0, t_2) < 0\right\},$$

where $\mathrm{JExp}(\boldsymbol{\ell}_0, t)$ denotes the Jacobian of $\mathrm{Exp}(\boldsymbol{\ell}, t)$ at $\boldsymbol{\ell}_0 = \boldsymbol{\lambda}(0)$.

The first conjugate point along $\boldsymbol{\lambda}$ is the point reached by the projection of $\boldsymbol{\lambda}$ at the first conjugate time. The set of all first conjugate points associated with extremals with initial condition equal to $\boldsymbol{q}_0$ is called the first conjugate locus.

2.5 The normal form

In this paper, we are considering a particular class of sub-Finsler L^1 structures, which we call *compatible with a sub-Riemannian structure* (see Definition 6 below). Loosely speaking, they are the sub-Finsler L^1 structures in which the vector fields f and g are closely related to the vector fields appearing in the normal form of some sub-Riemannian structure on M.

In order to give a precise definition of this notion, first of all we recall some basic facts on the sub-Riemannian normal form. Consider a sub-Riemannian manifold $(g, \mathcal{D}, M)$, where $\mathcal{D} \subset TM$ is a smooth 2-dimensional distribution of constant non-holonomic degree 2 ([4, 18]), and $g : \mathcal{D} \times \mathcal{D} \to \mathbb{R}$ is a positive definite quadratic form, smoothly depending on $\boldsymbol{q} \in M$, which defines a scalar product on $\mathcal{D}_{\boldsymbol{q}}$ for every $\boldsymbol{q}$ in M. Theorem 3.1 in [12] states that for every $\boldsymbol{q} \in M$ there exist an open neighborhood U of $\boldsymbol{q}$, a local coordinates chart (x, y, z) defined on U and an orthonormal basis $\{f, g\}$ for $g_{\boldsymbol{q}}$ such that, for every $\boldsymbol{q} \in U$, f and g can be written as

$$f(\boldsymbol{q}) = \begin{pmatrix} 1 + y^2\beta(x, y, z) \\ -xy\beta(x, y, z) \\ -\frac{y}{2}(1 + \gamma(x, y, z)) \end{pmatrix} \qquad g(\boldsymbol{q}) = \begin{pmatrix} -xy\beta(x, y, z) \\ 1 + x^2\beta(x, y, z) \\ \frac{x}{2}(1 + \gamma(x, y, z)) \end{pmatrix}, \tag{5}$$

where $\beta, \gamma : \mathbb{R}^3 \to \mathbb{R}$ are two smooth functions satisfying

$$\beta(0,0,\textbf{\textit{z}}) = \gamma(0,0,\textbf{\textit{z}}) = 0 \quad \forall \textbf{\textit{z}} \in \mathbb{R}, \tag{6}$$

$$\frac{\partial \gamma}{\partial \boldsymbol{x}}(0,0,\textbf{\textit{z}}) = \frac{\partial \gamma}{\partial \textbf{\textit{y}}}(0,0,\textbf{\textit{z}}) = 0 \quad \forall \textbf{\textit{z}} \in \mathbb{R}. \tag{7}$$

Definition 6 *Consider a sub-Riemannian manifold $(g, \mathcal{D}, M)$ and a sub-Finsler L^1 structure $(\varphi, \|\cdot\|_1)$ on M. We say that the sub-Finsler L^1 structure $(\varphi, \|\cdot\|_1)$ is (locally) compatible with $(g, M, \mathcal{D})$ at $\boldsymbol{q}_0 \in M$ if there exist a neighborhood U of $\boldsymbol{q}_0$ and a constant non-singular two dimensional square matrix $\mathbf{M}$ such that $\varphi(\{\boldsymbol{q}\} \times \mathbb{R}^2) = \mathcal{D}_{\boldsymbol{q}}$ for every $\boldsymbol{q} \in U$ and*

$$\begin{pmatrix} f(\boldsymbol{q}) \\ g(\boldsymbol{q}) \end{pmatrix} = \mathbf{M} \begin{pmatrix} \textbf{\textit{f}}(\boldsymbol{q}) \\ \textbf{\textit{g}}(\boldsymbol{q}) \end{pmatrix}, \qquad \boldsymbol{q} \in U, \tag{8}$$

where $f(\boldsymbol{q}) = \varphi(\boldsymbol{q}, e_1)$, $g(\boldsymbol{q}) = \varphi(\boldsymbol{q}, e_2)$, and $\textbf{\textit{f}}, \textbf{\textit{g}}$ are the two orthonormal vector fields in (5).

Up to rescaling the L^1 norm, we can always assume that $\det \mathbf{M} = 1$. The most particular case of a compatible L^1 metric is the one in which $f = \textbf{\textit{f}}$ and $g = \textbf{\textit{g}}$.

We can now make our first assumption.

Assumption 1 *The sub-Finsler L^1 structure $(\varphi, \|\cdot\|_1)$ is locally compatible at $\boldsymbol{q}_0$ with a sub-Riemannian structure $(g, M, \mathcal{D})$.*

Remark 2 *By straightforward computations it is easy to prove that, under Assumption 1, the vector fields f, g and $[f, g]$ are linearly independent on U. In particular, Assumption 1 implies Assumption 0.*

We now perform in U another coordinate change, that allows us to obtain a nice symmetric form of the two vector fields f, g defining the sub-Finsler structure of M.

Proposition 1 *Let $(g, M, \mathcal{D})$ be a sub-Riemannian structure, and consider a sub-Finsler L^1 structure $(\varphi, \|\cdot\|_1)$ locally compatible with $(g, M, \mathcal{D})$ at some $\boldsymbol{q}_0 \in M$. Let $(\boldsymbol{x}, \textbf{\textit{y}}, \textbf{\textit{z}})$ be the normal (sub-Riemannian) coordinates in which $\textbf{\textit{f}}$ and $\textbf{\textit{g}}$ assume the form* (5)*, and let $f = \varphi(\cdot, e_1)$ and $g = \varphi(\cdot, e_2)$.*

There exists a change of coordinates $\Phi : (\boldsymbol{x}, \textbf{\textit{y}}, \textbf{\textit{z}}) \mapsto (x, y, z)$ such that $\textbf{\textit{z}} = z$ and

$$f = \frac{\partial}{\partial x} + yW \qquad g = \frac{\partial}{\partial y} - xW, \tag{9}$$

where W is the vector field defined by

$$W(x,y,z) = \begin{pmatrix} xL_{11}(x,y,z) + yL_{12}(x,y,z) \\ xL_{21}(x,y,z) + yL_{22}(x,y,z) \\ -\frac{1}{2} + \mathcal{L}_3(x,y,z) \end{pmatrix},$$

$L_{ij} : \mathbb{R}^3 \to \mathbb{R}$ being smooth functions satisfying $L_{ij}(0,0,z) = 0$ for every z and $\mathcal{L}_3 : \mathbb{R}^3 \to \mathbb{R}$ being a smooth function such that $\mathcal{L}_3(0,0,z) = \frac{\partial \mathcal{L}_3}{\partial x}(0,0,z) = \frac{\partial \mathcal{L}_3}{\partial y}(0,0,z) = 0$ for every z.

Proof. The proofs relies on straightforward computations. Let

$$\mathbf{M} = \begin{pmatrix} m_{11} & m_{12} \\ m_{21} & m_{22} \end{pmatrix} \tag{10}$$

be the matrix appearing in equation (8), and assume without loss of generality that $\det \mathbf{M} = 1$. Set

$$\begin{pmatrix} x \\ y \end{pmatrix} = \mathbf{M}^{-T} \begin{pmatrix} \boldsymbol{x} \\ \textbf{\textit{y}} \end{pmatrix}, \qquad z = \textbf{\textit{z}}.$$

Then it is immediate to verify that

$$f = \frac{\partial}{\partial x} + yH(\Phi^{-1}(x,y,z)) \qquad g = \frac{\partial}{\partial y} - xH(\Phi^{-1}(x,y,z)),$$

where $H(\boldsymbol{x}, \textbf{\textit{y}}, \textbf{\textit{z}}) = \beta(\boldsymbol{x}, \textbf{\textit{y}}, \textbf{\textit{z}})\Big(\textbf{\textit{y}}\frac{\partial}{\partial x} - \boldsymbol{x}\frac{\partial}{\partial \textbf{\textit{y}}}\Big) - \frac{1}{2}(1 + \gamma(\boldsymbol{x}, \textbf{\textit{y}}, \textbf{\textit{z}}))\frac{\partial}{\partial \textbf{\textit{z}}}$.

Equations (6) and (7) yield

$$\beta(\Phi^{-1}(0,0,z)) = \gamma(\Phi^{-1}(0,0,z)) = 0 \quad \forall z \in \mathbb{R}$$
$$\frac{\partial(\gamma \circ \Phi^{-1})}{\partial x}(0,0,z) = \frac{\partial(\gamma \circ \Phi^{-1})}{\partial y}(0,0,z) = 0 \quad \forall z \in \mathbb{R},$$

and the Proposition is proved. □

The functions L_{ij}, $i,j = 1,2$, can be expanded in power series (about 0):

$$L_{ij}(x,y,z) = \mathrm{ax}_{ij}x + \mathrm{ay}_{ij}y + \frac{1}{2}\begin{pmatrix} x & y & z \end{pmatrix}\begin{pmatrix} \omega_{xxij} & \omega_{xyij} & \omega_{xzij} \\ \omega_{yxij} & \omega_{yyij} & \omega_{yzij} \\ \omega_{zxij} & \omega_{zyij} & \omega_{zzij} \end{pmatrix}\begin{pmatrix} x \\ y \\ z \end{pmatrix} + \phi_{ij}(x,y,z),$$

where ϕ_{ij} are smooth functions vanishing at all points $(0,0,z)$, together with all their first and second order derivatives with respect to x, y. Analogously, we expand also $\mathcal{L}_3$ in Taylor series

$$\begin{aligned}\mathcal{L}_3(x,y,z) = {} & \mathrm{ax}_{31}x^2 + \mathrm{ax}_{32}xy + \mathrm{ay}_{31}xy + \mathrm{ax}_{32}y^2 \\ & + \frac{x}{2}\begin{pmatrix} x & y & z \end{pmatrix}\begin{pmatrix} \omega_{xx31} & \omega_{xy31} & \omega_{xz31} \\ \omega_{yx31} & \omega_{yy31} & \omega_{yz31} \\ \omega_{zx31} & \omega_{zy31} & \omega_{zz31} \end{pmatrix}\begin{pmatrix} x \\ y \\ z \end{pmatrix} \\ & + \frac{y}{2}\begin{pmatrix} x & y & z \end{pmatrix}\begin{pmatrix} \omega_{xx32} & \omega_{xy32} & \omega_{xz32} \\ \omega_{yx32} & \omega_{yy32} & \omega_{yz32} \\ \omega_{zx32} & \omega_{zy32} & \omega_{zz32} \end{pmatrix}\begin{pmatrix} x \\ y \\ z \end{pmatrix} + \phi_3(x,y,z),\end{aligned}$$

where ϕ_3 is a smooth function vanishing at all points $(0,0,z)$, together with all its first and second order partial derivatives with respect to x, y. In analogy with the expansion of L_{ij}, $i,j = 1,2$, we set

$$L_{3j}(x,y,z) = \mathrm{ax}_{3j}x + \mathrm{ay}_{3j}y + \frac{1}{2}\begin{pmatrix} x & y & z \end{pmatrix}\begin{pmatrix} \omega_{xx3j} & \omega_{xy3j} & \omega_{xz3j} \\ \omega_{yx3j} & \omega_{yy3j} & \omega_{yz3j} \\ \omega_{zx3j} & \omega_{zy3j} & \omega_{zz3j} \end{pmatrix}\begin{pmatrix} x \\ y \\ z \end{pmatrix} + \phi_{3j}(x,y,z),$$

where ϕ_{31} and ϕ_{32} are chosen such that $\phi_{31} + \phi_{32} = \phi_3$ and that both ϕ_{31} and ϕ_{32}, together with all their first and second order partial derivatives, are null at $(0,0,z)$, $z \in \mathbb{R}$.

The constants $\mathrm{ax}_{ij}, \mathrm{ay}_{ij}, \omega_{\cdot\cdot ij}$ are called the *invariants* of the metric. As we will see in the following sections, some particular (linear) functions of the invariant play a major role in the loss of local and global optimality of bang-bang geodesics. These invariants are

$$C_1 = 8\mathrm{ax}_{31} \qquad C_2 = 8\mathrm{ay}_{32},$$
$$A = 4\mathrm{ax}_{32} + 4\mathrm{ay}_{31},$$
$$D_1 = 9\mathrm{ax}_{21} - 15\omega_{xx31} \qquad D_2 = -9\mathrm{ay}_{12} - 15\omega_{yy32}, \tag{11}$$
$$E_1 = 3\mathrm{ax}_{11} - 3\mathrm{ax}_{22} - 3\mathrm{ay}_{21} + 5\omega_{xx32} + 5\omega_{xy31} + 5\omega_{yx31}, \tag{12}$$
$$E_2 = -3\mathrm{ax}_{12} - 3\mathrm{ay}_{11} - 3\mathrm{ay}_{22} - 5\omega_{xy32} - 5\omega_{yx32} - 5\omega_{yy31}.$$

We also define the following constants

$$\begin{aligned} c_1 &= 4\mathrm{ax}_{12} + 7\mathrm{ax}_{21} + 4\mathrm{ay}_{11} - 12\mathrm{ay}_{22} + 15\omega_{xx31} + 20\omega_{xy32} + 20\omega_{yx32} + 20\omega_{yy31} \\ d_1 &= 4\mathrm{ax}_{22} + \mathrm{ay}_{12} + 4\mathrm{ay}_{21} + 15\omega_{yy32} \\ c_2 &= 12\mathrm{ax}_{11} - 4\mathrm{ax}_{22} - 7\mathrm{ay}_{12} - 4\mathrm{ay}_{21} + 20\omega_{xx32} + 20\omega_{xy31} + 20\omega_{yx31} + 15\omega_{yy32} \\ d_2 &= 4\mathrm{ax}_{12} + \mathrm{ax}_{21} + 4\mathrm{ay}_{11} - 15\omega_{xx31}, \end{aligned}$$

which do not affect the classification of the cut locus, but often appear in the computations.

We are ready to state the second assumption we are doing (its meaning will be more clear in Section 3.2).

Assumption 2 *The invariants A, C_2, D_1 and E_1 are non zero. Moreover, we assume that $|A| \neq |C_2|$ and $|D_1| \neq |E_1|$. The invariant C_1 is null.*

We finally notice that the control system (2b)-(2c)-(2d) inherits some symmetry properties from the vector fields (9), as the following Lemma shows. The proof follows from straightforward computation, and is thus omitted.

Lemma 4 *Let $\theta = \frac{k\pi}{2}$, $k \in 1, 2, 3$, denote with $\hat{R}_\theta$ (respectively, R_θ) the matrix of the (counterclockwise) rotation of angle θ in the two dimensional Euclidean space (respectively, around the axis z in three dimensional Euclidean space). Consider the vector fields*

$$\widetilde{f} = \begin{pmatrix} 1 + y(x\widetilde{L}_{11}(\mathbf{x}) + y\widetilde{L}_{12}(\mathbf{x})y) \\ y(x\widetilde{L}_{21}(\mathbf{x}) + y\widetilde{L}_{22}(\mathbf{x})y) \\ -\frac{y}{2} + y(x\widetilde{L}_{31}(\mathbf{x}) + y\widetilde{L}_{32}(\mathbf{x})y) \end{pmatrix} \quad \widetilde{g} = \begin{pmatrix} -x(x\widetilde{L}_{11}(\mathbf{x}) + y\widetilde{L}_{12}(\mathbf{x})) \\ 1 - x(x\widetilde{L}_{21}(\mathbf{x}) + y\widetilde{L}_{22}(\mathbf{x})) \\ \frac{x}{2} - x(x\widetilde{L}_{31}(\mathbf{x}) + y\widetilde{L}_{32}(\mathbf{x})) \end{pmatrix} \tag{13}$$

where

$$\begin{pmatrix} \widetilde{L}_{11}(\mathbf{x}) & \widetilde{L}_{12}(\mathbf{x}) \\ \widetilde{L}_{21}(\mathbf{x}) & \widetilde{L}_{22}(\mathbf{x}) \\ \widetilde{L}_{31}(\mathbf{x}) & \widetilde{L}_{32}(\mathbf{x}) \end{pmatrix} = R_\theta^{-1} \begin{pmatrix} L_{11}(R_\theta\mathbf{x}) & L_{11}(R_\theta\mathbf{x}) \\ L_{21}(R_\theta\mathbf{x}) & L_{22}(R_\theta\mathbf{x}) \\ L_{31}(R_\theta\mathbf{x}) & L_{32}(R_\theta\mathbf{x}) \end{pmatrix} \hat{R}_\theta.$$

Let $\widetilde{\boldsymbol{u}} : [0, T] \to Q$ be some measurable function and $\widetilde{\boldsymbol{\xi}}$ denote the solution of the Cauchy problem

$$\begin{cases} \dot{\widetilde{\boldsymbol{\xi}}}(t) = (\widetilde{u}_1\widetilde{f} + \widetilde{u}_2\widetilde{g}) \circ \widetilde{\boldsymbol{\xi}}(t), \\ \widetilde{\boldsymbol{\xi}}(0) = (0, 0, 0). \end{cases}$$

Then $R_\theta\widetilde{\boldsymbol{\xi}}(t)$ is the solution of the Cauchy problem (2b) *corresponding to the control $\boldsymbol{u}(t) = R_\theta\widetilde{\boldsymbol{u}}(t)$ with initial condition equal to* $(0, 0, 0)$.

The symmetric properties of the normal form (9) are inherited also by the extremals, as the Lemma here below states.

Lemma 5 *Assume that $(\boldsymbol{\mu}(t), \boldsymbol{\xi}(t))$ is an extremal of the optimal control problem* (2)*, associated with the control function $\boldsymbol{u}(t)$.*

Then the pair $(\widetilde{\boldsymbol{\mu}}(t), \widetilde{\boldsymbol{\xi}}(t)) = (R_\theta^{-1}\boldsymbol{\mu}(t), R_\theta^{-1}\boldsymbol{\xi}(t))$ is an extremal of the minimum time problem associated with the system

$$\dot{\widetilde{\boldsymbol{\xi}}}(t) = (\widetilde{u}_1\widetilde{f} + \widetilde{u}_2\widetilde{g}) \circ \widetilde{\boldsymbol{\xi}}(t),$$

where $\widetilde{f}$ and $\widetilde{g}$ are the vector fields defined in (13) *and $\widetilde{\boldsymbol{u}}(t) = \widehat{R}_\theta^{-1}\boldsymbol{u}(t)$.*

2.5.1 Genericity

In this section, we briefly discuss the notion of genericity we are considering, thus clarifying the statements done in the Introduction. The whole section relies on the results of the article [12].

Let $\mathrm{SubR}(M)$ denote the set of all sub-Riemannian structures on the manifold M, endowed with the Whitney topology ([15]). The set of all the sub-Finsler L^1 structures compatible with some sub-Riemannian structure on M, that we denote with $\overline{\mathrm{SF}}_1(M)$, can be identified with $\mathbb{R}^2 \times \mathrm{SubR}(M)$, endowed with the product topology.

Following [12, Theorem 1.3, Corollary 1.4, Corollary 2.8], we write the function γ in (5) as $\gamma(x, y, z) = c_1x^2 + c_2y^2 + 2c_3xy + V(x, y) + \chi(x, y, z)$, where V is a cubic function and χ, together with its partial derivatives with respect to x, y of order less than 4, vanishes at $(0, 0, z)$. By easy computations, we can see that $\mathrm{ax}_{31} = \frac{c_1}{m_{11}^2}$, $\mathrm{ay}_{32} = c_1m_{21}^2 + \frac{c_2}{m_{11}^2} - 2c_3m_{11}m_{21}$ and $\mathrm{ax}_{32} = \mathrm{ay}_{31} = -c_1m_{11}m_{21} + c_3$ where, without loss of generality, we assumed that the element m_{12} of $\mathbf{M}$ is null (this operation does not impact the structure of the small spheres).

Therefore, we can adapt the proof of [12, Theorem 1.5] and conclude that, for a generic sub-Finsler L^1 metric compatible with a sub-Riemannian structure, the set of points $\boldsymbol{q} \in M$ such that the normal form (9) has $\mathrm{ax}_{31} = 0$ (respectively, $\mathrm{ay}_{32} = 0$) form a 2-dimensional submanifold of M. Therefore, asking $\mathrm{ax}_{31}\mathrm{ay}_{32} \neq 0$, as done in [7], is a genericity assumptions.

In this paper, we are interested in sub-Finsler structure for which $\mathrm{ax}_{31} = 0$, while the invariants ay_{32}, D_1 and E_1 and defined in equations (11)-(12)) are non-zero. By easy computations, it can be proved that E_1 and D_1 are linear combinations of the invariants of the original sub-Riemannian metric (more precisely, the terms called V and l in [12]). Adapting again [12, Theorem 1.5], we get that, for a generic sub-Finsler L^1 metric compatible with

a sub-Riemannian structure, the set of points $\boldsymbol{q} \in M$ such that the normal form (9) has $\mathrm{ax}_{31} = D_1 = E_1 = 0$ has codimension 3 in M.

In other words, the assumption $D_1 E_1 \neq 0$ is generically true if we restrict ourselves to the non-generic set of points $\boldsymbol{q}$ for which the normal form has $\mathrm{ax}_{31} = 0$.

2.6 The Heisenberg system

The simplest case of the optimal control problem (2) corresponds to the nilpotent approximation of the vector fields f and g (also known as Heisenberg group, see for instance [4, 18]), that is

$$f = \not{f} = \begin{pmatrix} 1 \\ 0 \\ -y/2 \end{pmatrix} \qquad g = \not{g} = \begin{pmatrix} 0 \\ 1 \\ x/2 \end{pmatrix}.$$

We recall that $[f, g] = \left(\begin{smallmatrix} 0 \\ 0 \\ 1 \end{smallmatrix}\right)$.

The time-optimal problem for this system has already been studied in [9, 11, 19]. Since it constitutes a starting point for the study of the generic cases, it is worth recalling the main properties of its time-optimal synthesis from the initial point $\mathbf{x}_0 = (0, 0, 0)$.

First of all, we notice that the problem exhibits a discrete symmetry: it is invariant for rotations of $k\pi/2$, $k \in \mathbb{Z}$ around the vertical axis (z); moreover, it turns out that the unit sphere (that is, the set of all points reachable in time 1 from the origin) is symmetric with respect to the (x, y) plane, and that the geodesics that reach positive (respectively, negative) z are projections of extremals with $p_z^0 \geq 0$ (respectively, $p_z^0 \leq 0$). For these reasons, we discuss only the extremals whose initial adjoint vector $\boldsymbol{\mu}(0) = (p_x^0, p_y^0, p_z^0)$ satisfies $p_x^0 = 1$, $p_y^0 \in [-1, 1]$ and $p_z^0 \geq 0$; indeed, all other extremals can be recovered from these ones applying a suitable transformation.

First of all, consider any extremal with $|p_y^0| < 1$ and $p_z^0 > 0$: then, since $F(\boldsymbol{\lambda}(0)) = 1 > |p_y^0| = |G(\boldsymbol{\lambda}(0))|$, PMP implies that there exists some $\mathbb{T}_1 > 0$ such that on the interval $[0, \mathbb{T}_1)$ the control associated with the extremal is $(1, 0)$; in particular, $\mathbb{T}_1$ is the smallest (positive) time satisfying $F(\boldsymbol{\lambda}(\mathbb{T}_1)) = G(\boldsymbol{\lambda}(\mathbb{T}_1))$, which, by computations, turns out to be $\mathbb{T}_1 = \frac{1-p_y^0}{p_z^0}$. For $p_y^0 = -1$, both the controls $\boldsymbol{u} = (1, 0)$ and $\boldsymbol{u} = (0, -1)$ are admissible at $t = 0$; on the other hand, if $\boldsymbol{u} = (0, -1)$, then $F(\boldsymbol{\lambda}(t))$ is strictly increasing, so that the pair $(\boldsymbol{\lambda}(t), (0, -1))$ does not satisfy PMP for $t > 0$ small enough. Thus, the control associated with extremals with $\boldsymbol{\mu}(0) = (1, -1, p_z^0)$, $p_z^0 > 0$, is $(1, 0)$ for every $t \in [0, \mathbb{T}_1)$, $\mathbb{T}_1 = 2/p_z^0$.

In both cases ($|p_y| < 1$ and $p_y = -1$), for $t \in (\mathbb{T}_1, \mathbb{T}_2)$, where $\mathbb{T}_2 = \mathbb{T}_1 + 2/p_z^0$, the control associated with the extremal is equal to $(0, 1)$; $\mathbb{T}_2$ is indeed the smallest time greater than $\mathbb{T}_1$ such that $F(\boldsymbol{\lambda}(\mathbb{T}_2)) = -G(\boldsymbol{\lambda}(\mathbb{T}_2))$. For times greater than $\mathbb{T}_2$, the control switches every $\Delta T = 2/p_z^0$, following the vertexes of Q in the counterclockwise sense.

In the special case $p_x^0 = p_y^0 = 1$, explicitly integrating the Hamiltonian system and applying equation (3c), it is easy to see that the control associated with such extremals is equal to $(0, 1)$ on the interval $(0, \Delta T)$, and then it switches every ΔT, following the same sequence as above.

Let $(\widehat{\boldsymbol{\mu}}, \widehat{\boldsymbol{\xi}})$ be an extremal such that $\widehat{\boldsymbol{\mu}}(0) = (1, \widehat{p}_y^0, \widehat{p}_z^0)$, with $\widehat{p}_y^0 \in [-1, 1)$ and $\widehat{p}_z^0 > 0$; integrating the system, we see that, for $t \in [\mathbb{T}_4, 8/\widehat{p}_z^0]$, the expression of the geodesic is given by

$$\begin{cases} x(t) = t - 4\Delta T \\ y(t) = 0 \\ z(t) = \Delta T^2, \end{cases}$$

that is, its value depends only on t and on $\widehat{p}_z^0$, but not on $\widehat{p}_y^0$. In particular, at $t = \mathbb{T}_4 = \frac{7-\widehat{p}_y^0}{\widehat{p}_z^0}$, $\widehat{\boldsymbol{\xi}}$ meets all geodesics with $\boldsymbol{\mu}(0) = (1, p_y^0, \widehat{p}_z^0)$ and $\widehat{p}_y^0 < p_y^0 \leq 1$, and coincides with them, at least up to time $8/\widehat{p}_z^0$. Moreover, for every $\epsilon > 0$, we can always find some $p_y^0 > \widehat{p}_y^0$ such that the graph of the corresponding trajectory is ϵ-close in the C^0 norm to the graph of $\widehat{\boldsymbol{\xi}}$. In other words, at $t = \mathbb{T}_4$ the trajectory $\widehat{\boldsymbol{\xi}}$ loses its local optimality.

To verify if a geodesics loses its global optimality before its fourth switching time, we must look for intersections of the trajectory under study with some geodesics trajectories whose graph does not belong to a neighborhood of its graph, that is, whose initial control is not $(1, 0)$. By computations, it is possible to prove that such intersections occur either at the

fourth switching time, either at $8/\hat{p}_z$. Therefore, for every trajectory, the fourth switching time $\mathbb{T}_4$ is the cut time.

To complete the analysis, we now consider the extremals with $p_x^0 = p_y^0 = 1$ and $p_z^0 = 0$; we notice that every control of the form $(\alpha(t), 1-\alpha(t))$, with $\alpha(t) \in [0,1]$ $\forall t$, satisfies PMP. As $x(T) + y(T) = \int_0^T u_1(t) + u_2(t)\, dt = T$, such extremals are necessarily optimal; we can also prove that $z(T) \leq x(T)y(T)/2$. Conversely, every point $(x_T, y_T, z_T) \in \mathbb{R}^3$ with $|z_T| \leq |x_T y_T|/2$ can be reached in time $|x_T|+|y_T|$ by at least a singular trajectory. We conclude that the minimum time for reaching points $\{(x_T, y_T, z_T) : |z_T| \leq |x_T y_T|/2\}$ is $|x_T|+|y_T|$.

3 Non-generic case: bang-bang geodesics with controls switching in counterclockwise sense

3.1 Local expansions of the dynamics

As already anticipated in the introduction, we are interested in the local geometry of the L^1 sub-Finsler metric associated with $\{f, g\}$, or, equivalently, in the local optimal synthesis for the minimum time problem (2). Indeed, as in the sub-Riemannian case ([2, 12, 23]), it is interesting to see how a small perturbation of the nilpotent system affects the shape of the conjugate and the cut locus. We then study the optimal synthesis from some initial point $\boldsymbol{q}_0$ and final points sufficiently close to $\boldsymbol{q}_0$. More precisely, consider a neighborhood U of $\boldsymbol{q}_0$ on which the local coordinates of Proposition 1, centered at $\boldsymbol{q}_0$, are well defined; thanks to small-time local controllability, there exists an open neighborhood $V \subset U$ of $\boldsymbol{q}_0$ such that all time optimal trajectories from $\boldsymbol{q}_0$ to points in V are contained in U. We can shrink V further, in order to ensure that $|x|, |y|, |z| < 1$ for every $(x, y, z) \in V$ (here $|\cdot|$ denotes the Euclidean norm on $\mathbb{R}^3$), and that the minimum time for reaching any point in V from $\boldsymbol{q}_0$ is bounded by some $T \ll 1$.

When we restrict to final points contained in V, we also reduce the possible behaviors of the extremals we can consider. Indeed, computing explicitly Θ, we obtain that, for every extremal $\boldsymbol{\lambda}$ whose projection lies in V, the following estimate holds

$$\Theta(\boldsymbol{\lambda}(t)) = p_z(t)\big(1 + \mathcal{O}(x(t)^2, y(t)^2, z(t))\big) + \|(p_x(t), p_y(t))\|\mathcal{O}(x(t)^2, y(t)^2, z(t)).$$

Assume that $p_z(0) > 0$. We can have two possible cases; either the sign of $\Theta(\boldsymbol{\lambda}(t))$ is constant on $[0, T]$, or it is not. In the first case, the corresponding extremals are associated with controls that switch from vertex to vertex of Q in counterclockwise sense (as $\Theta(\boldsymbol{\lambda}(0)) > 0$), as for the nilpotent system. For the corresponding trajectories, the nilpotent part in f, g dominates, and the trajectories are close to those described in Section 2.6.

Let us now consider the second case: we recall that the time derivatives of $\boldsymbol{p}$ are linear in $\boldsymbol{p}$ (eventually multiplied by powers of x, y, z, that are small in V) and that both $|p_x(0)|$ and $|p_y(0)|$ are bounded by 1. Then, in some neighborhoods of the times where $\Theta(\boldsymbol{\lambda}(t))$ changes sign, $p_z(t)$ must be of the same order of magnitude of $\mathcal{O}(x(t)^2, y(t)^2, z(t))$; in particular, $|\Theta(\boldsymbol{\lambda}(t))| = \mathcal{O}(x(t)^2, y(t)^2, z(t)) = \mathcal{O}(T^2)$ on $[0, T]$. It follows that F and G vary very slowly along the extremal and the associated control is either constant or it assumes values that belong on one side of Q (see Section 5 for a brief description of such situations).

By straightforward computations, we can prove that the geodesics associated with extremal of the first kind satisfy the bound $|z(t)| \geq \frac{|x(t)y(t)|}{2} + \mathcal{O}(x(t)^4, y(t)^4)$ (as for the Heisenberg system), and that those associated with extremals of the second kind the bound $|z(t)| \leq \frac{|x(t)y(t)|}{2} + \mathcal{O}(x(t)^4, y(t)^4)$. In this paper we focus on the former extremals or, equivalently, we study the upper part of the sphere, that is, the part with $z(t) > \frac{|x(t)y(t)|}{2}$ (our description can be easily adapted to describe the part of the sphere with $z(t) < -\frac{|x(t)y(t)|}{2}$). In short times, these geodesics are characterized by very large values of $p_z(0)$ (that is, of the same order of magnitude of the inverse of the final time). In order to (approximately) compute such extremals, we derive a power expansion of the solution of the Hamiltonian system in terms of the small parameter $\rho_0 = 1/p_z(0)$.

Let $(\boldsymbol{\mu}(t), \boldsymbol{\xi}(t))$ be an extremal of (2) with $p_z(0) \gg 1$, and let $\boldsymbol{u}(t)$ be its associated control function. Following the same techniques used in [2, 7, 12], we perform the time

reparametrization

$$\tau(t) = \int_0^t p_z(s)\, ds, \tag{14}$$

and we define the new variables

$$\overline{p}_x = \frac{p_x}{p_z} \qquad \overline{p}_y = \frac{p_y}{p_z} \qquad \varrho = \frac{1}{p_z} \qquad \overline{\Theta} = \frac{\Theta}{p_z}.$$

Notation. *In the paper we are dealing with two time-scales: the real time t, of order $\mathcal{O}(\varrho)$, and the reparameterized time τ, of order $\mathcal{O}(1)$, related by equation* (14)*. In order to avoid ambiguities, we will use normal fonts $(t, T, \boldsymbol{T}, \ldots)$ to denote the real time, and script or Greek fonts $(\tau, \boldsymbol{\tau}, \mathscr{T}, \mathcal{T})$ to denote the reparameterized time.*

In order to compute the jets of the extremal $(\boldsymbol{\mu}(\tau), \boldsymbol{\xi}(\tau))$, we now expand its coordinates in power series of the parameter $\rho_0 = \varrho(0)$:

$$\begin{cases} x(\tau) = \rho_0 x_1(\tau) + \rho_0^2 x_2(\tau) + \rho_0^3 x_3(\tau) + \rho_0^4 x_4(\tau) + \rho_0^5 x_5(\tau) + \mathcal{O}(\rho_0^6) \\ y(\tau) = \rho_0 y_1(\tau) + \rho_0^2 y_2(\tau) + \rho_0^3 y_3(\tau) + \rho_0^4 y_4(\tau) + \rho_0^5 y_5(\tau) + \mathcal{O}(\rho_0^6) \\ z(\tau) = \rho_0 z_1(\tau) + \rho_0^2 z_2(\tau) + \rho_0^3 z_3(\tau) + \rho_0^4 z_4(\tau) + \rho_0^5 z_5(\tau) + \mathcal{O}(\rho_0^6) \\ \overline{p}_x(\tau) = \rho_0 \overline{p}_{x1}(\tau) + \rho_0^2 \overline{p}_{x2}(\tau) + \rho_0^3 \overline{p}_{x3}(\tau) + \rho_0^4 \overline{p}_{x4}(\tau) + \rho_0^5 \overline{p}_{x5}(\tau) + \mathcal{O}(\rho_0^6) \\ \overline{p}_y(\tau) = \rho_0 \overline{p}_{y1}(\tau) + \rho_0^2 \overline{p}_{y2}(\tau) + \rho_0^3 \overline{p}_{y3}(\tau) + \rho_0^4 \overline{p}_{y4}(\tau) + \rho_0^5 \overline{p}_{y5}(\tau) + \mathcal{O}(\rho_0^6) \\ \varrho(\tau) = \rho_0 + \rho_0 \varrho_1(\tau) + \rho_0^2 \varrho_2(\tau) + \rho_0^3 \varrho_3(\tau) + \rho_0^4 \varrho_4(\tau) + \rho_0^5 \varrho_5(\tau) + \mathcal{O}(\rho_0^6). \end{cases} \tag{15}$$

Plugging these expansions into the adjoint equation (3b), we can see that $\frac{d\varrho}{d\tau} = \mathcal{O}(\rho_0^5)$, that is, $\varrho(\tau) = \rho_0 + \mathcal{O}(\rho_0^5)$. The control system (2b) can be thus written as

$$\begin{aligned} \frac{dx}{d\tau} &= \dot{x}_1\rho_0 + \dot{x}_2\rho_0^2 + \dot{x}_3\rho_0^3 + \dot{x}_4\rho_0^4 + \mathcal{O}(\rho_0^5) \\ &= u_1\rho_0 + (u_2x_1 - u_1y_2)\big(\mathrm{ax}_{11}x_1^2 + (\mathrm{ax}_{12} + \mathrm{ay}_{11})x_1y_1 + \mathrm{ay}_{12}y_1^2\big)\rho_0^4 + \mathcal{O}(\rho_0^5) \\ \frac{dy}{d\tau} &= \dot{y}_1\rho_0 + \dot{y}_2\rho_0^2 + \dot{y}_3\rho_0^3 + \dot{y}_4\rho_0^4 + \mathcal{O}(\rho_0^5) \\ &= u_2\rho_0 + (u_2x_1 - u_1y_2)\big(\mathrm{ax}_{21}x_1^2 + (\mathrm{ax}_{22} + \mathrm{ay}_{21})x_1y_1 + \mathrm{ay}_{22}y_1^2\big)\rho_0^4 + \mathcal{O}(\rho_0^5) \\ \frac{dz}{d\tau} &= \dot{z}_1\rho_0 + \dot{z}_2\rho_0^2 + \dot{z}_3\rho_0^3 + \dot{z}_4\rho_0^4 + \dot{z}_5\rho_0^5 + \mathcal{O}(\rho_0^6) \\ &= \frac{1}{2}(u_2x_1 - u_1y_2)\rho_0^2 \\ &\quad + (u_2x_1 - u_1y_1)\big(\mathrm{ax}_{31}x_1^2 + (\mathrm{ax}_{32} + \mathrm{ay}_{31})x_1y_1 + \mathrm{ay}_{32}y_1^2\big)\rho_0^4 \\ &\quad + \frac{1}{2}\Big((u_2x_4 - u_1y_4) + (u_2x_1 - u_1y_2)\big(\omega_{xx31}x_1^3 + (\omega_{xx32} + \omega_{xy31} + \omega_{yx31})x_1^2y_1 \\ &\quad + (\omega_{xy32} + \omega_{yx32} + \omega_{yy31})x_1y_1^2 + \omega_{yy32}y_1^3\big)\Big)\rho_0^5 + \mathcal{O}(\rho_0^6), \end{aligned}$$

where, to avoid heavy notations, we omitted to explicitly write the time dependence of the functions x_i, y_i, z_i. Analogously, plugging (15) into the adjoint equation,we obtain

$$\begin{aligned} \frac{d\overline{p}_x}{d\tau} &= -\frac{u_2}{2}\rho_0 + \Big(3u_2\mathrm{ax}_{31}x_1^2 + 2u_2(\mathrm{ax}_{32} + \mathrm{ay}_{31})x_1y_1 + u_2\mathrm{ay}_{32}y_1^2 \\ &\qquad - 2u_1\mathrm{ax}_{31}x_1y_1 - u_1(\mathrm{ax}_{32} + \mathrm{ay}_{31})y_1^2\Big)\rho_0^3 + \mathcal{O}(\rho_0^4) \\ \frac{d\overline{p}_y}{d\tau} &= \frac{u_1}{2}\rho_0 + \Big(-3u_1\mathrm{ax}_{32}y_1^2 - 2u_1(\mathrm{ax}_{32} + \mathrm{ay}_{31})x_1y_1 - u_1\mathrm{ax}_{31}x_1^2 \\ &\qquad + 2u_2\mathrm{ay}_{32}x_1y_1 + u_2(\mathrm{ax}_{32} + \mathrm{ay}_{31})x_1^2\Big)\rho_0^3 + \mathcal{O}(\rho_0^4). \end{aligned}$$

These equations can be integrated at each order in ρ_0, in order to obtain the expression of the functions $x_i(\tau), y_i(\tau), z_i(\tau), \overline{p}_{xi}(\tau), \overline{p}_{yi}(\tau)$. To do that, we use the software Wolfram *Mathematica*; the program computing the jets of the extremal can be found in [16, Annexe C].

For the results contained in this paper, we are stopping at the *fourth* order for the x and y and at the *fifth* order for z; the expressions can be found in Appendix B.1. For what concerns $\overline{p}_x$ and $\overline{p}_y$, the third order terms suffice.

The power series for the switching times are computed analogously. Consider, for instance, an extremal with $p_x(0) = 1$ and $|p_y(0)| < 1$. The switching (reparameterized) time $\mathscr{T}_1$ is determined by the condition $F(t(\mathscr{T}_1)) = G(t(\mathscr{T}_1)) = 1$. Plugging the expansions for $(\boldsymbol{\mu}(t(\tau)), \boldsymbol{\xi}(t(\tau)))$ into $\overline{\Theta}$, we can compute the coefficients $\overline{\Theta}_k$ in

$$\begin{aligned}\overline{\Theta} &= 1 + \overline{\Theta}_1\rho_0 + \overline{\Theta}_2\rho_0^2 + \overline{\Theta}_3\rho_0^3 + \cdots \\ &= 1 - 4\big(\mathrm{ax}_{31}x_1^2 + \mathrm{ay}_{32}y_1^2 + (\mathrm{ax}_{32} + \mathrm{ay}_{31})x_1y_1\big)\rho_0^2 + \dots\end{aligned}$$

Developing $\mathscr{T}_1$ in powers of ρ_0 and imposing, at each order in ρ_0,

$$\begin{aligned}1 = G(t(\mathscr{T}_1)) &= p_y(0) + \int_0^{\mathscr{T}_1} \overline{\Theta}(\boldsymbol{\mu}(t(\tau)), \boldsymbol{\xi}(t(\tau)))d\tau \\ &= p_y(0) + \int_0^{\mathscr{T}_1^0} (1 + \rho_0\overline{\Theta}_1 + \cdots)d\tau + \int_{\mathscr{T}_1^0}^{\mathscr{T}_1^0 + \rho_0\mathscr{T}_1^1} (1 + \rho_0\overline{\Theta}_1 + \cdots)d\tau + \cdots,\end{aligned}$$

we can identify all the coefficients $\mathscr{T}_1^k$ of the expansion of $\mathscr{T}_1$. We proceed in the same way for the other switching times (see [16, Annexe C] for the *Mathematica* program we used); the first terms in the expansion of the switching times can be found in Appendix B.2.

Based on Lemmas 4-5, there is no need of computing the jets of the geodesics and the switching times for the bang-bang geodesics with large $p_z(0)$ and $p_x(0) \neq 1$, as they can be easily recovered from those just computed, by applying a suitable rotation and a permutation of the invariants, as explained in Appendix A.

We end this section by classifying the four different kinds of bang-bang geodesics associated with extremals with large positive $p_z(0)$, according to their initial velocity. For every $r > 0$ small enough, we define the set

$$\Gamma_f^r = \left\{ \boldsymbol{\xi} : [0, 10r] \to \mathbb{R}^3 : \left\{ \begin{array}{l} \boldsymbol{\lambda} = (\boldsymbol{\mu}, \boldsymbol{\xi}) \text{ is an extremal of the problem (2)} \\ \qquad\qquad \text{with control } \boldsymbol{u} \\ \boldsymbol{\xi}(0) = (0,0,0) \\ \boldsymbol{\mu}(0) = (1, p_y^0, p_z^0) \ \text{ with } p_y^0 \in [-1,1) \text{ and } p_z^0 \geq \frac{1}{r} - 1 \\ \exists\ 0 < \mathbb{T}_1 < \cdots < \mathbb{T}_5 \leq 10r \\ \qquad\qquad \text{such that } \left\{ \begin{array}{l} \boldsymbol{u}|_{(0,\mathbb{T}_1)} = (1,0) \\ \boldsymbol{u}|_{(\mathbb{T}_1,\mathbb{T}_2)} = (0,1) \\ \boldsymbol{u}|_{(\mathbb{T}_2,\mathbb{T}_3)} = (-1,0) \\ \boldsymbol{u}|_{(\mathbb{T}_3,\mathbb{T}_4)} = (0,-1) \\ \boldsymbol{u}|_{(\mathbb{T}_4,\mathbb{T}_5)} = (1,0) \end{array} \right. \end{array} \right. \right\}.$$

Γ_f^r is actually the set of bang-bang geodesics with $p_z(0)$ large enough and that behave qualitatively as the bang-bang geodesics of the nilpotent case with initial velocity f and switch at least five time in the time interval $[0, 10r]$. In an analogous way, we can define also Γ_{-f}^r, Γ_g^r and Γ_{-g}^r. In the following, r will always be fixed, so we will drop the super-script r from the definition of these sets.

3.2 Computation of conjugate times

For short times, all geodesics with constant bang control (i.e., only one bang arc) are optimal: indeed, if for instance $\boldsymbol{u} = (1,0)$, then $\boldsymbol{\xi}(t) = (t,0,0)$, and t is the minimum time for reaching the point $(t,0,0)$. Also regular bang-bang geodesics with large $p_z(0)$ and two bang arcs are locally optimal, as can be deduced, for instance, from [21, Remark 3.5]. On the other hand, a bound on the maximum number of switching times for an optimal geodesic has been provided in [24]: regular bang-bang geodesics with large $p_z(0)$ and more than five bang arcs cannot be locally optimal.

Summing up, for our purposes, it suffices to compute the Jacobian of the exponential map for bang-bang geodesics with at most 6 bang arcs. By long but simple computations (done with the help of the software *Mathematica*, see [16, Annexe C]), it is possible to compute its power expansion, which turns out to be constant (with respect to time), at least up to the

order we computed, along each bang arc. For extremals corresponding to geodesics in the sets $\Gamma_{\pm f}$, with $|p_x^0|=1$, $|p_y^0|\leq 1$ and $p_x^0 \neq p_y^0$, we obtain

$$\mathrm{JExp}|_{(p_y^0,p_z^0,\tau)}=\begin{cases}0 & \tau\in[0,\mathscr{T}_2(p_y^0,p_z^0))\\ 4\rho_0^3+\mathcal{O}(\rho_0^4) & \tau\in(\mathscr{T}_2(p_y^0,p_z^0),\mathscr{T}_3(p_y^0,p_z^0))\\ 8\rho_0^3+\mathcal{O}(\rho_0^4) & \tau\in(\mathscr{T}_3(p_y^0,p_z^0),\mathscr{T}_4(p_y^0,p_z^0))\\ 32C_1\rho_0^5 & \\ \quad+32\big(D_1p_y^0\pm E_1\big)\rho_0^6+\mathcal{O}(\rho_0^7) & \tau\in(\mathscr{T}_4(p_y^0,p_z^0),\mathscr{T}_5(p_y^0,p_z^0))\\ -8\rho_0^3+\mathcal{O}(\rho_0^4) & \tau\in(\mathscr{T}_5(p_y^0,p_z^0),\mathscr{T}_6(p_y^0,p_z^0)).\end{cases}$$

Analogously, for extremals corresponding to geodesics in the sets $\Gamma_{\pm g}$, we obtain

$$J\mathrm{Exp}|_{(p_x^0,p_z^0,\tau)}=\begin{cases}0 & \tau\in[0,\mathscr{T}_2(p_x^0,p_z^0))\\ 4\rho_0^3+\mathcal{O}(\rho_0^4) & \tau\in(\mathscr{T}_2(p_x^0,p_z^0),\mathscr{T}_3(p_x^0,p_z^0))\\ 8\rho_0^3+\mathcal{O}(\rho_0^4) & \tau\in(\mathscr{T}_3(p_x^0,p_z^0),\mathscr{T}_4(p_x^0,p_z^0))\\ 32C_2\rho_0^5 & \\ \quad-32\big(D_2p_x^0\mp E_2\big)\rho_0^6+\mathcal{O}(\rho_0^7) & \tau\in(\mathscr{T}_4(p_x^0,p_z^0),\mathscr{T}_5(p_x^0,p_z^0))\\ -8\rho_0^3+\mathcal{O}(\rho_0^4) & \tau\in(\mathscr{T}_5(p_x^0,p_z^0),\mathscr{T}_6(p_x^0,p_z^0)).\end{cases}$$

Definition 5 and the equations here above yield the following results.

Theorem 1 ([7]) *If $C_1<0$, then $\mathscr{T}_4$ is the (reparameterized) conjugate time for all extremals corresponding to geodesics in the sets $\Gamma_{\pm f}$ with $|p_x^0|=1$, $|p_y^0|\leq 1$ and $p_x^0\neq p_y^0$; if $C_1>0$ the conjugate time for these extremals coincides with $\mathscr{T}_5$.*

Analogously, the conjugate time for all extremals corresponding to geodesics in the sets $\Gamma_{\pm g}$ with $|p_y^0|=1$, $|p_x^0|\leq 1$ and $p_x^0\neq p_y^0$, coincides with $\mathscr{T}_4$ if $C_2<0$ and with $\mathscr{T}_5$ if $C_2>0$.

Theorem 2 *Assume that $C_1=0$ and $|E_1|\neq|D_1|$. If $E_1<-|D_1|$ (respectively, $E_1>|D_1|$), then the fourth (respectively, fifth) switching time is the conjugate time for every geodesic in the set Γ_f. If $|E_1|<|D_1|$, then the conjugate time of all geodesics of the kind Γ_f with $D_1p_y^0+E_1<0$ (respectively, $D_1p_y^0+E_1>0$) is their fourth (respectively, fifth) switching time.*

Remark 3 *If $C_1=0$ and $0<|E_1|<|D_1|$, to detect the conjugate times for the geodesic with initial covector $p_y^0=-\frac{E_1}{D_1}$, a higher order expansion of the Jacobian is needed, which, in turn, depends on higher order terms of x, y and z, and may require a higher order Taylor expansion of the vector fields f and g. As it is only one trajectory, and since we are interested in the cut points, we neglect this analysis.*

3.3 Suspension of the wavefronts

To characterize the Maxwell locus, we look for the self intersection of the front at some fixed time $\boldsymbol{T}$; in particular, as done in [7], we restrict the study to the suspension of the front, that is, the intersection of the set $\mathrm{Exp}(\cdot,\boldsymbol{T})$ with a plane with fixed vertical coordinate z (usually set to be equal to $4\zeta^2$, where ζ is some positive constant of the same order of magnitude of ρ_0). We stress that this can be done because the wavefronts are transversal to all planes with fixed z coordinate (as both vector fields f and g are transversal to such planes); therefore, the suspension of the wavefront is a planar curve; analyzing the self-intersections of a planar curve is much easier than analyzing the self-intersections of a surface.

For each fixed $\zeta>0$, the suspension of the Maxwell locus is thus described as the union of a finite number of curves of the form $(x_k(\zeta,s),y_k(\zeta,s))$, parameterized by some parameter s (typically coinciding with one component of the adjoint covector at time zero), taking values on some intervals I_k partitioning $[-1,1]$. The whole Maxwell locus can afterwards be recovered as the surface

$$\bigcup_k\{(x_k(\zeta,s),y_k(\zeta,s),4\zeta^2):\zeta>0,s\in I_k\}.$$

We can limit our attention to the study of the front of the geodesics in the set Γ_f, as the behavior of the others can be recovered applying suitable rotations of the coordinates and permutations of the parameters, as explained in Lemmas 4-5.

Let us fix a small positive parameter ζ and a time $\boldsymbol{T} = T_1\zeta + T_2\zeta^2 + T_3\zeta^3 + T_4\zeta^4 + \mathcal{O}(\zeta^5)$. In order to describe the intersection of

$$\{\mathrm{Exp}(\boldsymbol{\ell}, \boldsymbol{T}) : \boldsymbol{\ell} = (1, p_y^0, p_z^0, 0, 0, 0),\ |p_y^0| \leq 1,\ p_y^0 \geq \frac{1}{\zeta} - 1\}$$

with the plane $\{z = 4\zeta^2\}$, we must before compare, for each $\boldsymbol{p} = (1, p_y^0, p_z^0)$, the value of $\boldsymbol{T}$ with the switching times of the extremal emanating from $(\boldsymbol{p}, (0,0,0))$. Indeed, if, for instance, $\boldsymbol{T}$ is greater than the third switching time and less than the fourth one, then $\mathrm{Exp}(\boldsymbol{\ell}, \boldsymbol{T})$ is described by equations (B.1)-(B.2)-(B.3); if instead $\boldsymbol{T}$ is greater than the fourth switching time and less than the fifth one, we must use equations (B.4)-(B.5)-(B.6). As we are interested in the fourth and fifth bang fronts, T_1 is chosen to lie in the interval $[6, 10]$ (see Appendix B.2).

First of all, we focus on trajectories for which $\boldsymbol{T}$ is smaller than the fourth switching time, which implies that we restrict to $p_y^0 \in [-1, 7 - T_1]$. We call the set containing the value at $\boldsymbol{T}$ of all such geodesics the *fourth bang front*.

If we consider only the lowest order terms in equations (B.1)-(B.2)-(B.3), by simple computations we can see that the suspension of the fourth bang front on the plane $\{z = 4\zeta^2\}$ is given by the curve

$$\{(l\zeta, \big(-3l + 2\sqrt{2l^2 + 2lT_1 + 16} - T_1\big)\zeta) : l \in [T_1 - 8, 0]\},$$

up to higher order terms in ζ. However, for the purpose of detection of Maxwell points, we will need a more precise characterization of such front near the origin (in the affine plane $z = 4\zeta^2$), that is, for $T_1 \sim 8$, which correspond to geodesics with $p_y^0 \sim -1$; to analyze such curves, we thus set $p_y^0 = -1 + \sum_{k\geq 1} \gamma_k \rho_0^k$. By equation (14), the reparameterized time $\tau(\boldsymbol{T})$ along the geodesic with initial momentum $(1, p_y^0, 1/\rho_0)$ satisfies

$$\boldsymbol{T} = \rho_0\tau + \int_0^\tau \varrho_4(\tau)\rho_0^4 + \varrho_5(\tau)\rho_0^5\, d\tau + \mathcal{O}(\rho_0^6). \tag{16}$$

We write τ as the power series $\tau = \mathscr{T}_3 + \sum_{k\geq 0} \delta_k \rho_0^k$, $\mathscr{T}_3$ denoting the (reparameterized) third switching time of the considered geodesic; to find the coefficients δ_k, we develop ρ_0 in powers of ζ as follows

$$\rho_0 = \zeta + r_2\zeta^2 + r_3\zeta^3 + \cdots, \tag{17}$$

then we solve equation (16) at every order in ζ. This provides the expressions for all δ_k as functions of $T_2, T_3, \gamma_1, \gamma_2, \gamma_3, r_2, r_3, \ldots$.

We now substitute ρ_0 with (17) and $\hat{\tau}$ with $\sum_{k\geq 0} \delta_k \rho_0^k$ into equation (B.3) and we set $z(\tau(\boldsymbol{T})) = 4\zeta^2 + \mathcal{O}(\zeta^7)$. Solving this equation at every order in ζ, we obtain the expression of $r_k,\ k \geq 2$.

The suspension of the front is thus obtained by plugging (17) and $\hat{\tau} = \sum_{k\geq 0} \delta_k \rho_0^k$ into equations (B.1)-(B.2); we obtain

$$\begin{cases} x(\boldsymbol{T}) & = -\gamma_1\zeta^2 - \big(4C_2 + 4A + \gamma_2\big)\zeta^3 + \big((C_1 + C_2 + \frac{11}{2}A)\gamma_1 + \frac{T_2}{16}\gamma_1^2 \\ & \quad + \frac{1}{16}\gamma_1^3 - \gamma_3 + 4E_2 - \frac{8}{3}E_1 - \frac{4}{3}d_1 + \frac{4}{3}D_2\big)\zeta^4 + \mathcal{O}(\zeta^5) \\ y(\boldsymbol{T}) & = -(T_2 + \gamma_1)\zeta^2 - \big(T_3 + \frac{1}{6}(8C_2 - 16C_1 + 3(T_2\gamma_1 + \gamma_1^2 + 2\gamma_2))\big)\zeta^3 \\ & \quad + \big((-T_4 - \frac{1}{2}T_2\gamma_2 - \gamma_1\gamma_2 - \gamma_3 - \frac{A}{2}\gamma_1 - \frac{5}{3}(C_1 + C_2)\gamma_1 - 2T_2(A + C_2) \\ & \quad - \frac{1}{2}T_3\gamma_1 - \frac{3}{16}\gamma_1^2(T_2 + \gamma_1) + \frac{4}{3}(E_2 + D_2 - d_2)\big)\zeta^4 + \mathcal{O}(\zeta^5), \end{cases} \tag{18}$$

for $\gamma_1 \geq 0$. At the leading order in ζ, equation (18) describes a segment (parameterized by γ_1) of length $\mathcal{O}(\zeta^2)$ and of slope equal to $+1$.

We now consider the *fifth bang front* (of the geodesics of the set Γ_f), that is the set $\mathrm{Exp}(\boldsymbol{\ell}, \boldsymbol{T})$ for all $\boldsymbol{p} = (1, p_y^0, 1/\rho_0)$ with $|p_y^0| \leq 1$ such that $\mathbb{T}_4(p_y^0, 1/\rho_0) \leq \boldsymbol{T}$, $\mathbb{T}_4(p_y^0, 1/\rho_0)$ denoting the fourth switching time of the geodesic with initial momentum $(1, p_y^0, 1/\rho_0)$.

Analogously as above, we set $\hat{\tau} = \sum_{k\geq 0} \delta_k \rho_0^k$ and $\tau = \mathscr{T}_4 + \hat{\tau}$ (here $\tau = \mathscr{T}_4 + \sum_{k\geq 0} \delta_k \rho_0^k$, $\mathscr{T}_4$ denoting the reparametrization of $\mathbb{T}_4(p_y^0, 1/\rho_0)$) and, using equations (16) and (17), we can recover the expressions for δ_k as functions of the terms in the development of $\mathscr{T}_4$ and the coefficients $T_2, T_3, r_2, r_3, \ldots$. Afterwards, we compute $z(\tau(\boldsymbol{T}))$ (using equation (B.6)), where we substitute ρ_0 with its expansion (17), and we set $z(\tau(\boldsymbol{T})) = 4\zeta^2 + \mathcal{O}(\zeta^7)$, in order to get

the expression of r_k, $k \geq 2$. Finally, the suspension of the front is obtained by substituting the expansions for $\hat{\tau}$ and ρ_0 into equations (B.4)-(B.5), using the coefficients just computed. We obtain

$$\begin{cases} x(\boldsymbol{T}) &= (T_1-8)\zeta + T_2\zeta^2 + \Big(T_3 + \big(2(p_y^0)^2 + 2(T_1-8)p_y^0 - \frac{2}{3}\big)C_1 \\ &- \frac{8}{3}C_2 - 2(T_1-8)A\Big)\zeta^3 \\ &+ \Big(T_4 + \frac{4}{3}D_1(p_y^0)^3 + 2E_1(p_y^0)^2 + 2T_2C_1p_y^0 - 2AT_2 \\ &+ (T_1-8)(D_1(p_y^0)^2 + 2E_1p_y^0 - \frac{1}{3}c_1) - \frac{2}{3}(E_1+2d_1)\Big)\zeta^4 + \mathcal{O}(\zeta^5) \\ y(\boldsymbol{T}) &= 4\big(A - C_1p_y^0\big)\zeta^3 + \big(\frac{2}{3}c_1 - 2D_1(p_y^0)^2 - 4E_1p_y^0\big)\zeta^4 + \mathcal{O}(\zeta^5). \end{cases} \tag{19}$$

For fixed $\boldsymbol{T}$, equation (19) describes a parameterized curve of parameter p_y^0. As already observed in [7] (see also [16]), if $C_1 \neq 0$, at the leading order it describes an arc of parabola of length $\mathcal{O}(\zeta^3)$. If instead $C_1 = 0$, third and lower order terms of the development are constant with respect to p_y^0, and we must consider the fourth order terms. In particular, $y(\boldsymbol{T})$ is, up to some constant, a quadratic function of p_y^0, with derivative vanishing for $p_y^0 = -\frac{E_1}{D_1}$. Then, if $\left|\frac{E_1}{D_1}\right| \geq 1$, we have that $\frac{\partial y(\boldsymbol{T})}{\partial p_y^0} \neq 0$ for every $p_y^0 \in (-1,1)$, so that $x(\boldsymbol{T})$ can be written as a smooth function of $y(\boldsymbol{T})$. If instead $\left|\frac{E_1}{D_1}\right| < 1$, then $y(\boldsymbol{T})$ is not monotone on the interval $[-1,1]$. In particular, computing the first and second order derivatives of $x(\boldsymbol{T}), y(\boldsymbol{T})$ with respect to p_y^0, we deduce that the front has a cusp for $p_y^0 = -\frac{E_1}{D_1}$ (see [22]). We can then distinguish six main cases.

$\boldsymbol{A}_\pm$ These are the cases in which $|E_1| > |D_1|$ and $E_1 > 0$ (respectively, $E_1 < 0$). As remarked before, the front of the fifth arc is a smooth curve. In particular, $\frac{d^2x}{dy^2}$ has the same sign as E_1 for $p_y^0 \in [-1,1]$. An example of such a front (for $T_1 = 8$) is plotted in Figure 1.

$\boldsymbol{B}_\pm$ These are the cases in which $D_1 > |E_1|$ and $E_1 > 0$ (respectively, $E_1 < 0$). An example of such a front (for $T_1 = 8$) is plotted in Figure 2.

$\boldsymbol{C}_\pm$ These are the cases in which $D_1 < -|E_1|$ and $E_1 > 0$ (respectively, $E_1 < 0$). An example of such a front (for $T_1 = 8$) is plotted in Figure 3.

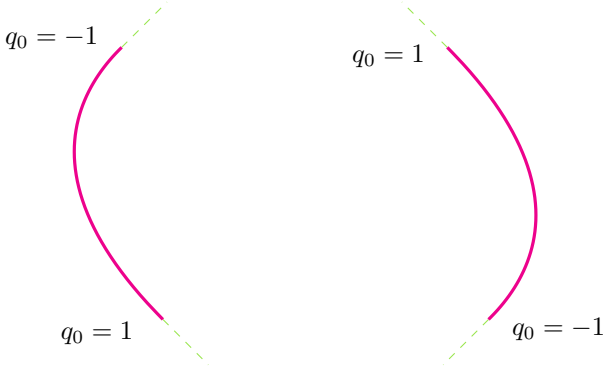

Figure 1: Fronts (fifth arc) of the kind A_+ (on the left) and A_- (on the right). In green: the tangents at $q_0 = 0, 1, -1$.

To recover the front of the trajectories of set Γ_{-f}, we apply a rotation of π around the axis z and the permutation of the invariants ♦ (see Appendix A). Notice that this permutation, that leaves A, C_1 and C_2 unchanged, sends D_1 into $-D_1$ and E_1 into $-E_1$. The suspension of the fourth front at time $\boldsymbol{T} = 8\zeta + \sum_{k\geq 2} T_k\zeta^k$ is thus

$$\begin{cases} x(\boldsymbol{T}) &= -\nu_1\zeta^2 + \big(4C_2 + 4A - \nu_2\big)\zeta^3 + \mathcal{O}(\zeta^4) \\ y(\boldsymbol{T}) &= (T_2 - \nu_1)\zeta^2 + \big(T_3 + \frac{1}{6}(8C_2 - 16C_1 \\ &\quad -3(T_2\nu_1 - \nu_1^2 + 2\nu_2))\big)\zeta^3 + \mathcal{O}(\zeta^4), \end{cases} \tag{20}$$

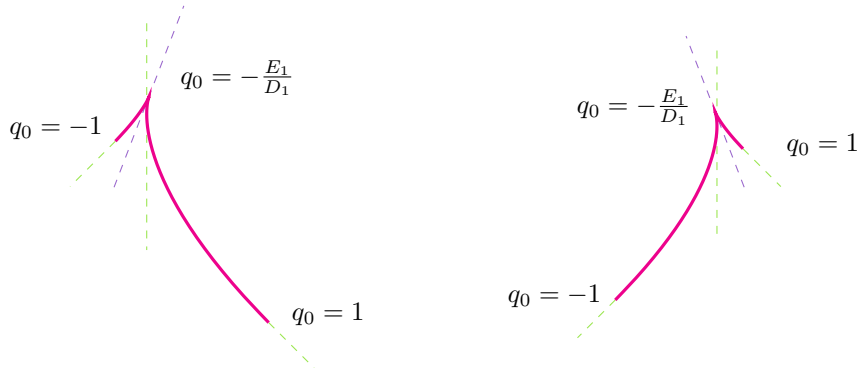

Figure 2: Fronts (fifth arc) of the kind B_+ (on the left) and B_- (on the right). In green: the tangents at $q_0 = 0, 1, -1$. In purple: the tangent at $q_0 = -\frac{E_1}{D_1}$ (the cusp).

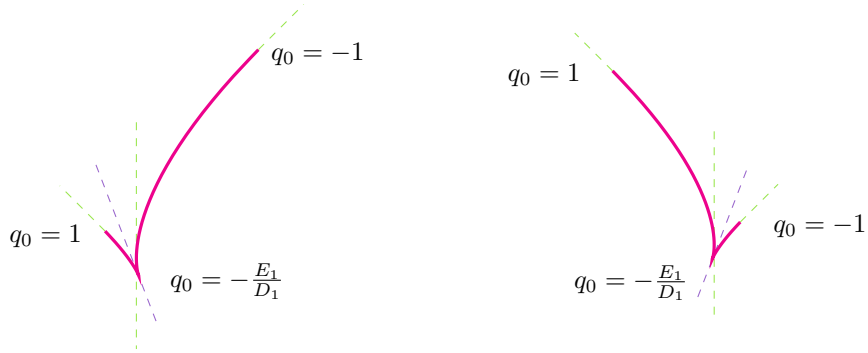

Figure 3: Fronts (fifth arc) of the kind C_+ (on the left) and C_- (on the right). In green: the tangents at $q_0 = 0, 1, -1$. In purple: the tangent at $q_0 = -\frac{E_1}{D_1}$ (the cusp).

for $\nu_1 \leq 0$. We recall that the initial adjoint vector associated to such trajectories is $(-1, p_y^0, 1/\rho_0)$, with $p_y^0 = 1 + \sum_{k\geq 2} \nu_k \rho_0^k$.

The suspension of the fifth front at time $\boldsymbol{T} = \sum_{k\geq 1} T_k \zeta^k$ is given by

$$\begin{cases} x(\boldsymbol{T}) &= -(T_1-8)\zeta - T_2\zeta^2 - \Big(T_3 + (2(p_y^0)^2 \\ &- 2(T_1-8)p_y^0 - \frac{2}{3})C_1 - \frac{8}{3}C_2 - 2(T_1-8)A\Big)\zeta^3 \\ &+ \Big(-T_4 - \frac{4}{3}D_1(p_y^0)^3 + 2E_1(p_y^0)^2 + 2T_2C_1p_y^0 + 2AT_2 \\ &+ (T_1-8)(D_1(p_y^0)^2 - 2E_1p_y^0 - \frac{2}{3}c_1) - \frac{2}{3}(E_1+d_1)\Big)\zeta^4 \\ &+ \mathcal{O}(\zeta^5) \\ y(\boldsymbol{T}) &= -4\big(A + C_1p_y^0\big)\zeta^3 + \big(\frac{2}{3}c_1 - 2D_1(p_y^0)^2 + 4E_1p_y^0\big)\zeta^4 + \mathcal{O}(\zeta^5), \end{cases} \tag{21}$$

parameterized by $p_y^0 \in [-1, 1]$.

The suspensions of the fronts of the geodesics of the sets $\Gamma_{\pm g}$ can be recovered from equations (18)-(19) too, by applying a suitable rotation around the vertical axis and the corresponding permutation of parameters. For the sake of completeness, we write them here below.

For a small fixed $\zeta > 0$, the intersection of the front $\mathcal{G}_4$ at time $\boldsymbol{T} = 8\zeta + \sum_{k\geq 2} T_k\zeta^k$ with the plane $z = 4\zeta^2$ is given by

$$\begin{cases} x(\boldsymbol{T}) &= (T_2 - \beta_1)\zeta^2 + \big(T_3 + \frac{1}{6}(8C_1 - 16C_2 \\ &\quad +3(-T_2\beta_1 + \beta_1^2 - 2\beta_2))\big)\zeta^3 + \mathcal{O}(\zeta^4) \\ y(\boldsymbol{T}) = &\ \beta_1\zeta^2 + (4A + \beta_2 - 4C_1)\zeta^3 + \mathcal{O}(\zeta^4), \end{cases} \tag{22}$$

where $p_y^0 = -1 + \sum_{k\geq 1} \beta_k \rho_0^k$. Analogously, the intersection of the front $\bar{\mathcal{G}}_4$ with the plane $z = 4\zeta^2$ is given by

$$\begin{cases} x(\boldsymbol{T}) & = -(T_2 + \eta_1)\zeta^2 - \big(T_3 + \frac{1}{6}(8C_1 - 16C_2 \\ & \quad +3(T_2\eta_1 + \eta_1^2 + 2\eta_2))\big)\zeta^3 + \mathcal{O}(\zeta^4) \\ y(\boldsymbol{T}) & = \eta_1\zeta^2 - (4A - \eta_2 - 4C_1)\zeta^3 + \mathcal{O}(\zeta^4), \end{cases} \tag{23}$$

with $p_y^0 = 1 + \sum_{k\geq 1} \eta_k \rho_0^k$.

Concerning the fifth bang front, if $\boldsymbol{T}$ is greater than the fourth switching time and less than the fifth one, we have

$$\begin{cases} x = 4(\pm A - g_0 C_2)\zeta^3 + \mathcal{O}(\zeta^4) \\ y = \pm(T_1 - 8)\zeta \pm T_2\zeta^2 \pm \big(T_3 - \frac{2}{3}C_2 \\ \quad +2C_2 g_0^2 + 2(T_1 - 8)(A \mp C_2 g_0) - \frac{8}{3}C_1\big)\zeta^3 + \mathcal{O}(\zeta^4), \end{cases} \tag{24}$$

where g_0 denotes the first component of the initial covector (i.e, $g_0 = p_x^0$).

Notation. In the following, we will use the following notations:

- $\mathcal{F}_4(\boldsymbol{T})$ (respectively, $\bar{\mathcal{F}}_4(\boldsymbol{T}), \mathcal{G}_4(\boldsymbol{T}), \bar{\mathcal{G}}_4(\boldsymbol{T})$)) denotes the fourth bang front at time $\boldsymbol{T}$ of the trajectories of the set Γ_f (respectively, $\Gamma_{-f}, \Gamma_g, \Gamma_{-g}$), that is, the set

$$\left\{ \boldsymbol{\xi}(\boldsymbol{T}) : \begin{array}{l} \boldsymbol{\xi} \in \Gamma_f \\ \mathbb{T}_3(\boldsymbol{\xi}) \leq \boldsymbol{T} \leq \mathbb{T}_4(\boldsymbol{\xi}) \end{array} \right\},$$

  where $\mathbb{T}_3(\boldsymbol{\xi})$ and $\mathbb{T}_4(\boldsymbol{\xi})$ denote the third and fourth switching times of the geodesics $\boldsymbol{\xi}$.
- $\mathcal{F}_5(\boldsymbol{T})$ (respectively, $\bar{\mathcal{F}}_5(\boldsymbol{T}), \mathcal{G}_5(\boldsymbol{T}), \bar{\mathcal{G}}_5(\boldsymbol{T})$)) denotes the fifth bang front at time $\boldsymbol{T}$ of the trajectories of the set Γ_f (respectively, $\Gamma_{-f}, \Gamma_g, \Gamma_{-g}$). The definition is analogous to the previous one.

To avoid heavy notations, in the following we are omitting the dependence on the time $\boldsymbol{T}$ from the symbols denoting the fronts.

4 Local structure of the cut locus for small spheres

In this section we provide the main result of the paper, that is, a description of the cut points of bang-bang geodesics with large $p_z(0)$; this result permit to characterize the upper part of small spheres.

In order to find the cut locus, we must compute and analyze the (first) Maxwell locus, that is, the set of points where the geodesics meet at the same time. In Section 4.1 we detail the computations of four examples of these intersections, thus providing a quite complete insight on the methods we use; in particular, for these cases, we obtain a set of existence conditions (on the values of the invariants of the normal form and on the adjoint covector associated with the involved geodesics at time 0). More details on all the interesting intersection (that is, those that give to first Maxwell points) can be found in Appendix D.

The classification of the possible cut loci (depending on the values of the invariants) is provided in Section 4.2, where we highlight the main features and the main peculiarities of the possible cases. A detailed analysis is given in Appendix C.

4.1 Computation of the first Maxwell points along bang-bang geodesics

In general terms, the method we use to detect Maxwell points consists in parameterizing two families of geodesics by the value of their initial adjoint covectors, and impose that they meet at the same time, by equating the jets at each order. This provides a set of constraints for the values of the initial adjoint covectors and on the intersection time, producing a set of existence conditions for the intersection, in terms of the values of the main invariants.

More specifically, the exact steps of such procedure depend on the pair of geodesics under concern and on the relative position of their fourth switching times with respect to the intersection time. For this reason, here below we detail four examples, that represent quite completely the cases we may encounter and the procedure to study them.

Intersection between the fronts $\mathcal{F}_4$ and $\mathcal{G}_4$ The aim of this section is to compute (if it takes place) the intersection, *occurring at the same real time* $\boldsymbol{T}$, between a geodesic of the set Γ_f and a geodesic of the set Γ_g, assuming that both of them have already passed their third switching time, but they have not passed their fourth one yet.

These intersections (together with their counterparts $\mathcal{G}_4 \cap \bar{\mathcal{F}}_4$, $\bar{\mathcal{F}}_4 \cap \bar{\mathcal{G}}_4$ and $\bar{\mathcal{G}}_4 \cap \mathcal{F}_4$) are the source of the loss of optimality of the geodesics in the Heisenberg system (except for those losing optimality at $\boldsymbol{T} = 8/p_z^0$). Their suspensions at the plane $\{z = 4\zeta^2\}$ are, up to higher order terms in ζ, segments of length $\sim 2\zeta$. This is a remarkable property, as the suspensions of all other intersections are "shorter" (that is, curves of length at most $\mathcal{O}(\zeta^3)$), as we will see here below.

Let us fix $\rho_0 > 0$ small enough, $\gamma \in [-1, 1)$ and a time $\boldsymbol{T} > 0$. Let $\boldsymbol{\xi}_f$ be the geodesic associated with the extremal $(\boldsymbol{\mu}_f, \boldsymbol{\xi}_f)$ such that $\boldsymbol{\mu}_f(0) = (1, \gamma, 1/\rho_0)$, and let $\boldsymbol{\xi}_g$ be the geodesic associated with the extremal $(\boldsymbol{\mu}_g, \boldsymbol{\xi}_g)$ such that $\boldsymbol{\mu}_g(0) = (\beta, 1, 1/\widehat{\rho}_0)$; we assume moreover that $\boldsymbol{\xi}_f$ belongs to Γ_f and $\boldsymbol{\xi}_g$ to Γ_g. For the intersection between these curves to exist, $\widehat{\rho}_0$ must be close to ρ_0; to guarantee this, we write $\widehat{\rho}_0 = \rho_0 + \sum_{k\geq 2} \alpha_k \rho_0^k$, where the α_k will be determined later. Inspired from the nilpotent case, we are also expecting that the two geodesics intersect only if β is close to 1; we then set $\beta = 1 + \sum_{k\geq 1} \beta_k \rho_0^k$. As the expressions for the trajectories (Appendix B.1) are given in terms of the reparameterized times, we must also ensure that the reparameterized times along the two geodesics correspond to the same (real) time $\boldsymbol{T}$; to do so, we define

$$\mathcal{T} = \mathscr{T}_3 + \delta_0 + \delta_1\rho_0 + \delta_2\rho_0^2 + \cdots \quad \text{and} \quad \widehat{\mathcal{T}} = \widehat{\mathscr{T}_3} + \widehat{\delta}_0 + \widehat{\delta}_1\rho_0 + \widehat{\delta}_2\rho_0^2 + \cdots, \tag{25}$$

$\mathscr{T}_3$ and $\widehat{\mathscr{T}_3}$ being the third switching times of $\boldsymbol{\xi}_f$ and $\boldsymbol{\xi}_g$ respectively, and we impose that

$$\boldsymbol{T} = \int_0^{\mathcal{T}} \varrho_f(s)ds = \int_0^{\widehat{\mathcal{T}}} \widehat{\varrho}_g(s)ds. \tag{26}$$

Keeping in mind that, in the nilpotent case, such intersections occur at the fourth switching time (of the geodesics in Γ_f), we can already set $\delta_0 = 2$. Then, plugging the expansion of $\widehat{\rho}_0$ in powers of ρ_0 and equations (25) into equation (26), imposing the equality for each power of ρ_0, we obtain the expression of $\widehat{\delta}_k$ in terms of the coefficients δ_k and α_k, for $k \geq 1$.

Using equations (B.1)-(B.2)-(B.3), we compute the jets of $\boldsymbol{\xi}_f(t(\mathcal{T}))$ and $\boldsymbol{\xi}_g(t(\widehat{\mathcal{T}}))$ and we impose the equality $\boldsymbol{\xi}_f(t(\mathcal{T})) = \boldsymbol{\xi}_g(t(\widehat{\mathcal{T}}))$, up to the fourth order in ρ_0 for the coordinates x, y and to the fifth one for the coordinate z. Thanks to this, we recover the values for the coefficients $\alpha_k, \beta_k, \delta_k$, $k \leq 3$, as functions of the invariants and of γ. In particular, we obtain

$$\beta = 1 + 2(1-\gamma)C_1\rho_0^2 + 2(1-\gamma)\big(E_1 + \frac{\gamma+2}{3}D_1\big)\rho_0^3 + \mathcal{O}(\rho_0^4). \tag{27}$$

As β must be contained in the interval $[-1, 1]$, this intersection occurs only if $C_1 \leq 0$ and, when $C_1 = 0$, if, in addition,

$$E_1 + \frac{\gamma+2}{3}D_1 \leq 0. \tag{28}$$

We obtain also

$$\mathscr{T}_4 - \mathcal{T} = 2(\gamma-1)C_1\rho_0^2 + 2(\gamma-1)\big(E_1 + \frac{1+2\gamma}{3}D_1)\rho_0^3;$$

then, this intersection takes place only if $C_1 \leq 0$ and, when $C_1 = 0$, if moreover

$$E_1 + \frac{1+2\gamma}{3}D_1 \leq 0. \tag{29}$$

Conditions (28)-(29) are the necessary existence conditions of this intersection, in the non-generic case considered in this paper.

In order to portray this intersection, we compute its suspension on the plane $\{z = 4\zeta^2\}$, for some $\zeta = \rho_0 + \mathcal{O}(\rho_0^2)$; to do so, we set $\rho_0 = \zeta + \sum_{k\geq 2} r_k\zeta^k$ and we find those r_k that guarantee $z_f(t(\mathcal{T})) = 4\zeta^2 + \mathcal{O}(\zeta^6)$. Then, we plug the expansion for ρ_0 into the expressions of $x_f(t(\mathcal{T}))$ and $y_f(t(\mathcal{T}))$. If $C_1 = 0$, we obtain the parameterized curve

$$\begin{cases} x = -(1+\gamma)\zeta + \big((1+12\gamma-5\gamma^2)\frac{A}{4} + (\gamma-3)C_2\big)\zeta^3 + \mathcal{O}(\zeta^4) \\ y = 4A\zeta^3 - \frac{2}{3}\big(D_1\gamma^2 + (3E_1+D_1)(1+\gamma) - \mathscr{e}_1\big)\zeta^4 + \mathcal{O}(\zeta^5). \end{cases} \qquad \gamma \in [-1, 1) \tag{30}$$

Up to fourth order terms in ζ, it is a horizontal segment of length $\sim 2\zeta$.

From these computations, we can also deduce the existence condition, the value of the intersection time and the expression of the suspension for other similar intersections, that is, $\bar{\mathcal{G}}_4 \cap \mathcal{F}_4$, $\bar{\mathcal{F}}_4 \cap \bar{\mathcal{G}}_4$ and $\mathcal{G}_4 \cap \bar{\mathcal{F}}_4$: it it suffices rotate the suspension (30) of a suitable angle and to apply the corresponding permutation of the invariants, according to Lemmas 4-5.

Intersection between the fronts $\mathcal{G}_4$ and $\bar{\mathcal{G}}_4$ In the nilpotent case, the intersection between geodesics with opposite initial velocity occur only close to the vertical axis, at times $\boldsymbol{T} \sim 8/p_z(0)$. If we are considering only fourth bang fronts, then only few geodesics are involved, as $\mathbb{T}_4 = (7 \pm q_0)/p_z(0) + \mathcal{O}(1/p_z(0)^2)$, where $q_0 \in [-1, 1]$ is one component of the momentum at time 0; in the case of the sets Γ_g and Γ_{-g}, it concerns the geodesics with $p_x^0 \sim 1$ and $p_x^0 \sim -1$, respectively.

Thus, to study such intersections, we consider a geodesic of the set Γ_g, associated with the adjoint vector $\boldsymbol{\mu}_g$ such that $\boldsymbol{\mu}_g(0) = (\beta, 1, 1/\rho_0)$, and geodesic in the set Γ_{-g} associated with an adjoint vector $\boldsymbol{\mu}_{-g}$ such that $\boldsymbol{\mu}_{-g}(0) = (\eta, -1, 1/\widetilde{\rho}_0)$, where $\eta = \sum_{k\geq 0} \eta_k \rho_0^k$, $\widetilde{\rho}_0 = \rho_0 + \mathcal{O}(\rho_0^2)$ and $\beta = \sum_{k\geq 0} \beta_k \rho_0^k$; since we are close to the vertical axis, we also set $\boldsymbol{T} = 8\rho_0 + \mathcal{O}(\rho_0^2)$. Equating the jets of the two geodesics, we find the following constraints

$$\eta_0 = -1 \quad \beta_0 = 1$$
$$\eta_1 = \beta_1 = 0$$
$$\eta_2 - \beta_2 = 8(A - C_1)$$

that implies that, under the hypothesis that $C_1 = 0$, these intersections occur only for $A \geq 0$.

The suspension of the intersection at the plane $\{z = 4\zeta^2\}$ is given by the parameterized curve

$$\begin{cases} x = (4A + \eta_2)\zeta^3 + \mathcal{O}(\zeta^4) \\ y = -(4A + \eta_2)\zeta^3 + \mathcal{O}(\zeta^4), \end{cases} \qquad \eta_2 \in [0, 8A]. \tag{31}$$

Intersection between the fronts $\bar{\mathcal{F}}_5$ and $\mathcal{G}_5$ The analysis of such intersection is straightforward in the generic case $C_1 C_2 \neq 0$, as both fronts have length $\mathcal{O}(\zeta^3)$ (see for instance [16]). However, when $C_1 = 0$, the front $\bar{\mathcal{F}}_5$ has length $\mathcal{O}(\zeta^4)$, and the analysis is more delicate.

Let us consider the expressions of the two fronts (equations (21) and (24), respectively) at some time $\boldsymbol{T} = T_1\zeta + T_2\zeta^2 + T_3\zeta^3 + T_4\zeta^4 + \mathcal{O}(\zeta^5)$. First of all, we recall that it makes sense to consider such intersections only when $C_2 > 0$ and $D_1 p_y^0 - E_1 > 0$ (otherwise, the considered geodesics are not optimal). By naively imposing the equality of the jets of both coordinates, up to the fourth order in ζ, we obtain the constraints

$$T_1 = 8, \qquad T_2 = 0, \qquad T_3 = -4A - \frac{4}{3}C_2, \qquad g_0 = -1$$

and the two pairs of solutions

$$p_y^0 = 1, \qquad T_4 = 4(E_1 - E_2) - \frac{4}{3}(D_1 + D_2)$$
$$p_y^0 = -\frac{1}{2} + \frac{3E_1}{2D_1}, \qquad T_4 = \frac{3}{2D_1}\Big(E_1 + \frac{D_1}{3}\Big)^2 - 4\Big(E_2 + \frac{D_2}{3}\Big).$$

Since there are only two (pairs of) solutions, it seems that the fronts intersect only in two points (that is, only two pairs of geodesics intersect); this conclusion is not satisfactory as, when studying the cut locus in some particular cases (as, for instance, in the case $\boldsymbol{A}_-$ with $C_2 > 0$), it would imply that the geodesics of the set Γ_{-f} have no Maxwell points before the conjugate time.

A finer analysis is thus in order: to do so, we set $\boldsymbol{T} = 8\zeta - \big(4A + \frac{4}{3}C_2\big)\zeta^3 + T_r(p_y^0, \zeta)$, where T_r is some continuous function, to be determined. The system (21)=(24) becomes

$$\begin{cases} 4C_2(1 + g_0) - T_r(p_y^0, \zeta) + \\ \quad + \big(-\frac{4}{3}D_1(p_y^0)^3 + 2E_1(p_y^0)^2 + 2E_1 - 2D_2 g_0^2 + 4E_2 g_0 + \frac{2}{3}D_2\big)\zeta = o(\zeta) \\ 2C_2(1 - g_0^2) - T_r(p_y^0, \zeta) + \\ \quad + \big(\frac{4}{3}D_2 g_0^3 - 2E_2 g_0^2 - 2E_2 - 2D_1(p_y^0)^2 + 4E_1 p_y^0 + \frac{2}{3}D_1\big)\zeta = o(\zeta) \end{cases}$$

where the right-hand sides of the equations here above depend on g_0, p_y^0 and T_r. Summing the two equations and factorizing the result, we obtain

$$\begin{aligned}\eta(p_y^0,\zeta)^2\big(3C_2+(3D_2+3E_2+2D_2\eta(p_y^0,\zeta))\zeta\big)+\\ +(1-p_y^0)^2\big(-2D_1p_y^0+3E_1-D_1\big)\zeta=R(\eta,T_r,p_y^0,\zeta),\end{aligned}\tag{32}$$

where we set $g_0=-1+\eta(p_y^0,\zeta)$ and R is some function such that $R\big(0,\mathbb{T}_4-8\zeta+\big(4A+\frac{4}{3}C_2\big)\zeta^3,1,\zeta\big)=0\ \forall\zeta$ (here $\mathbb{T}_4$ denotes the fourth switching time of the Γ_g geodesics). Moreover, R goes to zero faster than ζ as ζ approaches zero, uniformly with respect to the other variables on compact sets. Let us, for now, neglect the term R in (32), and let us solve the equation

$$\eta^2\big(3C_2+(3E_2+3D_2+2D_2\eta)\zeta\big)+(1-p_y^0)^2\big(-2D_1p_y^0+3E_1-D_1\big)\zeta=0\tag{33}$$

with respect to the unknown η. For $p_y^0=1$, the equation (33) has the double root $\{\eta=0\}$ and the simple one $\{\eta=-\frac{3}{2}-\frac{3E_2}{2D_2}-\frac{3C_2}{2D_2}\frac{1}{\zeta}\}$, where the latter does not provide an admissible value for the adjoint vector, if ζ is small enough. Since $(-2D_1p_y^0-D_1+3E_1)<0$ for all relevant p_y^0, we can see that, for $p_y^0\neq1$, the double root of (33) splits into two distinct roots, one strictly smaller and one strictly greater than 0, continuously depending on p_y^0; if ζ is small enough, then these two roots will stay close to 0 and, in particular, the latter is always non-negative.

The same argument holds for equation (32). Indeed, R is null for $g_0=-1$, $p_y^0=1$ and $\boldsymbol{T}$ equal to the switching time, and goes to zero faster than ζ; then, for every $p_y^0\in[-1,1)$ there exists $\bar\zeta$ such that

$$(1-p_y^0)^2(-2D_1p_y^0+3E_1-D_1)\zeta-R(\eta,T,p_y^0,\zeta)>0$$

for $\zeta<\bar\zeta$, $|\eta|<1/2$ and T close enough to the switching time. Then the graph of the function defined in the right-hand side of (32) is close to the one of the function defined in the right-hand side of (33); for ζ small enough, we can write the root (which gives an admissible value for g_0) of equation (32) as

$$\eta(p_y^0,\zeta)=\sqrt{\frac{-3E_1+2p_y^0D_1+D_1}{3C_2}}(1-p_y^0)\sqrt{\zeta}+\mathcal{O}(\zeta).\tag{34}$$

We also obtain $T_r(p_y^0,\zeta)=-4C_2\eta(p_y^0,\zeta)$.

We will see in the following that the intersection between these two fronts participate to the cut locus in three cases: when $E_1<-|D_1|$, when $D_1>E_1>0$ and $\frac{3E_1}{D_1}<1$ and when $D_1>-E_1>0$ and $\frac{3E_1}{D_1}<-1$. In the first and third cases, $(-2D_1p_y^0-D_1+3E_1)<0$ for all $p_y^0\in[-1,1]$. In the second one, this is true (and, therefore, the intersection occurs) only for $p_y^0>\frac{3E_1}{2D_1}-\frac{1}{2}>-1$.

The suspension of the intersection between the fronts $\mathcal{G}_5$ and $\bar{\mathcal{F}}_5$ is thus obtained by substituting the values of $\boldsymbol{T}$ into equation (21), and is described by the parameterized curve

$$\begin{cases}x(p_y^0) &= 4(A+C_2)\zeta^3+4\sqrt{\frac{(D_1+2p_y^0D_1-3E_1)C_2}{3}}(1-p_y^0)\zeta^{7/2}+\mathcal{O}(\zeta^4)\\ y(p_y^0) &= -4A\zeta^3+\mathcal{O}(\zeta^4),\end{cases},$$

with $p_y^0\in[-1,1]\cap\big(\frac{3E_1}{2D_1}-\frac{1}{2},1\big]$.

Remark 4 *The usual procedure of developing the component p_x^0 of the covector of the trajectory of the set Γ_g in powers of ζ (or ρ_0, which has the same order of magnitude) in this case does not work. Indeed, as equation* (34) *shows, p_x^0 should be rather developed in powers of $\sqrt{\zeta}$.*

Self-intersections of the front of geodesics of the set Γ_f In the cases $\boldsymbol{B}_\pm$ and $\boldsymbol{C}_\pm$, corresponding to the fact that the invariant D_1 is larger, in absolute value, than the invariant E_1, a peculiar phenomenon arises: the self-intersections between the fourth and the fifth bang fronts of bang-bang geodesics with the same initial control (that is, both belonging to the set Γ_f or Γ_{-f}); this does not occur when $C_1C_2\neq0$. Here below, we explain in details the case B_+, that is, $0<E_1<D_1$, which is illustrated in Figures 4-5; the other cases can be

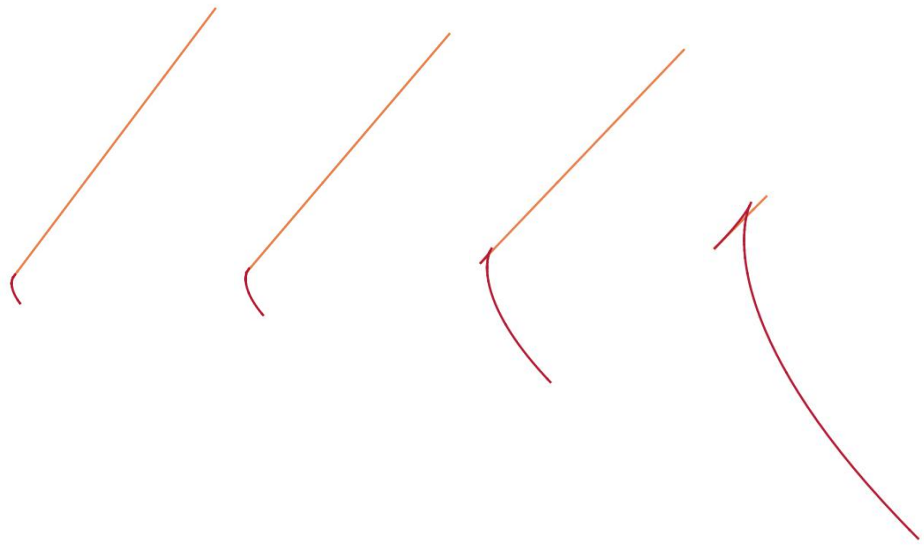

Figure 4: Suspension of the front of geodesics of the set Γ_f, for $D_1 > E_1 > 0$. In orange, the fourth bang arc ($\mathcal{F}_4$); in red, the fifth bang arc ($\mathcal{F}_5$). From left to right: $T = 7.5\zeta$, $T = 7.7\zeta$, $T = 7.9\zeta$ and $T = 7.99\zeta$. This picture (and the following ones) is illustrating the phenomena only qualitatively, as proportions between the length of the arcs are not fully respected.

easily derived by applying the suitable symmetries and the corresponding permutation of the invariants.

As previously, we fix $\rho_0 > 0$ and we consider two geodesics $\boldsymbol{\xi}_f$ and $\widetilde{\boldsymbol{\xi}}_f$ of the set Γ_f, associated respectively with the adjoint covectors $\boldsymbol{\mu}, \widetilde{\boldsymbol{\mu}}$, where $\boldsymbol{\mu}(0) = (1, \gamma, 1/\rho_0)$ and $\widetilde{\boldsymbol{\mu}}(0) = (1, \eta, 1/\widetilde{\rho}_0)$, and we set $\widetilde{\rho}_0 = \rho_0 + \sum_{k\geq 2} \alpha_k \rho_0^k$ and $\gamma = \gamma_0 + \sum_{k\geq 1} \gamma_k \rho_0^k$.

We want to evaluate both $\boldsymbol{\xi}_f$ and $\widetilde{\boldsymbol{\xi}}_f$ near the fourth switching time of $\boldsymbol{\xi}_f$, that is, at some time $\boldsymbol{T} = (7 - \gamma_0)\rho_0 + \sum_{k\geq 2} T_k \rho_0^k$. First of all, we notice that, whenever $\gamma_0 < \eta$, then we can choose the terms $T_k, k \geq 2$, in such a way that $\boldsymbol{T}$ is smaller than the fourth switching time of $\boldsymbol{\xi}_f$ and greater than the fourth switching time of $\widetilde{\boldsymbol{\xi}}_f$; then, we assume that $\gamma_0 \leq \eta$.

We now solve the equation $\boldsymbol{\xi}_f(\boldsymbol{T}) = \widetilde{\boldsymbol{\xi}}_f(\boldsymbol{T})$ by equating the jets at each order. We find that γ_0 and η must satisfy one of these equations:

$$\begin{aligned} \gamma_0 &= \eta \\ \gamma_0 + 2\eta &= -3\frac{E_1}{D_1} \end{aligned} \tag{35}$$

If $\gamma_0 = \eta$, carrying out the computations we find also $\alpha_k = 0\ \forall k \leq 3$ and that $\boldsymbol{T}$ is equal (up to the third order in ρ_0) to the fourth switching time of both trajectories (higher order are not inspected): indeed, in this case $\boldsymbol{\xi}_f$ and $\widetilde{\boldsymbol{\xi}}_f$ are the same trajectory, and we are evaluating it at the switching time between the fourth and the fifth arc. If instead $\gamma_0 + 2\eta = -3\frac{E_1}{D_1}$, combining the equality with the constraints $\eta, \gamma_0 \in [-1, 1]$ and $\gamma_0 \leq \eta$, we obtain that this

intersection may occur for $\gamma_0 \in [-1, -\frac{E_1}{D_1}]$ and $\eta \in [-\frac{E_1}{D_1}, \frac{1}{2} - \frac{3E_1}{2D_1}]$; in this case, we find

$$\boldsymbol{T} = (7-\gamma_0)\rho_0 - \gamma_1\rho_0^2 + \Big(\frac{20}{3}C_2 - 8A\gamma_0\Big)\rho_0^3 + \mathcal{O}(\rho_0^4) \tag{36}$$
$$\widetilde{\rho}_0 = \rho_0 - \frac{9}{4}A\Big(\gamma_0 + \frac{E_1}{D_1}\Big)\rho_0^3 + \mathcal{O}(\rho_0^4).$$

The suspension at $z = 4\zeta^2$ of this intersection is the parameterized curve

$$\begin{cases} x = -(1+\gamma_0)\zeta - \gamma_1\zeta^2 + \big((\gamma_0 - 3)C_2 + (1 + 12\gamma_0 - 5\gamma_0^2)\frac{A}{4} - \gamma_2\big)\zeta^3 + \mathcal{O}(\zeta^4) \\ y = 4A\zeta^3 + \mathcal{O}(\zeta^4), \end{cases}$$

with $\gamma_0 \in \Big[-1, -\frac{E_1}{D_1}\Big]$. Its graph is a horizontal segment of length $\Big(1 - \frac{E_1}{D_1}\Big)\zeta$, up to higher orders in ζ (see Figure 5).

We conclude by noticing that, in the case $\boldsymbol{B}_+$, there is no intersection between the fourth and the fifth front of the geodesics of the set Γ_{-f}, as can be seen in Figure 5.

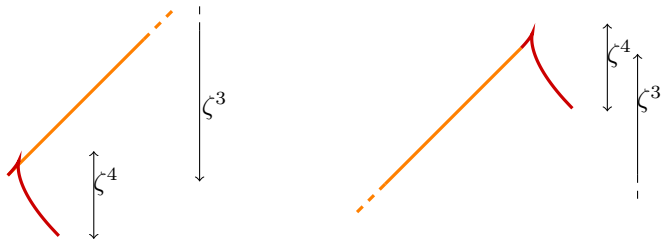

Figure 5: On the left (right): self intersection (suspension) of the front of trajectories of the set Γ_f (Γ_{-f}). Orange: front of the fourth bang arc; red: front of the fifth bang arc.

4.2 Main results

Assume that we have found all Maxwell points along a certain geodesic (or, at least, all those that occur at times smaller than the conjugate time): we must now identify which Maxwell point occurs before (that is, at smaller times than) the other ones; this one is, indeed, the cut point of the considered geodesic.

In order to determine which intersection occurs before the others, either we explicitly compute the intersection times or we rely on some geometric considerations, as explained in the example here below.

Example 1 *In Figure 6, we plot the suspensions of fronts at different times (the closer the curve to the origin, the larger the time); the arrows show the directions in which suspensions are evolving as time increases.*

For instance, in the figure on the left (that illustrates the case in which $E_1 < -|D_1|$, $C_2 < 0$ and $A > 0$), we see that all trajectories of the set Γ_f are going to intersect either the front $\mathcal{G}_4$ or the front $\bar{\mathcal{G}}_4$ before possibly intersecting some geodesics of the set Γ_{-f}; this last kind of intersection can then be neglected, as it involves geodesics of the set Γ_f that have already met other geodesics, and therefore have already lost their optimality.

The figure on the right shows the case in which $E_1 < -|D_1|$, $C_2 < 0$ and $A < 0$.

Based on this analysis, we describe the possible shapes of the cut locus for bang-bang extremal with large $p_z(0)$, so that we can figure out the upper part of small spheres. This classification depends on the relative values of the invariants $A, C_1, C_2, E_1, E_2, D_1, D_2$. Under Assumption 2, we distinguish 60 different cases, that can be reduced to 30, thanks to the symmetry properties of the normal form: indeed, the cases $\boldsymbol{A}_+$, $\boldsymbol{C}_+$ and $\boldsymbol{C}_-$ can be deduced from the cases $\boldsymbol{A}_-$, $\boldsymbol{B}_-$ and $\boldsymbol{B}_+$, respectively, just exchanging the behaviors of the part of the front made of trajectories of the class Γ_f with the one made of trajectories of the class Γ_{-f}; at this order of jets, this corresponds to a rotation of an angle π with respect to the vertical

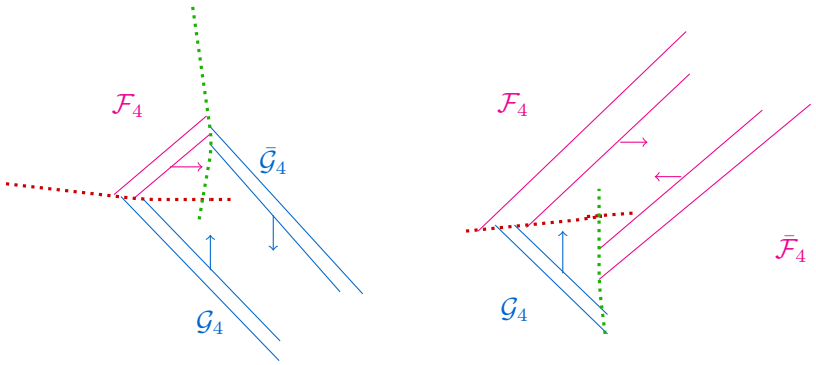

Figure 6: Example of intersection of the suspensions of fronts. The arrows denote the direction in which the suspensions move as time increases.

axis (together with the suitable permutation of invariants). Thus, in this paper, we analyze the following three cases: $E_1 < -|D_1|$ (case $\boldsymbol{A}_-$), $D_1 > E_1 > 0$ (case $\boldsymbol{B}_+$) and $-D_1 < E_1 < 0$ (case $\boldsymbol{B}_-$).

In order to highlight the difference with the generic case, we are recalling, in Figure 7, the possible forms of the cut locus and its suspension for geodesic with large $p_z(0)$ (see [7, 16] for more details).

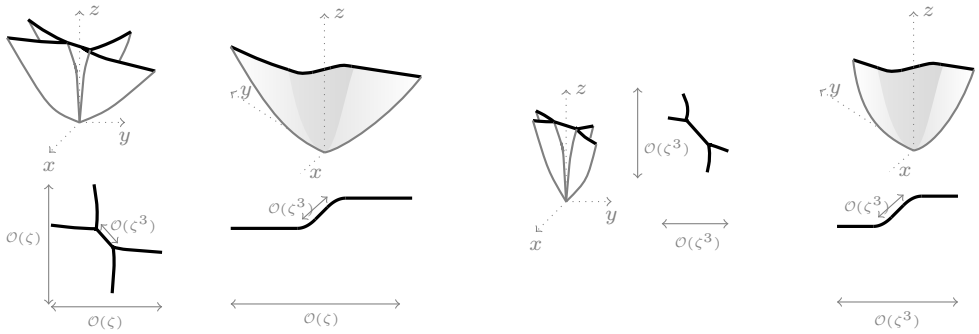

Figure 7: The possible structures of the cut locus in the generic case and, below, the corresponding suspension. The leftest picture shows the cut locus in the case in which both C_1 and C_2 are negative; the second, from the left, shows the case in which one invariant is positive and one negative; the two on the right show the possible shapes of the cut locus when both invariants C_1 and C_2 are positive.

In general, between the generic case and the non-generic one, we remark two major differences:

- the generic case presents a symmetry between the geodesics of the set Γ_f with those of the set Γ_{-f}, and the geodesics of the set Γ_g with those of the set Γ_{-g}, which results in cut symmetric cut loci (at least, up to the orders considered in the expansion in ρ_0). In the non-generic case, there is no more symmetry between the geodesics of the sets $\Gamma_{\pm f}$; this breaks the symmetry of the cut locus;
- in the generic case, when both the invariants C_1 and C_2 are positive, the intersections of the kind $\mathcal{F}_4 \cap \mathcal{G}_4$ (and their analogous) do not occur, which implies that the cut times are all of the order of $8\rho_0$ and that the suspension of the cut locus at the plane $\{z = 4\zeta^2\}$ is contained in some neighborhood of radius $\mathcal{O}(\zeta^3)$ of the origin; on the contrary, when at least one between C_1 and C_2 is negative, then the suspension of the cut locus possesses branches of length $\mathcal{O}(\zeta)$, and there are geodesics losing global optimality close to their fourth switching time. In the non-generic case, there are always geodesics whose conjugate

time coincides with the fourth switching time: this implies that the suspension of cut locus always has branches of length $\mathcal{O}(\zeta)$, and the cut time of the involved geodesics is smaller than $8\rho_0$.

More details about the computations and a careful description of the cut points are given in Appendix C. In this section, we are instead portraying the suspension of the cut locus for all 30 cases, giving a qualitative description of their "shape" and emphasizing their peculiarities.

4.2.1 Case A_-

This is the case presenting less differences with the generic one; this is mostly due to the fact that the location of the first conjugate time (that is, the fact that it coincides with the fourth or the fifth switching time) of the geodesics of the classes $\Gamma_{\pm f}$ is completely determined by the value of the invariant E_1, regardless of the value of the adjoint covector. For instance, at a first sight, the suspension of the cut locus when $C_2 < 0$ may seem a sort of "hybrid" between the two structures shown at the left of Figure 7 (possibly up to rotations).

However, some major differences appear. As pointed out above, there is no more symmetry between the geodesics of the class Γ_f and those of the class Γ_{-f}, as the first ones lose their local optimality at the fourth switching time, while the latter are locally optimal up to the fifth switching time. This results in asymmetric cut loci.

Another important feature is given by the fact that even suspensions of the cut locus made by one branch can be non-smooth: this happens when pieces of the intersections $\bar{\mathcal{F}}_5 \cap \bar{\mathcal{G}}_5$ or $\bar{\mathcal{F}}_5 \cap \mathcal{G}_5$ belong to be cut locus.

Summing up, in the case $\boldsymbol{A}_-$, the suspensions of the cut locus can be made by three C^1 branches, when $C_2 < 0$, or by one piecewise-C^1 branch (when $C_2 > 0$). The suspensions are portrayed in Figures 8-9, while an illustration of the corresponding cut loci is given in Figure 10.

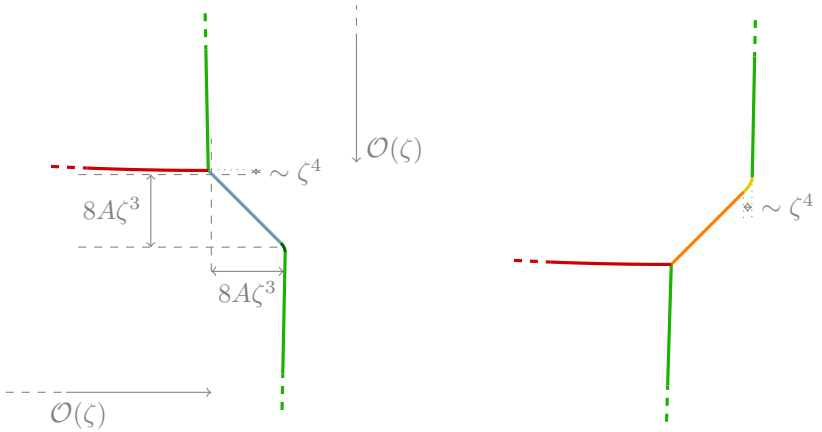

Figure 8: Suspension of the cut locus for the case A_- with $C_2 < 0$. On the left, $A > 0$, on the right, $A < 0$. The wavefront intersections participating to the cut locus are highlighted in different colors: in red, we plot (the part of) the intersection $\mathcal{F}_4 \cap \mathcal{G}_4$ (that belongs to the cut locus); in green, the intersections $\bar{\mathcal{G}}_4 \cap \mathcal{F}_4$ and $\mathcal{G}_4 \cap \bar{\mathcal{F}}_4$; in sugarpaper, $\mathcal{G}_4 \cap \bar{\mathcal{G}}_4$; in dark green, $\mathcal{G}_4 \cap \bar{\mathcal{F}}_5$; in orange, $\mathcal{F}_4 \cap \bar{\mathcal{F}}_4$; finally, in yellow $\mathcal{F}_4 \cap \bar{\mathcal{F}}_5$.

4.2.2 Case B_+

Differently from the previous case, this one is very rich and presents ten different subcases. Indeed, as D_1 is greater than E_1, the quantity $D_1 p_y^0 \pm E_1$, which determines the location of the conjugate times of the geodesics of the classes $\Gamma_{\pm f}$, respectively, changes sign for $p_y^0 \in [-1, 1]$. Moreover, the existence conditions for the intersections $\bar{\mathcal{F}}_4 \cap \bar{\mathcal{G}}_4$ (given in equation (D.1)) is not satisfied for some values of p_y^0, if D_1 is larger than $3E_1$. Thus, the six sub-cases we

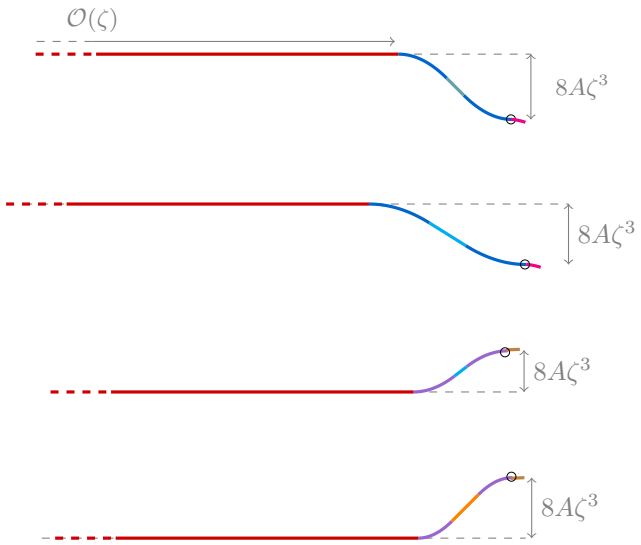

Figure 9: Suspension of the cut locus for the case A_-, respectively, from top to bottom, in the subcases $A > C_2$, $C_2 > A > 0$, $0 > A > -C_2$ and $0 > -C_2 > A$. Red: $\mathcal{F}_4 \cap \mathcal{G}_4$; blue: $\mathcal{G}_4 \cap \bar{\mathcal{G}}_5$ and $\bar{\mathcal{G}}_4 \cap \mathcal{G}_5$; sugarpaper: $\mathcal{G}_4 \cap \bar{\mathcal{G}}_4$; magenta $\mathcal{G}_5 \cap \bar{\mathcal{F}}_5$; purple: $\mathcal{F}_4 \cap \mathcal{G}_5$ and $\bar{\mathcal{F}}_4 \cap \bar{\mathcal{G}}_5$; cyan: $\mathcal{G}_5 \cap \bar{\mathcal{G}}_5$; orange: $\mathcal{F}_4 \cap \bar{\mathcal{F}}_4$; brown: $\bar{\mathcal{F}}_5 \cap \bar{\mathcal{G}}_5$. The circle denotes the point where the cut locus fails to be C^1.

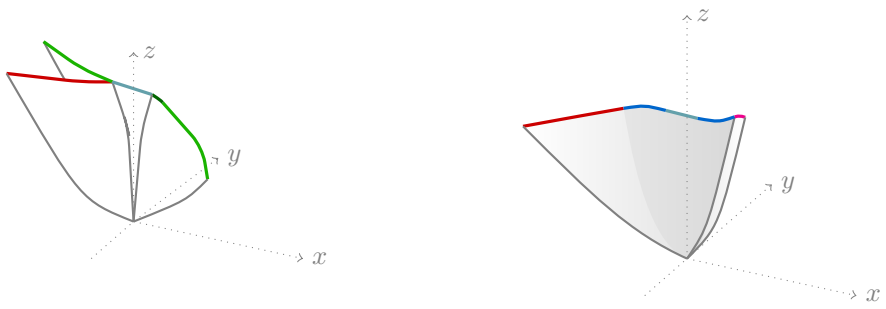

Figure 10: Cut locus in the case A_-, with $C_2 < 0$ and $A > 0$ (left) with $A > C_2 > 0$ (right). The colors of the branches correspond to the same code as in Figures 8-9.

encountered in Section 4.2.1 split, each one, into 2 further sub-cases, according to fact that $\frac{3E_1}{D_1}$ is less than one or is not.

We can summarize the influence of the value of the invariants as follows:

- when $C_2 < 0$ the suspension is "ramified", due to the fact that the intersections $\bar{\mathcal{G}}_4 \cap \mathcal{F}_4$ and $\mathcal{G}_4 \cap \bar{\mathcal{F}}_4$ (with suspension of length $\sim \mathcal{O}(\zeta)$) are admitted and participate to the cut locus; if $C_2 > 0$, then we may have suspension made by one branch or by three branches;
- as claimed above, if $\frac{3E_1}{D_1} < 1$, then the existence condition (D.1) is violated for some admissible values of the adjoint covector. This ends up in a cut locus whose suspension is *disconnected*;
- the value of A influences mostly the "central" part of the suspension (loosely speaking, that one belonging to a neighborhood of radius $\mathcal{O}(\zeta^3)$ of the origin).

4.2.3 Case B_-

At last, we consider the case in which again $|D_1| > |E_1|$, but the two invariants have opposite sign; in particular, we assume that D_1 is positive and E_1 negative. This case presents some

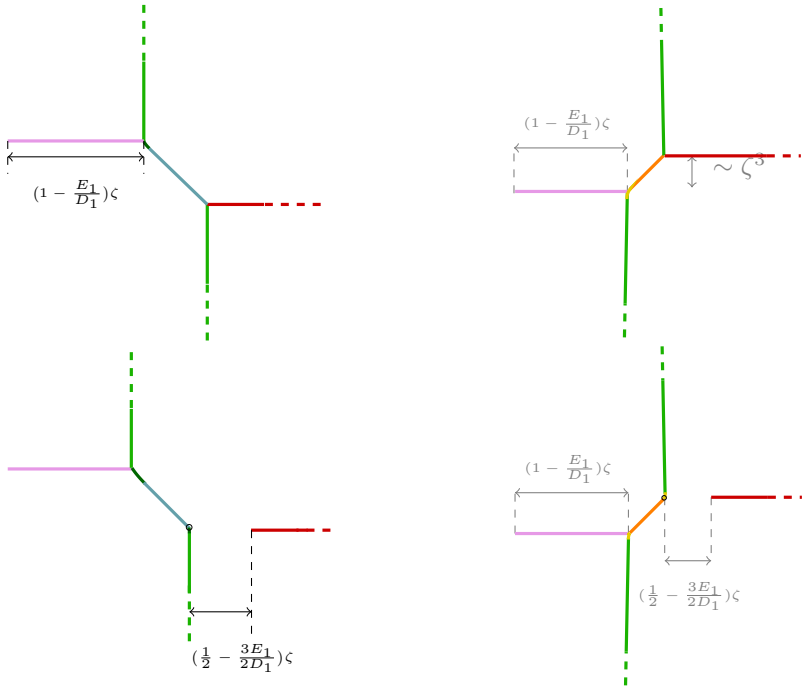

Figure 11: Suspension of the cut locus for the case B_+ with $C_2 < 0$. On the left, the cases with $A > 0$, on the right those with $A < 0$; on the top, we consider the cases with $\frac{3E_1}{D_1} \geq 1$ (connected suspension), on the bottom those with $\frac{3E_1}{D_1} < 1$ (disconnected suspension). Pink: $\mathcal{F}_4 \cap \mathcal{G}_4$; red: $\bar{\mathcal{F}}_4 \cap \bar{\mathcal{G}}_4$; green: $\mathcal{G}_4 \cap \bar{\mathcal{F}}_4$ and $\bar{\mathcal{G}}_4 \cap \mathcal{F}_4$; sugarpaper: $\mathcal{G}_4 \cap \bar{\mathcal{G}}_4$; dark green: $\mathcal{F}_5 \cap \bar{\mathcal{G}}_4$ and $\bar{\mathcal{F}}_5 \cap \mathcal{G}_4$; yellow: $\mathcal{F}_5 \cap \bar{\mathcal{F}}_4$ and $\bar{\mathcal{F}}_5 \cap \mathcal{F}_4$; orange: $\mathcal{F}_4 \cap \bar{\mathcal{F}}_4$. The circles show the points where the suspension is not C^1.

Figure 12: Cut locus in the case $\boldsymbol{B}_+$, with $C_2 < 0$ and $A > 0$. On the left, $\frac{3E_1}{D_1} \geq 1$, on the right $\frac{3E_1}{D_1} < 1$.

novelties with respect to the generic one; the main peculiarity is the fact that the suspension of the cut locus is always disconnected.

However, even if the intersections causing a loss of optimality may differ from the cases studied in Section 4.2.2, qualitatively the shapes of the suspensions of the cut locus are the same; the differences between the two cases can be appreciated only entering into the detailed description of Appendix C. We are nevertheless providing, here below, the plot of the suspensions of the cur loci.

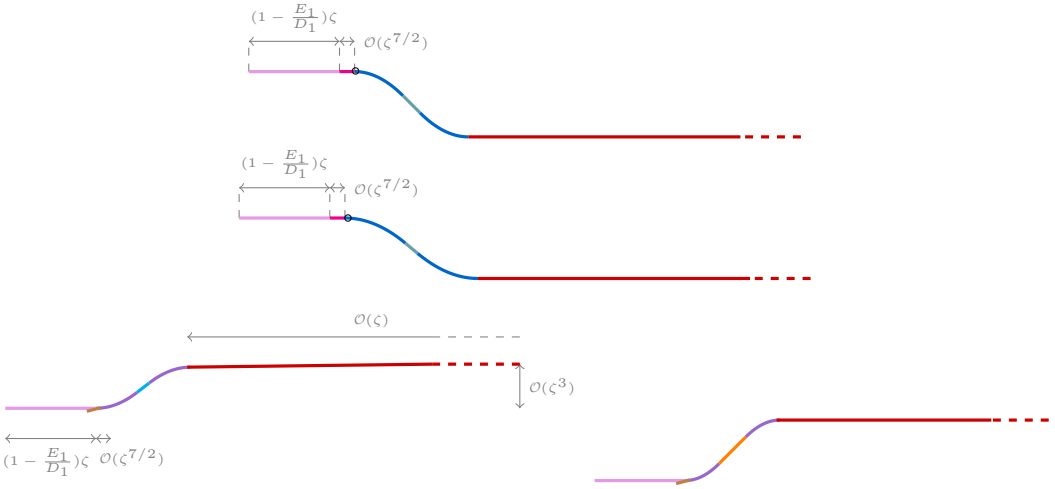

Figure 13: Suspension of the cut locus for the case B_+ with $\frac{3E_1}{E_1} \geq 1$, in the subcases $A > C_2$, $C_2 > A > 0$, $0 > A > -C_2$ and $0 > C_2 > A$ (from top to bottom). Pink: $\mathcal{F}_4 \cap \mathcal{F}_5$; magenta: $\mathcal{F}_5 \cap \bar{\mathcal{G}}_5$ and $\mathcal{G}_5 \cap \bar{\mathcal{F}}_5$; red: $\bar{\mathcal{F}}_4 \cap \bar{\mathcal{G}}_4$; blue: $\mathcal{G}_4 \cap \bar{\mathcal{G}}_5$ and $\bar{\mathcal{G}}_4 \cap \mathcal{G}_5$; sugarpaper: $\mathcal{G}_4 \cap \bar{\mathcal{G}}_4$; brown $\mathcal{F}_5 \cap \mathcal{G}_5$ and $\bar{\mathcal{F}}_5 \cap \bar{\mathcal{G}}_5$; orange: $\mathcal{F}_4 \cap \bar{\mathcal{F}}_4$. The circles point out the non-smooth junctions.

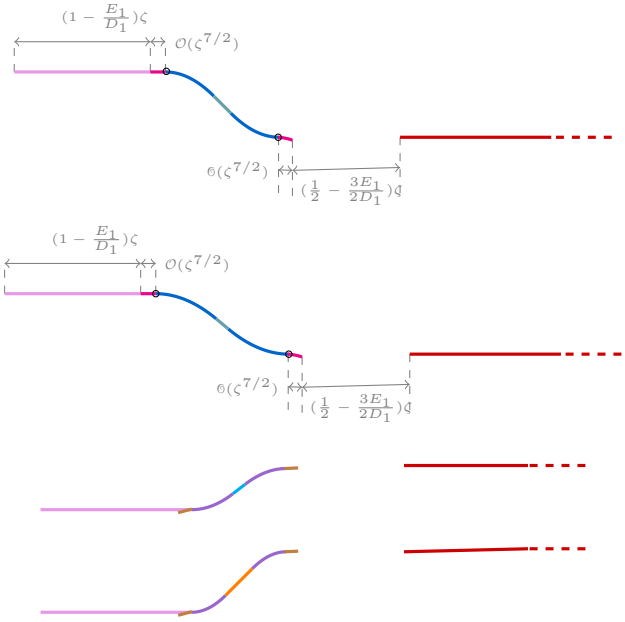

Figure 14: Suspension of the cut locus for the case B_+ with $\frac{3E_1}{E_1} < 1$, in the subcases $A > C_2$, $C_2 > A > 0$, $0 > A > -C_2$ and $0 > C_2 > A$ (from top to bottom). Pink: $\mathcal{F}_4 \cap \mathcal{F}_5$; magenta: $\mathcal{F}_5 \cap \bar{\mathcal{G}}_5$ and $\mathcal{G}_5 \cap \bar{\mathcal{F}}_5$; red: $\bar{\mathcal{F}}_4 \cap \bar{\mathcal{G}}_4$; blue: $\mathcal{G}_4 \cap \bar{\mathcal{G}}_5$ and $\bar{\mathcal{G}}_4 \cap \mathcal{G}_5$; sugarpaper: $\mathcal{G}_4 \cap \bar{\mathcal{G}}_4$; brown $\mathcal{F}_5 \cap \mathcal{G}_5$ and $\bar{\mathcal{F}}_5 \cap \bar{\mathcal{G}}_5$; orange: $\mathcal{F}_4 \cap \bar{\mathcal{F}}_4$. The circles point out the non-smooth junctions.

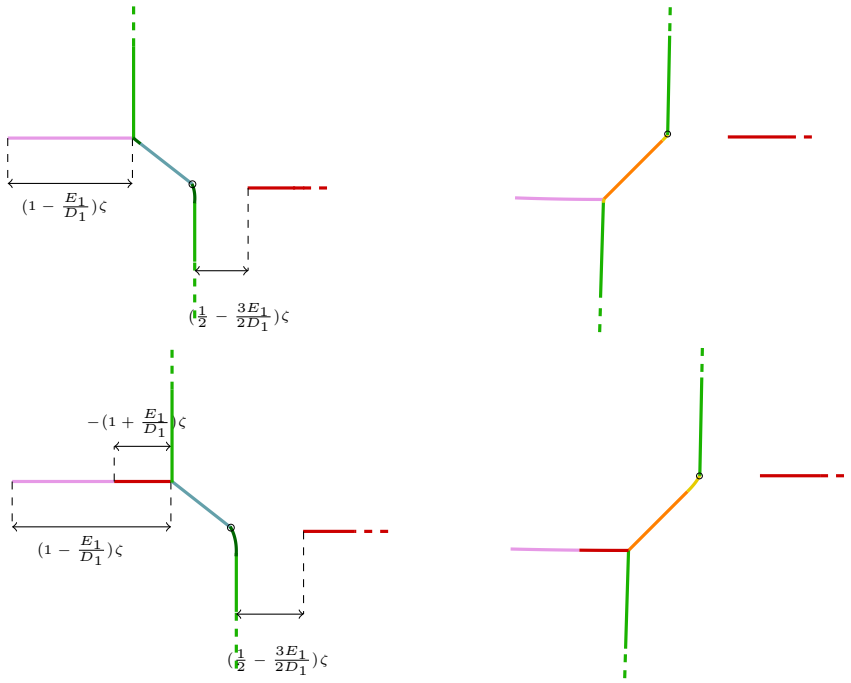

Figure 15: Suspension of the cut locus for the case B_- with $C_2 < 0$. On the left, the cases with $A > 0$, on the right those with $A < 0$; on the top, we consider the cases with $\frac{3E_1}{D_1} \geq 1$, on the bottom those with $\frac{3E_1}{D_1} < 1$. Pink: $\mathcal{F}_4 \cap \mathcal{G}_4$; red: $\bar{\mathcal{F}}_4 \cap \bar{\mathcal{G}}_4$ and $\mathcal{F}_4 \cap \mathcal{G}_4$; green: $\mathcal{G}_4 \cap \bar{\mathcal{F}}_4$ and $\bar{\mathcal{G}}_4 \cap \mathcal{F}_4$; sugarpaper: $\mathcal{G}_4 \cap \bar{\mathcal{G}}_4$; dark green: $\mathcal{F}_5 \cap \bar{\mathcal{G}}_4$ and $\bar{\mathcal{F}}_5 \cap \mathcal{G}_4$; orange: $\mathcal{F}_4 \cap \bar{\mathcal{F}}_4$; yellow: $\mathcal{F}_4 \cap \bar{\mathcal{F}}_5$ and $\mathcal{F}_5 \cap \bar{\mathcal{F}}_5$. The circles denote the points where the junction between two intersections is not C^1.

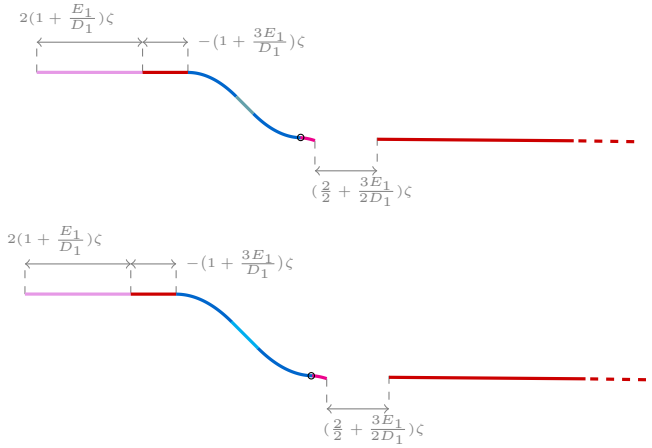

Figure 16: Cut locus for the case B_- with $C_2 > 0$, $A > 0$ and $\frac{3E_1}{E_1} < -1$. The upper plot shows the case, $A > C_2$, the lower one the case $A < C_2$: pink: $\mathcal{F}_4 \cap \mathcal{F}_5$; magenta: $\bar{\mathcal{F}}_5 \cap \mathcal{G}_5$; red: $\mathcal{F}_4 \cap \mathcal{G}_4$ and $\bar{\mathcal{F}}_4 \cap \bar{\mathcal{G}}_4$; blue: $\mathcal{G}_4 \cap \bar{\mathcal{G}}_5$ and $\bar{\mathcal{G}}_4 \cap \mathcal{G}_5$; sugarpaper: $\mathcal{G}_4 \cap \bar{\mathcal{G}}_4$; cyan: $\mathcal{G}_5 \cap \bar{\mathcal{G}}_5$. The circles show the points where the junction is not C^1.

5 Open Problems and final remarks

In this paper, all results hold true for the jets of the geodesics with respect to the small parameter ρ_0, up to the fourth order for the coordinates x, y and the fifth order for the

Figure 17: Cut locus for the case B_- with $C_2 > 0$, $A < 0$ and $\frac{3E_1}{D_1} < -1$. Upper plot: $-C_2 < A$; lower plot $A < -C_2$; rose: $\mathcal{F}_4 \cap \mathcal{F}_5$; red: $\mathcal{F}_4 \cap \mathcal{G}_4$ and $\bar{\mathcal{F}}_4 \cap \bar{\mathcal{G}}_4$ purple: $\mathcal{F}_4 \cap \mathcal{G}_5$ and $\bar{\mathcal{F}}_4 \cap \bar{\mathcal{G}}_5$; brown $\bar{\mathcal{F}}_5 \cap \bar{\mathcal{G}}_5$; orange: $\mathcal{F}_4 \cap \bar{\mathcal{F}}_4$.

coordinate z. Once the cut locus for the jets of the dynamics has been described, the natural question to be answered concerns the shape of the cut locus for the true geodesics of the system. As already observed in [7] for the generic case ($C_1 \neq 0$), all cut points of geodesics with initial covector (p_x^0, p_y^0, p_z^0) with $|p_x^0| \neq |p_y^0|$ correspond to transversal self-intersections of the wavefront and are therefore stable. In the case considered in the present paper, some problems may arise in studying the behavior of the intersections of the kind $\mathcal{F}_5 \cap \mathcal{G}_5$ (respectively, $\bar{\mathcal{F}}_5 \cap \mathcal{G}_5$, $\bar{\mathcal{F}}_5 \cap \bar{\mathcal{G}}_5$ and $\mathcal{F}_5 \cap \bar{\mathcal{G}}_5$): indeed, from the analysis carried out in the preceding sections, it is not completely clear if the wavefronts are transversal (even if some simulations in some concrete cases seems to suggest it); for what concerns other wavefronts intersection, involving geodesics associated with initial adjoint vectors with $|p_x^0| \neq |p_y^0|$ or $|p_x^0| = 1$ and $p_y^0 \neq -\frac{E_1}{D_1}$, we can say, in analogy with [7], that they are transversal.

Therefore, the cut loci computed above represent a good approximation for the cut loci of the true dynamics, except for the extremals with those particular value of the initial covector. To understand what happens in these cases, a stability analysis should be done. The question is particularly tricky, because the class in which one should study the stability of these singularities is not completely clear, as it is, for instance, for the caustics in sub-Riemannian geometry, which are stable in the class of Lagrangian maps (see [2, 12, 23]).

Another open problem concerns the study of the cut points of geodesics with final point (x_T, y_T, z_T) satisfying $|z_T| \leq \frac{x_T y_T}{2}$. We recall that, for the Heisenberg system, such points are reached in optimal time $|x_T| + |y_T|$ by means of a trajectory with at most two bang arc and/or by a singular trajectory; the "central part" of the unit sphere is thus made by the surface $\{(x, y, z) : |x| + |y| = 1 \text{ and } |z| \leq |xy|/2\}$.

To study the "central part" of the sphere in the generic case, some remarks are in order. First of all, we notice that, under some generic assumptions, there is no singular extremal; indeed, singular extremals are characterized by the constraint $|F(\boldsymbol{\lambda}(t))| \equiv |G(\boldsymbol{\lambda}(t))|$ along the whole singular interval. In particular, this implies that $\Theta(\boldsymbol{\lambda}(t)) \equiv 0$ and that all time derivatives of Θ along the extremal are null on the interval, i.e.

$$\langle \boldsymbol{\lambda}(t), \mathrm{ad}^k_{u_1 f + u_2 g}[f, g](\boldsymbol{\xi}(t)) \rangle = 0 \ \forall t \in I, \ \forall k \geq 1. \tag{37}$$

In particular, (37) gives a list of orthogonality constraints that the singular extremal and its associated control must satisfy; for a generic pair of vectors f, g, these constraints have maximal rank and thus impose that the covector is null, which is prohibited by the PMP.

On the other hand, differently from the nilpotent case, the sign of Θ may change along an extremal, which could lead to controls switching several times between two particular controls sharing the same side of Q (see [7]). In order to have such a behavior in short times, we must have $|\Theta(\boldsymbol{\lambda}(0))| \ll 1$. Indeed, if $|\Theta(\boldsymbol{\lambda}(0))| \sim 1$, then Θ cannot change sign in small time, because $\dot{\Theta}$ is bounded (and close to 0 at the initial time). This in particular shows that bang-bang extremals with several switches in small times may have only two behaviors: either the control switches from vertex to vertex of Q always in the same sense (that corresponds to Θ of constant sign along the extremal, and to the situation we analyzed throughout the paper), or it switches several times between two vertices of Q sharing the same side (which correspond to the fact that both $|F|$ and $|G|$ stay close to 1). A preliminary analysis (carried out for geodesics with three bang arcs) shows that the behavior of such geodesics is dominated by the value of the invariants $\mathrm{ax}_{ij}, \mathrm{ay}_{ij}$ with $i, j = 1, 2$, and their combinations, and that the invariants A, C_1, C_2, D_1 and E_1 are not involved. It thus seems that the behavior of the upper

part and the central one of the cut locus are not related (that is, we could have almost every possible combination). The question is surely interesting and will be the subject of future analyses of the authors'.

Finally, one must study also the part of the sphere with $z < -|xy|/2$. It is opinion of the authors that the problem can be solved just by finding the proper "symmetry" of the system, that is, the set of transformations and permutations of invariants that allow to compute the geodesics attaining points with negative z from the one studied in this paper.

Acknowledgments

The authors gratefully acknowledge Grégoire Charlot for fruitful exchanges they had with him and for his several inputs, that had led to the present paper. They also thank Ugo Boscain, Eric Busvelle and Jean-Paul Gauthier for useful discussions.

Declarations

- Funding : this research has been supported by the project *Partenariat Hubert Curien - Tassili 2015 PHC15MDU941* and by the funding CARTT-IUT.
- Availability of data and materials : not applicable

A Permutations of the invariants

In Lemma 4, we saw that the geodesics of the sets Γ_{-f} and $\Gamma_{\pm g}$ can be recovered from the Γ_f ones, by applying a rotation around the z axis and a suitable permutation of the invariants. For the sake of clarity, in this section we provide these permutations, for the main invariants.

♣ to obtain the coordinates (of the switching times) of a geodesics of the set Γ_g, starting from the corresponding expression associated with a geodesics belonging to the set Γ_f one, we must perform a rotation of $\pi/2$ around the vertical axis (both in the space of the coordinates and in the momentum space) and apply the following transformations:

$$
\begin{array}{cccc}
 & A \mapsto -A & & \\
 & C_1 \mapsto C_2 & C_2 \mapsto C_1 & \\
D_1 \mapsto D_2 & D_2 \mapsto -D_1 & E_1 \mapsto E_2 & E_2 \mapsto -E_1 \\
c_1 \mapsto c_2 & d_1 \mapsto d_2 & c_2 \mapsto -c_1 & d_2 \mapsto -d_1
\end{array}
$$

♦ analogously, to obtain the quantities associated with a geodesic of the set Γ_{-f} from those associated with a geodesic of the set Γ_f, we must perform a rotation of π around the vertical axis (in both spaces), and apply the following transformations:

$$
\begin{array}{cccc}
D_1 \mapsto -D_1 & D_2 \mapsto -D_2 & E_1 \mapsto -E_1 & E_2 \mapsto -E_2 \\
c_1 \mapsto -c_1 & d_1 \mapsto -d_1 & c_2 \mapsto -c_2 & d_2 \mapsto -d_2
\end{array}
$$

♠ finally, to obtain the quantities associated with a geodesic of the set Γ_{-g} geodesic from a Γ_f from those associated with a geodesic of the set Γ_f, we must perform a rotation of $3\pi/2$ around the vertical axis (in both spaces), and apply the following transformations:

$$
\begin{array}{cccc}
 & A \mapsto -A & & \\
 & C_1 \mapsto C_2 & C_2 \mapsto C_1 & \\
D_1 \mapsto -D_2 & D_2 \mapsto D_1 & E_1 \mapsto -E_2 & E_2 \mapsto E_1 \\
c_1 \mapsto -c_2 & d_1 \mapsto -d_2 & c_2 \mapsto c_1 & d_2 \mapsto d_1
\end{array}
$$

Remark 5 *We remark that* $\spadesuit = \clubsuit \circ \blacklozenge = \blacklozenge \circ \clubsuit$.

B Jets of the dynamics

B.1 Jets of the geodesics

Consider a geodesics of the set Γ_f, with initial adjoint covector $\boldsymbol{\mu}_f(0) = (1, p_y^0, 1/\rho_0)$. Let τ and $\mathscr{T}_3$ denote, respectively, the reparameterized time and the reparameterized third switching time, and set $\hat{\tau} = \tau - \mathscr{T}_3$. Then the jets of the geodesics are given by the following expressions:

$$
\begin{aligned}
x(\mathscr{T}_3 + \hat{\tau}) = {} & -(p_x^0 + p_y^0)\rho_0 + \Big(4Ap_x^0 p_y^0 - \frac{1}{6}C_1(p_x^0 + p_y^0)^3 - 4C_2(p_x^0)^3\Big)\rho_0^3 \\
& + \frac{1}{24}\Big(- p_y^0\big(24(p_y^0)^2\hat{\tau}\mathrm{ax}_{11} + 12p_y^0\hat{\tau}^2(\mathrm{ax}_{12} + \mathrm{ay}_{11}) + 8\hat{\tau}^3\mathrm{ay}_{12} + (p_y^0)^3(17\mathrm{ax}_{21} - 15\omega_{xx31})\big) \\
& + 4p_x^0\big(- 6(p_y^0)^2\hat{\tau}(3\mathrm{ax}_{11} - 2(\mathrm{ax}_{12} + \mathrm{ay}_{11})) - 6p_y^0\hat{\tau}^2(\mathrm{ax}_{12} + \mathrm{ay}_{11} - 2\mathrm{ay}_{12}) - 2\hat{\tau}^3\mathrm{ay}_{12} \\
& + (p_y^0)^3(4\mathrm{ax}_{11} - 9\mathrm{ax}_{21} + 15\omega_{xx31})\big) - 6(p_x^0)^2\big(4p_y^0\hat{\tau}(3\mathrm{ax}_{11} - 4(\mathrm{ax}_{12} + \mathrm{ay}_{11} - \mathrm{ay}_{12})) \\
& + 2\hat{\tau}^2(\mathrm{ax}_{12} + \mathrm{ay}_{11} - 4\mathrm{ay}_{12}) + (p_y^0)^2(16\mathrm{ax}_{11} + 8\mathrm{ax}_{12} + \mathrm{ax}_{21} - 24\mathrm{ax}_{22} + 8\mathrm{ay}_{11} - 24\mathrm{ay}_{21} - 15\omega_{xx31} \\
& + 40\omega_{xx32} + 40\omega_{xy31} + 40\omega_{yx31})\big) + 4(p_x^0)^3\big(- 6\hat{\tau}(\mathrm{ax}_{11} - 2(\mathrm{ax}_{12} + \mathrm{ay}_{11} - 2\mathrm{ay}_{12})) \\
& + p_y^0(12\mathrm{ax}_{11} + 48\mathrm{ax}_{12} + 7\mathrm{ax}_{21} + 48\mathrm{ay}_{11} + 16\mathrm{ay}_{12} - 72\mathrm{ay}_{22} + 15\omega_{xx31} + 120\omega_{xy32} \\
& + 120\omega_{yx32} + 120\omega_{yy31})\big) - (p_x^0)^4\big(32\mathrm{ax}_{11} + 48\mathrm{ax}_{12} - 15\mathrm{ax}_{21} + 80\mathrm{ax}_{22} + 48\mathrm{ay}_{11} + 256\mathrm{ay}_{12} \\
& + 80\mathrm{ay}_{21} - 15\omega_{xx31} + 80\omega_{xx32} + 80\omega_{xy31} + 80\omega_{yx31} + 960\omega_{yy32}\big)\Big)\rho_0^4 + \mathcal{O}(\rho_0^5)
\end{aligned}
\tag{B.1}
$$

$$
\begin{aligned}
y(\mathscr{T}_3 + \hat{\tau}) = {} & (2p_x^0 - \hat{\tau})\rho_0 + \Big(C_1 p_x^0(p_y^0 - p_x^0)^2 - 2A(p_x^0)^2(p_y^0 - p_x^0) + \frac{4}{3}C_2(p_x^0)^3\Big)\rho_0^3 \\
& + \frac{1}{6}\Big(- p_y^0\hat{\tau}(6(p_y^0)^2\mathrm{ax}_{21} + 3p_y^0\hat{\tau}(\mathrm{ax}_{22} + \mathrm{ay}_{21}) + 2\hat{\tau}^2\mathrm{ay}_{22}) \\
& + 2p_x^0\big((p_y^0)^2\hat{\tau}(-9\mathrm{ax}_{21} + 6(\mathrm{ax}_{22} + \mathrm{ay}_{21})) - 3p_y^0\hat{\tau}^2(\mathrm{ax}_{22} + \mathrm{ay}_{21} - 2\mathrm{ay}_{22}) - \hat{\tau}^3\mathrm{ay}_{22} \\
& + 15(p_y^0)^3(\mathrm{ax}_{21} - \omega_{xx31})\big) + 3(p_x^0)^2\big(2p_y^0\hat{\tau}(-3\mathrm{ax}_{21} + 4(\mathrm{ax}_{22} + \mathrm{ay}_{21} - \mathrm{ay}_{22})) \\
& - \hat{\tau}^2(\mathrm{ax}_{22} + \mathrm{ay}_{21} - 4\mathrm{ay}_{22}) + 2(p_y^0)^2(3\mathrm{ax}_{11} - 11\mathrm{ax}_{21} + 5(-\mathrm{ax}_{22} - \mathrm{ay}_{21} + 3\omega_{xx31} \\
& + \omega_{xx32} + \omega_{xy31} + \omega_{yx31}))) - 2(p_x^0)^3\big(3\hat{\tau}(\mathrm{ax}_{21} - 2(\mathrm{ax}_{22} + \mathrm{ay}_{21} - 2\mathrm{ay}_{22})) \\
& + p_y^0(18\mathrm{ax}_{11} + 4\mathrm{ax}_{12} + 3\mathrm{ax}_{21} - 30\mathrm{ax}_{22} + 4\mathrm{ay}_{11} - 30\mathrm{ay}_{21} - 20\mathrm{ay}_{22} + 45\omega_{xx31} \\
& + 30\omega_{xx32} + 30\omega_{xy31} + 20\omega_{xy32} + 30\omega_{yx31} + 20\omega_{yx32} + 20\omega_{yy31})\big) \\
& + 2(p_x^0)^4\big(9\mathrm{ax}_{11} + 4\mathrm{ax}_{12} + 5\mathrm{ax}_{21} + 9\mathrm{ax}_{22} + 4\mathrm{ay}_{11} + 2\mathrm{ay}_{12} + 9\mathrm{ay}_{21} - 36\mathrm{ay}_{22} \\
& + 15\omega_{xx31} + 15\omega_{xx32} + 15\omega_{xy31} + 20\omega_{xy32} + 15\omega_{yx31} + 20\omega_{yx32} + 20\omega_{yy31} + 30\omega_{yy32}\big)\Big)\rho_0^4 + \mathcal{O}(\rho_0^5)
\end{aligned}
\tag{B.2}
$$

$$
\begin{aligned}
z(\mathscr{T}_3+\hat\tau) &= \frac{1}{2}\big(6(p_x^0)^2+p_y^0(\hat\tau-2p_x^0)+\hat\tau p_x^0\big)\rho_0^2 \qquad\qquad (B.3)\\
&+\frac{1}{6}\Big(4(p_x^0)^4(19\mathrm{ax}_{31}+15\mathrm{ax}_{32}+15\mathrm{ay}_{31}+44\mathrm{ay}_{32})-p_y^0\hat\tau\big(2(p_y^0)^2\mathrm{ax}_{31}+3(p_y^0)\hat\tau(\mathrm{ax}_{32}+\mathrm{ay}_{31})\\
&+2\hat\tau^2\mathrm{ay}_{32}\big)-2p_x^0\big(10(p_y^0)^3\mathrm{ax}_{31}+3(p_y^0)^2\hat\tau(\mathrm{ax}_{31}-2(\mathrm{ax}_{32}+\mathrm{ay}_{31}))\\
&+3p_y^0\hat\tau^2(\mathrm{ax}_{32}+\mathrm{ay}_{31}-2\mathrm{ay}_{32})+\hat\tau^3\mathrm{ay}_{32}\big)+3(p_x^0)^2\big(4(p_y^0)^2(11\mathrm{ax}_{31}+\mathrm{ax}_{32}+\mathrm{ay}_{31})\\
&-\hat\tau^2(\mathrm{ax}_{32}+\mathrm{ay}_{31}-4\mathrm{ay}_{32})-2p_y^0\hat\tau(\mathrm{ax}_{31}+4(\mathrm{ax}_{32}+\mathrm{ay}_{31}+\mathrm{ay}_{32}))\big)\\
&-2(p_x^0)^3\big(p_y^0(78\mathrm{ax}_{31}+60\mathrm{ax}_{32}+60\mathrm{ay}_{31}+8\mathrm{ay}_{32})+\hat\tau(\mathrm{ax}_{31}-6(\mathrm{ax}_{32}+\mathrm{ay}_{31}+6\mathrm{ay}_{32}))\big)\Big)\rho_0^4\\
&+\frac{1}{48}\Big(2(p_x^0)^5\big(100\mathrm{ax}_{11}+32\mathrm{ax}_{12}+131\mathrm{ax}_{21}+180\mathrm{ax}_{22}+32\mathrm{ay}_{11}-184\mathrm{ay}_{12}+180\mathrm{ay}_{21}\\
&-16\mathrm{ay}_{22}+171\omega_{xx31}+204\omega_{xx32}+204\omega_{xy31}+208\omega_{xy32}+204\omega_{yx31}+208\omega_{yx32}\\
&+208\omega_{yy31}+888\omega_{yy32}\big)+p_y^0\hat\tau\big((p_y^0)^3(17\mathrm{ax}_{21}+9\omega_{xx31})\\
&+12(p_y^0)^2\hat\tau(\mathrm{ax}_{11}+\omega_{xx32}+\omega_{xy31}+\omega_{yx31})+4p_y^0\hat\tau^2(\mathrm{ax}_{12}+\mathrm{ay}_{11}+2(\omega_{xy32}+\omega_{yx32}+\omega_{yy31}))\\
&+2\hat\tau^3(\mathrm{ay}_{12}+3\omega_{yy32})\big)-2p_x^0((p_y^0)^4(53\mathrm{ax}_{21}-51\omega_{xx31})+2(p_y^0)^3\hat\tau\big(4\mathrm{ax}_{11}+3(-3\mathrm{ax}_{21}\\
&-3\omega_{xx31}+4\omega_{xx32}+4\omega_{xy31}+4\omega_{yx31})\big)-6(p_y^0)^2\hat\tau^2(3\mathrm{ax}_{11}-2\mathrm{ax}_{12}-2\mathrm{ay}_{11}+3\omega_{xx32}\\
&+3\omega_{xy31}-4\omega_{xy32}+3\omega_{yx31}-4\omega_{yx32}-4\omega_{yy31})-4p_y^0\hat\tau^3\big(\mathrm{ax}_{12}+\mathrm{ay}_{11}+2(-\mathrm{ay}_{12}\\
&+\omega_{xy32}+\omega_{yx32}+\omega_{yy31}-3\omega_{yy32})\big)-\hat\tau^4(\mathrm{ay}_{12}+3\omega_{yy32}))+2(p_x^0)^2\big(-4(p_y^0)^3(11\mathrm{ax}_{11}\\
&-69\mathrm{ax}_{21}+9(-\mathrm{ax}_{22}-\mathrm{ay}_{21}+11\omega_{xx31}+\omega_{xx32}+\omega_{yx31}+\omega_{yx31}))+3(p_y^0)^2\hat\tau(16\mathrm{ax}_{11}\\
&+8\mathrm{ax}_{12}+\mathrm{ax}_{21}-24\mathrm{ax}_{22}+8\mathrm{ay}_{11}-24\mathrm{ay}_{21}+9\omega_{xx31}+16\omega_{xx32}+16\omega_{xy31}+16\omega_{xy32}+16\omega_{yx31}\\
&+16\omega_{yx32}+16\omega_{yy31})+2\hat\tau^3(\mathrm{ax}_{12}+\mathrm{ay}_{11}+2(-2\mathrm{ay}_{12}+\omega_{xy32}+\omega_{yx32}+\omega_{yy31}-6\omega_{yy32}))\\
&+6p_y^0\hat\tau^2(3\mathrm{ax}_{11}-4\mathrm{ax}_{12}-4\mathrm{ay}_{11}+4\mathrm{ay}_{12}+3\omega_{xx32}+3\omega_{xy31}-8\omega_{xy32}+3\omega_{yx31}\\
&-8\omega_{yx32}-8\omega_{yy31}+12\omega_{yy32})\big)+4(p_x^0)^3\big(3(p_y^0)^2(26\mathrm{ax}_{11}-25\mathrm{ax}_{21}-46\mathrm{ax}_{22}-46\mathrm{ay}_{21}-8\mathrm{ay}_{22}\\
&+111\omega_{xx31}+62\omega_{xx32}+62\omega_{xy31}+8\omega_{xy32}+62\omega_{yx31}+8\omega_{yx32}+8\omega_{yy31})\\
&+3\hat\tau^2(\mathrm{ax}_{11}-2\mathrm{ax}_{12}-2\mathrm{ay}_{11}+4\mathrm{ay}_{12}+\omega_{xx32}+\omega_{xy31}-4\omega_{xy32}+\omega_{yx31}\\
&-4\omega_{yx32}-4\omega_{yy31}+12\omega_{yy32})-p_y^0\hat\tau(12\mathrm{ax}_{11}+48\mathrm{ax}_{12}+7\mathrm{ax}_{21}+48\mathrm{ay}_{11}+16\mathrm{ay}_{12}\\
&-72\mathrm{ay}_{22}-9\omega_{xx31}+36\omega_{xx32}+36\omega_{xy31}+72\omega_{xy32}+36\omega_{yx31}+72\omega_{yx32}+72\omega_{yy31}+48\omega_{yy32})\big)\\
&+(p_x^0)^4\big(-8(p_y^0)(69\mathrm{ax}_{11}-16\mathrm{ax}_{12}+55\mathrm{ax}_{21}-15\mathrm{ax}_{22}-16\mathrm{ay}_{11}-2\mathrm{ay}_{12}-15\mathrm{ay}_{21}-104\mathrm{ay}_{22}\\
&+159\omega_{xx31}+87\omega_{xx32}+87\omega_{xy31}+136\omega_{xy32}+87\omega_{yx31}+136\omega_{yx32}+136\omega_{yy31}+18\omega_{yy32})\\
&+\hat\tau(32\mathrm{ax}_{11}+48\mathrm{ax}_{12}-15\mathrm{ax}_{21}+80\mathrm{ax}_{22}+48\mathrm{ay}_{11}+256\mathrm{ay}_{12}+80\mathrm{ay}_{21}+9\omega_{xx31}+32\omega_{xx32}\\
&+32\omega_{xy31}+96\omega_{xy32}+32\omega_{yx31}+96\omega_{yx32}+96\omega_{yy31}+768\omega_{yy32})\big)\Big)\rho_0^5
\end{aligned}
$$

Consider a geodesics of the set Γ_f, with initial adjoint covector $(1, p_y^0, 1/\rho_0)$. Set now

$\hat\tau = \tau - \mathscr{T}_4$. Then

$$x(\mathscr{T}_4+\hat\tau) = x(\mathscr{T}_4) + \hat\tau\rho_0 + \mathcal{O}(\rho_0^5) \tag{B.4}$$

$$y(\mathscr{T}_4+\hat\tau) = y(\mathscr{T}_4) + \mathcal{O}(\rho_0^5) \tag{B.5}$$

$$\begin{aligned} z(\mathscr{T}_4+\hat\tau) = z(\mathscr{T}_4) &+ 2(p_x^0)^2\hat\tau(C_1p_y^0 - Ap_x^0)\rho_0^4 \\ &+ \hat\tau\big((p_y^0)^2D_1 + 2E_2p_y^0p_x^0 - \frac{1}{3}c_1(p_x^0)^2\big)(p_x^0)^2\rho_0^5 + \mathcal{O}(\rho_0^6) \end{aligned} \tag{B.6}$$

B.2 Switching times of the geodesics of the set Γ_f

$$\begin{aligned} \mathscr{T}_1 &= (p_x^0 - p_y^0) + \frac{4}{3}\mathrm{ax}_{31}(p_x^0-p_y^0)^3\rho_0^2 \\ &\quad + \frac{1}{24}\rho_0^3\left(15\mathrm{ax}_{21}(p_x^0-p_y^0)^4 + 32p_x^0\mathrm{ax}_{11}(p_x^0-p_y^0)^3 + 32p_y^0\mathrm{ax}_{21}(p_x^0-p_y^0)^3 + 15\omega_{xx31}(p_x^0-p_y^0)^4\right) \end{aligned}$$

$$\begin{aligned} \mathscr{T}_2 &= \mathscr{T}_1 + 2p_x^0 + \frac{2}{3}\left(12(p_x^0)^2\mathrm{ax}_{32}(p_x^0-p_y^0) + 12p_x^0\mathrm{ax}_{31}(p_x^0-p_y^0)^2 + 16(p_x^0)^3\mathrm{ay}_{32} + 12(p_x^0)^2\mathrm{ay}_{31}(p_x^0-p_y^0)\right)\rho_0^2 \\ &\quad + \frac{1}{24}\Big(32(p_x^0)^3\mathrm{ax}_{12}(p_x^0-p_y^0) + 72(p_x^0)^2\mathrm{ax}_{11}(p_x^0-p_y^0)^2 + 120(p_x^0)^2\mathrm{ax}_{22}(p_x^0-p_y^0)^2 \\ &\quad + 192(p_x^0)^2p_y^0\mathrm{ax}_{22}(p_x^0-p_y^0) + 120p_x^0\mathrm{ax}_{21}(p_x^0-p_y^0)^3 + 192p_x^0p_y^0\mathrm{ax}_{21}(p_x^0-p_y^0)^2 + 16(p_x^0)^4\mathrm{ay}_{12} \\ &\quad + 32(p_x^0)^3\mathrm{ay}_{11}(p_x^0-p_y^0) + 160(p_x^0)^3\mathrm{ay}_{22}(p_x^0-p_y^0) + 256(p_x^0)^3p_y^0\mathrm{ay}_{22} + 120(p_x^0)^2\mathrm{ay}_{21}(p_x^0-p_y^0)^2 \\ &\quad + 192(p_x^0)^2p_y^0\mathrm{ay}_{21}(p_x^0-p_y^0) + 240(p_x^0)^4\omega_{yy32} + 160(p_x^0)^3\omega_{xy32}(p_x^0-p_y^0) \\ &\quad + 160(p_x^0)^3\omega_{yx32}(p_x^0-p_y^0) + 160(p_x^0)^3\omega_{yy31}(p_x^0-p_y^0) + 120(p_x^0)^2\omega_{xx32}(p_x^0-p_y^0)^2 + 120(p_x^0)^2\omega_{xy31}(p_x^0-p_y^0)^2 \\ &\quad + 120(p_x^0)^2\omega_{yx31}(p_x^0-p_y^0)^2 + 120p_x^0\omega_{xx31}(p_x^0-p_y^0)^3\Big)\rho_0^3 \end{aligned}$$

$$\begin{aligned} \mathscr{T}_3 &= \mathscr{T}_2 + 2p_x^0 + \left(\frac{8}{3}(p_x^0)^3\mathrm{ax}_{31} - 16(p_x^0)^2p_y^0\mathrm{ax}_{32} + 8p_x^0(p_y^0)^2\mathrm{ax}_{31} + 32(p_x^0)^3\mathrm{ay}_{32} - 16(p_x^0)^2p_y^0\mathrm{ay}_{31}\right)\rho_0^2 \\ &\quad + \frac{1}{3}\rho_0^3\Big(-2(p_x^0)^4\mathrm{ax}_{11} + 10(p_x^0)^4\mathrm{ax}_{22} + 12(p_x^0)^3(p_y^0)\mathrm{ax}_{12} - 7(p_x^0)^3p_y^0\mathrm{ax}_{21} - 6(p_x^0)^2(p_y^0)^2\mathrm{ax}_{11} \\ &\quad - 18(p_x^0)^2(p_y^0)^2\mathrm{ax}_{22} + 9(p_x^0)(p_y^0)^3\mathrm{ax}_{21} - 24(p_x^0)^4\mathrm{ay}_{12} + 10(p_x^0)^4\mathrm{ay}_{21} + 12(p_x^0)^3(p_y^0)\mathrm{ay}_{11} + 36(p_x^0)^3(p_y^0)\mathrm{ay}_{22} \\ &\quad - 18(p_x^0)^2(p_y^0)^2\mathrm{ay}_{21} + 10(p_x^0)^4\omega_{xx32} + 10(p_x^0)^4\omega_{xy31} + 10(p_x^0)^4\omega_{yx31} + 120(p_x^0)^4\omega_{yy32} - 15(p_x^0)^3p_y^0\omega_{xx31} \\ &\quad - 60(p_x^0)^3p_y^0\omega_{xy32} - 60(p_x^0)^3p_y^0\omega_{yx32} - 60(p_x^0)^3p_y^0\omega_{yy31} + 30(p_x^0)^2(p_y^0)^2\omega_{xx32} + 30(p_x^0)^2(p_y^0)^2\omega_{xy31} \\ &\quad + 30(p_x^0)^2(p_y^0)^2\omega_{yx31} - 15p_x^0(p_y^0)^3\omega_{xx31}\Big) \end{aligned}$$

$$\begin{aligned} \mathscr{T}_4 &= \mathscr{T}_3 + 2p_x^0 + \Big(8(p_x^0)^3\mathrm{ax}_{31} - 8(p_x^0)^3\mathrm{ax}_{32} + 16(p_x^0)^2p_y^0\mathrm{ax}_{31} - 8(p_x^0)^2p_y^0\mathrm{ax}_{32} + 8p_x^0(p_y^0)^2\mathrm{ax}_{31} - 8(p_x^0)^3\mathrm{ay}_{31} \\ &\quad + \frac{32}{3}(p_x^0)^3\mathrm{ay}_{32} - 8(p_x^0)^2p_y^0\mathrm{ay}_{31}\Big)\rho_0^2 \\ &\quad + \frac{1}{3}\Big(9(p_x^0)^4\mathrm{ax}_{11} - 4(p_x^0)^4\mathrm{ax}_{12} - 15(p_x^0)^4\mathrm{ax}_{21} + 15(p_x^0)^4\mathrm{ax}_{22} + 18(p_x^0)^3(p_y^0)\mathrm{ax}_{11} - 4(p_x^0)^3p_y^0\mathrm{ax}_{12} \\ &\quad - 21(p_x^0)^3p_y^0\mathrm{ax}_{21} + 6(p_x^0)^3p_y^0\mathrm{ax}_{22} + 9(p_x^0)^2(p_y^0)^2\mathrm{ax}_{11} + 3(p_x^0)^2(p_y^0)^2\mathrm{ax}_{21} - 9(p_x^0)^2(p_y^0)^2\mathrm{ax}_{22} \\ &\quad + 9p_x^0(p_y^0)^3\mathrm{ax}_{21} - 4(p_x^0)^4\mathrm{ay}_{11} + 2(p_x^0)^4\mathrm{ay}_{12} + 15(p_x^0)^4\mathrm{ay}_{21} - 20(p_x^0)^4\mathrm{ay}_{22} - 4(p_x^0)^3p_y^0\mathrm{ay}_{11} \\ &\quad + 6(p_x^0)^3(p_y^0)\mathrm{ay}_{21} + 12(p_x^0)^3p_y^0\mathrm{ay}_{22} - 9(p_x^0)^2(p_y^0)^2\mathrm{ay}_{21} - 15(p_x^0)^4\omega_{xx31} + 15(p_x^0)^4\omega_{xx32} + 15(p_x^0)^4\omega_{xy31} \\ &\quad - 20(p_x^0)^4\omega_{xy32} + 15(p_x^0)^4\omega_{yx31} - 20(p_x^0)^4\omega_{yx32} - 20(p_x^0)^4\omega_{yy31} \\ &\quad + 30(p_x^0)^4\omega_{yy32} - 45(p_x^0)^3(p_y^0)\omega_{xx31} + 30(p_x^0)^3(p_y^0)\omega_{xx32} + 30(p_x^0)^3p_y^0\omega_{xy31} - 20(p_x^0)^3p_y^0\omega_{xy32} \\ &\quad + 30(p_x^0)^3p_y^0\omega_{yx31} - 20(p_x^0)^3p_y^0\omega_{yx32} - 20(p_x^0)^3p_y^0\omega_{yy31} - 45(p_x^0)^2(p_y^0)^2\omega_{xx31} + 15(p_x^0)^2(p_y^0)^2\omega_{xx32} \\ &\quad + 15(p_x^0)^2(p_y^0)^2\omega_{xy31} + 15(p_x^0)^2(p_y^0)^2\omega_{yx31} - 15p_x^0(p_y^0)^3\omega_{xx31}\Big)\rho_0^3 \end{aligned}$$

C Analysis of the upper part of the cut locus

In this Section we provide the details of the analysis that leads to the main results of the article. For each of the three considered cases ($\boldsymbol{A}_-$,$\boldsymbol{B}_+$ and $\boldsymbol{B}_-$), we consider separately the

sub-cases $C_2 < 0$ (in which all geodesics of the sets $\Gamma_{\pm g}$ lose optimality before the fourth switching time) and $C_2 > 0$ (in which they may lose optimality after the fourth switching time, see Section 3.2).

Notation. For the sake of readability, in the following we will sometimes omit to specify that we are providing only the leading terms in the expansion with respect to ζ and ρ_0; in particular, this will be done in two cases: when we specify the intersection points (for instance, the value of the intersection between the fronts $\mathcal{F}_4$, $\mathcal{G}_4$ and $\bar{\mathcal{G}}_4$ is given by equation (C.1) up to fifth order terms in ζ); when we describe the behavior of the geodesics according to the value of the initial adjoint vector (for instance, when we say that the geodesics with $p_y^0 \in [-1, -1+c\rho_0^2]$ behave in some particular way, we mean $p_y^0 \in [-1, -1 + c\rho_0^2 + \mathcal{O}(\rho_0^3)]$).

C.1 $E_1 < -|D_1|$ (case $\boldsymbol{A}_-$)

$C_2 < 0$

First of all, we focus on the Maxwell points of the geodesics belonging to the set Γ_f. In the nilpotent case, such geodesics lose optimality at the fourth swicthing time, when intersecting the front $\mathcal{G}_4$ and, in the case under concern, this intersection of fronts occurs (as sufficient conditions are satisfied); this suggest this intersection to cause global optimality loss for the geodesics of the class Γ_f, except maybe those with extreme values of the momentum, i.e. $|p_y^0| \sim 1$. To inspect more closely these ones, we look at the intersections $\mathcal{F}_4 \cap \mathcal{G}_4$, $\mathcal{G}_4 \cap \bar{\mathcal{F}}_4$ and $\bar{\mathcal{G}}_4 \cap \mathcal{F}_4$ close to the origin, by taking the limits of equations (30)-(D.5) and as $\gamma \to -1$, $\eta \to -1$ and $\beta \to 1$, respectively. We see that the reciprocal position of the intersections depend on the sign of the invariant A: indeed, the curve described by equation (30) crosses the one described by (D.6) if $A > 0$, and the curve described by (D.5) if $A < 0$, as can bee seen in Figure 6. In the first case, the lines $\mathcal{F}_4 \cap \mathcal{G}_4$ and $\bar{\mathcal{G}}_4 \cap \mathcal{F}_4$ "bound" the front $\mathcal{F}_4$ (so, we guess that the cut locus of the geodesics of the set Γ_f is contained in the union of these two lines); in the second one, it is the front $\mathcal{G}_4$ to be constrained (see Figure 6).

For this reason, we must study the two cases separately.

$A > 0$ The reasoning carried out few lines above suggests that, if $A > 0$, the (suspension of the) cut locus of the geodesics of the set Γ_f is contained in the union of the intersections $\mathcal{F}_4 \cap \mathcal{G}_4$ and $\bar{\mathcal{G}}_4 \cap \mathcal{F}_4$. In order to associate, with each geodesics, its cut point, we analyze the intersection among the suspension of three fronts $\mathcal{F}_4$, $\mathcal{G}_4$ and $\bar{\mathcal{G}}_4$. We find that, at time

$$\boldsymbol{T} = 8\zeta + \Big(\frac{8}{3}C_2 - 4A\Big)\zeta^3 + \mathcal{O}(\zeta^5)$$

the three fronts are intersecting at the point

$$\Big(-4A\zeta^3 - \frac{4}{3}\big(2E_1 + d_1\big)\zeta^4, 4A\zeta^3 - \frac{4}{3}\big(2E_2 + d_2\big)\zeta^4\Big). \tag{C.1}$$

The values of the corresponding adjoint vectors at time zero are respectively

$$\begin{aligned}
\boldsymbol{\mu}_f(0) &= -1 - 4C_2\zeta^2 + \mathcal{O}(\zeta^3)\\
\boldsymbol{\mu}_g(0) &= 1 + 4\big(E_1 + \frac{1}{3}D_1\big)\zeta^3 + \mathcal{O}(\zeta^4)\\
\boldsymbol{\mu}_{-g}(0) &= -1 + 8A\zeta^2 + \mathcal{O}(\zeta^3).
\end{aligned}$$

We can conclude that the geodesic associated with $\boldsymbol{\mu}_f(0) = (1, p_y^0, 1/\rho_0)$ loses its global optimality by intersecting the geodesics belonging to the set Γ_{-g} if $p_y^0 \in [-1, -1 - 4C_2\rho_0^2]$ (we took indeed $\zeta = \rho_0 + \mathcal{O}(\rho_0^2)$ here above), and those of the set Γ_g otherwise.

We now consider the geodesics of the set Γ_{-f}. We recall that, since, for all of them, the conjugate time coincides with the fifth switching time, the cut time could be greater than the fourth switching time. However, as the geodesics of the set Γ_{-f} cannot intersect neither those of the set Γ_f (see Appendix D-δ)-ε)) nor those of the set Γ_{-g} (because of (D.2)), we shall investigate their intersection with the trajectories of the set Γ_g.

From Appendix D-β) we see that the intersection $\mathcal{G}_4 \cap \bar{\mathcal{F}}_4$ involves only few geodesics of the set Γ_{-f}, that is, those associated with an adjoint vector $p_y^0 \sim -1$; thus, we must consider also the intersection $\mathcal{G}_4 \cap \bar{\mathcal{F}}_5$ (detailed in Appendix D-ι)). We can then conclude that all

geodesics of the set Γ_{-f} lose their optimality by intersecting the trajectories from Γ_g; those with $p_y^0 \in [1 + 4C_2\rho_0^2, 1]$ lose optimality before their fourth switching times, the other ones after it.

We are left to describe the Maxwell set associated with the geodesics of the sets $\Gamma_{\pm g}$. Part of their Maxwell locus is already contained in the intersections pointed out above; for geodesics intersecting close to the origin, we are considering the only other intersection involving fourth bang fronts, that is, $\mathcal{G}_4 \cap \bar{\mathcal{G}}_4$. Summing up, we can say that

- the geodesics of the set Γ_g with initial momentum $(p_x^0, 1, 1/\rho_0)$ lose their optimality during their fourth bang arc, when intersecting the fourth arcs of Γ_f (for $p_x^0 \in [1+4\big(E_1+\frac{D_1}{3}\big)\rho_0^2, 1]$), Γ_{-g} (for $p_x^0 \in [1 - 8A\rho_0^2, 1 + 4\big(E_1 + \frac{D_1}{3}\big)\rho_0^2, 1]$) and the trajectories of the set Γ_{-f}.
- the geodesics of the set Γ_{-g} with initial momentum $(p_x^0, -1, 1/\rho_0)$ lose their optimality during their fourth bang arc, when intersecting the fourth arcs of Γ_f (for $p_y^0 \in [-1+8A\rho_0^2, 1]$) and Γ_g, otherwise.

The suspension of the cut locus has three branches, each of that is at least C^1, at least up to the approximation in ζ that we considered. The graph of the suspension of the cut locus has been shown in Figure 8 (left), and the cut locus itself in Figure 10 (left).

$A < 0$ Looking at Figure 6, we guess that, when $A < 0$, the (suspension of the) cut locus for the geodesics of the set Γ_g is contained in the union of the intersections $\mathcal{F}_4 \cap \mathcal{G}_4$ and $\mathcal{G}_4 \cap \bar{\mathcal{F}}_4$. To determine exactly, for each geodesics, which intersections causes the loss of optimality, we proceed as above: we compare the suspension of the fronts (18), (20) and (22). By computations, we find that they meet at time $\boldsymbol{T} = 8\zeta + \big(\frac{8}{3}C_2 + 4A\big)\zeta^3 + \mathcal{O}(\zeta^5)$ at the point

$$\Big(4A\zeta^3 - \frac{4}{3}(2E_1 + \not{d}_1)\zeta^4, 4A\zeta^3 - \frac{4}{3}\big(2E_2 + \not{d}_2\big)\zeta^4\Big).$$

The values of the adjoint vectors at time zero are respectively $\boldsymbol{\mu}_f(0) = (1, \gamma, \rho_0)$, $\boldsymbol{\mu}_f(0) = (\beta, 1, \widetilde{\rho}_0)$ and $\boldsymbol{\mu}_{f-}(0) = (-1, \nu, \widetilde{\rho}_0)$, with $\rho_0, \widetilde{\rho}_0, \widehat{\rho}_0$ of order $\mathcal{O}(\zeta)$ and

$$\gamma_1 = \beta_1 = \nu_1 = 0$$
$$\gamma_2 = -4C_2 - 8A \quad \beta_2 = 0 \quad \nu_2 = 4C_2$$
$$\beta_3 = 4\big(E_1 + \frac{1}{3}D_1\big).$$

We can conclude that all geodesics of the set Γ_g with $p_x^0 \in [1 + 4(E_1 + D_1/3)\rho_0^3, 1]$ lose their optimality when intersecting the geodesics of the set Γ_f, whereas the others lose optimality by intersecting the geodesics of the set Γ_{-f}.

On the other hand, the geodesics of the set Γ_{-g} meet (before the conjugate time) only the geodesics of the set Γ_f: then, these intersections constitute their cut point.

Let us now focus on the geodesics of the set $\Gamma_{\pm f}$. First of all, we notice that the front $\mathcal{F}_4$ intersects both the fronts $\bar{\mathcal{F}}_4$ and $\bar{\mathcal{F}}_5$ (see Appendices D-δ)–D-ε)), while $A < 0$ forbids the intersection $\mathcal{G}_4 \cap \bar{\mathcal{F}}_5$. Moreover, equating the jets of the expressions (18), (23) and (21), we can prove that the three fronts $\mathcal{F}_4$, $\bar{\mathcal{G}}_4$ and $\bar{\mathcal{F}}_5$ meet at the point

$$\Big(-4A\zeta^3 - \frac{4}{3}(2E_1 + \not{d}_1)\zeta^4, -4A\zeta^3 - 2\big(2E_1 + D_1 - \frac{1}{3}\not{c}_1\big)\zeta^4\Big).$$

Indeed, putting $p_y^0 = -1$ in (21); $\gamma_1 = 0$, $\gamma_2 = -4C_2$ and $\gamma_3 = 4E_2 + \frac{4}{3}D_2$ in (18); $\eta_1 = \eta_2 = \eta_3 = 0$ in (23); $\boldsymbol{T} = 8\zeta + \big(4A + \frac{8}{3}C_2\big)\zeta^3$ in all of them, we see that the three expression are equal up to the third order in x, y and to the fourth order in ζ. We conclude that

- the geodesics of the set Γ_f with initial momentum $(1, p_y^0, \rho_0)$, with $p_y^0 \in [-1, -1 - 4C_2\rho_0^2 + 4(E_2 + D_2/3)\rho_0^3]$, lose optimality by intersecting the front $\bar{\mathcal{G}}_4$; those with $p_y^0 \in [-1 - 4(C_2 + 2A)\rho_0^2 + 4(E_2 + D_2/3)\rho_0^3, 1]$, by intersecting the front $\mathcal{G}_4$; the others, when they meet the geodesics of the set Γ_{-f}.
- the geodesics of the set Γ_{-f} with initial momentum $(-1, p_y^0, \rho_0)$ lose optimality in the following ways: for $p_y^0 \in [1 + 4(E_1 + \frac{1}{3}D_1)\rho_0^3, 1]$, intersecting, before the fourth switching time, the geodesics of the set Γ_g. The others, by intersecting the geodesics of the set Γ_f, after their fourth switching time if $p_y^0 \geq 1 + (8A + 4C_2)\rho_0^2$, before it otherwise.

As in the preceding case, the cut locus has three branches and each branch of the cut locus is at least C^1. Its suspension has been shown in Figure 8 (right).

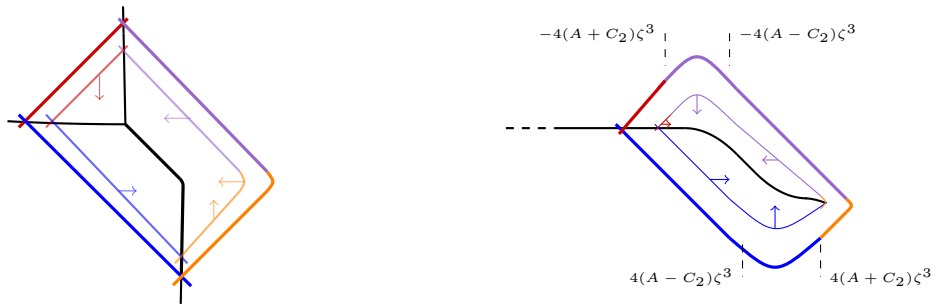

Figure 18: The formation of the cut locus in the cases A_- with $C_2 < 0$ and $A > 0$ (on the left) and A_- with $A > C_2 > 0$ (on the right). The arrows show the direction in which the front evolves in time; when the front self-intersects, it gives rise to the cut locus (shown in black). In red (respectively, blue, orange, purple) the front $\mathcal{F}$ (respectively $\mathcal{G}, \bar{\mathcal{F}}, \bar{\mathcal{G}}$)

$C_2 > 0$

When $C_2 > 0$, the conjugate time of the trajectories of the sets $\Gamma_{\pm g}$ coincide with their fifth switching time. Further, intersections of the kind $\mathcal{G}_4 \cap \bar{\mathcal{F}}_4$ and $\bar{\mathcal{G}}_4 \cap \mathcal{F}_4$ do not occur. Thus, in order to describe the cut locus, we must also consider the wavefront made by the geodesics in $\Gamma_{\pm g}$ that have already passed the fourth switching time. From equation (24), we can see that the front $\mathcal{G}_5$ is constrained between the vertical lines $\{x = 4(A-C_2)\zeta^3\}$ and $\{x = 4(A+C_2)\zeta^3\}$ (up to fourth order terms in ζ); for the fifth bang front $\bar{\mathcal{G}}_5$, an analogous bound holds. Then, to understand how the fronts coming from different strategies may intersect (and, in particular, if the intersection $\mathcal{G}_5 \cap \bar{\mathcal{G}}_5$ may occur), we must look at the relative values of A and C_2; we have four cases, all shown in Figure 9.

$A > C_2$ The suspension of the cut locus is a piecewise C^1 curve, composed by the concatenation of (pieces of) the following intersection between fronts:

$$\mathcal{F}_4 \cap \mathcal{G}_4, \quad \mathcal{G}_4 \cap \bar{\mathcal{G}}_5, \quad \mathcal{G}_4 \cap \bar{\mathcal{G}}_4, \quad \bar{\mathcal{G}}_4 \cap \mathcal{G}_5 \quad \bar{\mathcal{F}}_5 \cap \mathcal{G}_5.$$

In order to prove this, first of all we take advantage of the results of Section C.1, to conclude that all geodesics of the set Γ_f lose their optimality during the fourth bang arc, by intersections with the geodesics of Γ_g (as $C_2 > 0$ forbids the intersection with the front $\bar{\mathcal{G}}_4$ and $A > 0$ forbids those with the fronts $\bar{\mathcal{F}}_4$ and $\bar{\mathcal{F}}_5$).

We then focus on the geodesics of the set Γ_{-f}. We recall that the front $\bar{\mathcal{F}}_4$ cannot intersect neither the front $\mathcal{G}_4$ nor the front $\bar{\mathcal{G}}_4$; we thus consider also the intersections between $\bar{\mathcal{F}}_5$ and $\mathcal{G}_5$ (all computations were detailed at page 21).

Let us now concentrate on the geodesics of the set Γ_g. From Figure 18 (right), we see that the front arising from the geodesics of the set Γ_g may cross the fronts $\mathcal{F}_4, \bar{\mathcal{G}}_4, \bar{\mathcal{G}}_4$ and $\bar{\mathcal{F}}_5$; on the other hand, equation (27) tells that the geodesics that lose their optimality by intersecting the front $\mathcal{F}_4$ are those whose initial momentum $\boldsymbol{\mu}_g(0) = (p_x^0, 1, 1/\rho_0)$ satisfies $p_x^0 \in [1 - 4(E_1 + D_1/3)\rho_0^3, 1]$. To see what happens for $p_x^0 < 1 - 4(E_1 + D_1/3)\rho_0^3$ we now look at the intersection between the front $\mathcal{G}_4$ and the fronts $\bar{\mathcal{G}}_4$ and $\bar{\mathcal{G}}_5$; the detailed computations are provided, respectively, at page 21 and in the Appendix D-ζ).

From (D.9), we can see that the suspension of the first intersection describes, up to higher order terms in ζ, an arc of parabola (with concavity $-C_2$) connecting the points $(-4(A + C_2)\zeta^3, 4A\zeta^3)$ and $(-4(A-C_2)\zeta^3, 4(A-C_2)\zeta^3)$. From equation (D.8), we see that the geodesics of the set Γ_g involved in this intersection are those such that $p_x^0 \geq 1 - 4C_2\rho_0^2$.

Analogously, the suspension of the intersection $\bar{\mathcal{G}}_4 \cap \mathcal{G}_5$ (that can be recovered by applying to the intersection $\mathcal{G}_4 \cap \bar{\mathcal{G}}_5$ a rotation of π around the z axis and the corresponding permutation of the invariants ⧫), describes an arc of parabola of concavity C_2 connecting the points $(4(A - C_2)\zeta^3, -4(A - C_2)\zeta^3)$ and $(4(A + C_2)\zeta^3, -4A\zeta^3)$.

As we have already pointed out, the front $\bar{\mathcal{G}}_5$ is confined in the region $x < -4(A - C_2)\zeta^3$, and the front $\mathcal{G}_5$ in the region $x > 4(A - C_2)\zeta^3$; then, as $A > C_2$, to describe the part of the cut locus for $|x| < 4(A - C_2)\zeta^3$, we must also consider the intersection $\mathcal{G}_4 \cap \bar{\mathcal{G}}_4$. Equation (31)

tells us that the suspension of this intersection is indeed a segment that joins the points $(-4(A+C_2)\zeta^3, 4A\zeta^3)$ and $(-4(A-C_2)\zeta^3, 4(A-C_2)\zeta^3)$. We thus conclude that the geodesics of the set Γ_g (with $\boldsymbol{\mu}_g(0) = (p_x^0, 1, 1/\rho_0)$) lose optimality in the following ways:

- if $p_x^0 \geq 1 + 4(E_1 + 1/3D_1)\rho_0^3 + \mathcal{O}(\rho_0^4)$, the geodesic loses its optimality by intersecting $\mathcal{F}_4$.
- if $1-4C_2\rho_0^2 \leq p_x^0 \leq 1+4(E_1+1/3D_1)\rho_0^3$, then the geodesic loses its optimality by intersecting $\bar{\mathcal{G}}_5$ (see equation (D.9)).
- for $1-8A\rho_0^2 \leq p_x^0 \leq 1-4C_2\rho_0^2$, then the geodesic loses its optimality during its fourth bang arc, by intersecting $\bar{\mathcal{G}}_4$ (see equation (31)).
- all geodesics with $p_x^0 \leq -1+2\sqrt{\zeta}\sqrt{\frac{-D_1-3E_1}{3C_2}}$ lose their optimality during the fifth bang arc, by intersecting the front $\bar{\mathcal{F}}_5$ (see page 21);
- finally, all geodesics of the set Γ_g with $-1+2\sqrt{\zeta}\sqrt{\frac{-D_1-3E_1}{3C_2}} \leq p_x^0 \leq 1-8A\rho_0^2+\mathcal{O}(\rho_0^3)$ lose their optimality during the fifth bang arc, by intersecting the front $\bar{\mathcal{G}}_4$.

Last of all, the loss of optimality of the geodesics of the set Γ_{-g} is analogous to the one of the trajectories Γ_g (with the difference that they do not meet other trajectories than those of the set Γ_g).

The cut locus is shown in Figure 10 (right).

$0 < A < C_2$ This case is very similar to the precedent one, with one major exception: if $A < C_2$, then the intersection between the fourth arcs of the geodesics of the sets Γ_g and Γ_{-g} does not occur, so that we look at the intersection between the fronts $\mathcal{G}_5$ and $\bar{\mathcal{G}}_5$. Such intersections involve only those geodesics of the set Γ_{-g} that are associated with an initial covector $\boldsymbol{\mu}_{-g}(0) = (\eta, -1, 1/\rho_0)$ satisfying $\eta \geq 1-\frac{2A}{C_2}$; besides, the intersection $\mathcal{G}_5 \cap \bar{\mathcal{G}}_5$ requires $\eta \geq \frac{2A}{C_2} - 1$ to exist. Then, the cut locus contains: the part of $\mathcal{G}_4 \cap \bar{\mathcal{G}}_5$ between the points $(-4(A+C_2)\zeta^3, 4A\zeta^3)$ and $(4(A-C_2)\zeta^3, (-4A^2/C_2+4A)\zeta^3)$; the part of the intersection $\bar{\mathcal{G}}_4 \cap \mathcal{G}_5$ between the points $(4(A+C_2)\zeta^3, -4A\zeta^3)$ and $(-4(A-C_2)\zeta^3, (4A^2/C_2-4A)\zeta^3)$; the portion of the intersection between $\mathcal{G}_5 \cap \bar{\mathcal{G}}_5$ joining the points $(4(A-C_2)\zeta^3, (-4A^2/C_2+4A)\zeta^3)$ and $(-4(A-C_2)\zeta^3, (4A^2/C_2-4A)\zeta^3)$; this last part is a segment of slope $-A/C_2$.

Thus, the cut locus has one branch and is given by the concatenation of (pieces of) the following intersections:

$$\mathcal{F}_4 \cap \mathcal{G}_4, \quad \mathcal{G}_4 \cap \bar{\mathcal{G}}_5, \quad \mathcal{G}_5 \cap \bar{\mathcal{G}}_5, \quad \bar{\mathcal{G}}_4 \cap \mathcal{G}_5, \quad \bar{\mathcal{F}}_5 \cap \mathcal{G}_5.$$

It can be easily verified that all junctions are C^1, except the one involving $\bar{\mathcal{F}}_5 \cap \mathcal{G}_5$.

$-C_2 < A < 0$ We are showing that the cut locus has one branch and is given by the concatenation of (pieces of) the following intersections:

$$\mathcal{F}_4 \cap \mathcal{G}_4, \quad \mathcal{F}_4 \cap \mathcal{G}_5, \quad \mathcal{G}_5 \cap \bar{\mathcal{G}}_5, \quad \bar{\mathcal{F}}_4 \cap \bar{\mathcal{G}}_5, \quad \bar{\mathcal{F}}_5 \cap \bar{\mathcal{G}}_5.$$

We start by considering the geodesics of the set Γ_g; first of all, we notice that the intersections with the geodesics of the set Γ_{-f} are forbidden (see equation (D.4) and Appendix-D-ι)); on the other hand, the only allowed intersection between the geodesics of the sets Γ_g and Γ_{-g} is $\mathcal{G}_5 \cap \bar{\mathcal{G}}_5$ that involves only some of the geodesics of the set Γ_g (see Appendix-D-η)). Then, to detect the loss of optimality of the geodesics of the set Γ_g, we study their intersections with those of the set Γ_f. Consider the geodesics of the set Γ_g associated with the initial covector $\boldsymbol{\mu}_g(0) = (p_x^0, 1, 1/\rho_0)$. We already saw that those with $p_x^0 \geq 1 + 4\big(E_1 + D_1/3\big)\rho_0^3 + \mathcal{O}(\rho_0^4)$ are intersecting the front $\mathcal{F}_4$, before their fourth switching time; we now evaluate the intersection that may occur after the forth switching time (the details can be found in Section D-κ)). We find that these intersections occur, and cause a loss of global optimality, if $p_x^0 \in [1 + \frac{2A}{C_2}, 1 + 4\big(E_1 + D_1/3\big)\rho^3]$; equation (D.11) shows that the suspension (on the plane $\{z = 4\zeta^2\}$, with $\zeta = \rho_0 + \mathcal{O}(\rho_0^2)$) of this intersection describes an arc of parabola; in particular, the arc joining the points $(4(A-C_2)\zeta^3, 4A\zeta^3)$ and $(-4(A+C_2)\zeta^3, 4(A+A^2/C_2)\zeta^3)$ (corresponding respectively to $p_x^0 = 1 + \mathcal{O}(\rho_0^3)$ and to $p_x^0 = 1 + \frac{2A}{C_2}$) belongs to the cut locus.

We can repeat the same reasoning for the fronts $\bar{\mathcal{F}}_4$ and $\bar{\mathcal{G}}_5$ and see that the symmetric arc of parabola joining the points $(-4(A-C_2)\zeta^3, -4A\zeta^3)$ and $(4(A+C_2)\zeta^3, -4(A+A^2/C_2)\zeta^3)$ belongs to the cut locus.

Finally, all trajectories of the set Γ_g with $p_x^0 \in [-1, 1 + \frac{2A}{C_2}]$ lose their optimality along the fifth bang arc, by intersecting the fifth bang front $\bar{\mathcal{G}}_5$.

It is left to prove how the trajectories of the set Γ_{-f} with initial covector $(-1, p_y^0, \rho_0)$ and $p_y^0 \leq 1 + 8A\rho_0^3$ lose optimality. By geometric considerations on the position of the fronts, the only possibility is an intersection with the front $\bar{\mathcal{G}}_5$. To find such intersection, we proceed exactly as we did when studying the intersection $\bar{\mathcal{F}}_5 \cap \mathcal{G}_5$ (see page 21). As in that case, we obtain expressions for the intersection time and the momentum depending on powers of $\sqrt{\zeta}$. Thus, the suspension of the intersection is the parameterized curve

$$\begin{cases} x = -4(A - C_2)\zeta^3 - 4\sqrt{\frac{(2D_1 p_y^0 - D_1 - 3E_1)C_2}{3}}(1 + p_y^0)\zeta^{7/2} + \mathcal{O}(\zeta^4) \\ y = -4A\zeta^3 + \mathcal{O}(\zeta^4) \end{cases} \tag{C.2}$$

As above, we can prove that all the junctions, except the one with (C.2), are at least C^1, up to higher order terms.

$A < -C_2 < 0$ This case looks alike the precedent one; with respect to it, we spot two main differences: first of all, the intersection between the fronts $\mathcal{F}_4$ and $\mathcal{G}_5$ (as well as its symmetric) is allowed for every $p_x^0 \in [-1, 1]$ (p_x^0 denotes the first component of the adjoint covector associated at time 0 with the geodesic of the set Γ_g); also, the intersection between the fifth fronts of the geodesics of the sets Γ_g and Γ_{-g} does not occur: the part of the cut locus closer to the origin of the plane $\{z = 4\zeta^2\}$ is given by the intersection $\mathcal{F}_4 \cap \bar{\mathcal{F}}_4$, which is studied in Section D-δ).

The cut locus has one branch and is given by the concatenation of (pieces of) the following intersections:

$$\mathcal{F}_4 \cap \mathcal{G}_4, \quad \mathcal{F}_4 \cap \mathcal{G}_5, \quad \mathcal{F}_4 \cap \bar{\mathcal{F}}_4, \quad \bar{\mathcal{F}}_4 \cap \bar{\mathcal{G}}_5, \quad \mathcal{F}_5 \cap \bar{\mathcal{G}}_5.$$

Again, we can prove that all the junctions, except the one with (C.2), are C^1.

C.2 $0 < E_1 < D_1$ (case B_+)

When $\frac{|E_1|}{|D_1|} < 1$, the conjugate locus of the geodesics belonging to the sets $\Gamma_{\pm f}$ does not depend only on the values of the invariants, but also on the value of the associated adjoint vector at time 0. Moreover, the cut locus does not depend on the values of the two invariants C_2 and A only, but also on the ratio between E_1 and D_1, as it will be seen in the following. In particular, the last invariant that determines the shape of the cut locus is the ratio $\frac{3E_1}{D_1}$. We will study all the cases in details.

$C_2 < 0$

There are four subcases, depending on the values of $\frac{3E_1}{D_1}$ and of A. The suspensions of the cut loci have been illustrated in Figure 11.

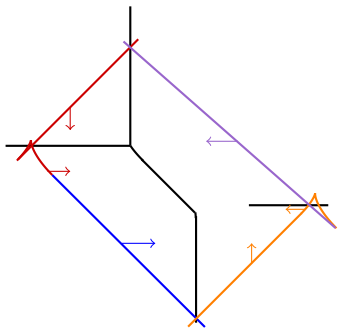

Figure 19: The formation of the cut locus in the case B_+ with $C_2 < 0$, $A > 0$ and $\frac{3E_1}{D_1} < 1$. The arrows show how the fronts deplace as time increases.

$A > 0$ For these values of the invariants, the evolution of the suspensions of the front as time increases is sketched in Figure 19. To understand how the whole front self-intersects,

we first concentrate on the geodesics of the set Γ_f. The "natural" intersection $\mathcal{F}_4 \cap \mathcal{G}_4$ does not occur, as condition (27) is never satisfied, but the front $\mathcal{F}_4$ does intersect the front $\mathcal{F}_5$. Moreover, the geodesics of the set Γ_f with p_y^0 close to -1 are also intersecting, before the fourth switching time, the front $\bar{\mathcal{G}}_4$ (as already seen in Section C.1); on the other hand, the intersection $\mathcal{F}_5 \cap \bar{\mathcal{G}}_4$ is allowed (see Appendix D-θ)). To understand which parts of these intersections actually belong to the cut locus, we search for an intersection of the three fronts: we fix some $\zeta > 0$ and a time $\boldsymbol{T} = 8\zeta + \mathcal{O}(\zeta^2)$, and we consider these three geodesics: the two geodesics (of the set Γ_f) with initial covector given respectively by $(1, \gamma, 1/\rho_0)$ and $(1, \widetilde{\gamma}, 1/\widetilde{\rho}_0)$ and the geodesic (of the set Γ_{-g}) geodesic with initial covector $(\eta, -1, 1/\widehat{\rho}_0)$, where $\rho_0, \widetilde{\rho}_0$ and $\widehat{\rho}_0$ are chosen in such a way that the third coordinate of each of the three trajectories equals $4\zeta^2$, up to sixth order powers of ζ. Imposing the equality (at each order of the jets) for the other coordinates, we find that the intersection occurs at time

$$\boldsymbol{T} = 8\zeta + \Big(\frac{8}{3}C_2 - 4A\Big)\zeta^3 - \frac{3(E_1 + D_1/3)^2}{2D_1}\zeta^4 + \mathcal{O}(\zeta^5)$$

and for

$$\gamma = -1 - 4C_2\zeta^2 + 4(E_2 + D_2/3)\zeta^3 + \mathcal{O}(\zeta^4)$$
$$\widetilde{\gamma} = \frac{1}{2} - \frac{3E_1}{2D_1} + \mathcal{O}(\zeta)$$
$$\eta = -1 + 8A\zeta^2 + \big(5E_1 + \frac{3E_1^2}{2D_1} + \frac{3D_1}{2}\big)\zeta^3 + \mathcal{O}(\zeta^4).$$

Summing up these elements, we can describe the cut points of the geodesics belonging to the set Γ_f. Let $\boldsymbol{\mu}_f(0) = (1, p_y^0, 1/\rho_0)$ be the associated adjoint vector; then:

- the geodesics with $p_y^0 \in [-1, -1 - 4C_2\rho_0^2)$ lose global optimality because of the intersection $\mathcal{F}_4 \cap \bar{\mathcal{G}}_4$.
- the geodesics with $p_y^0 \in [-1 - 4C_2\rho_0^2, \frac{1}{2} - \frac{3E_1}{2D_1})$ lose global optimality due to the intersection of $\mathcal{F}_4$ with $\mathcal{F}_5$, as described in Section 4.1.
- the geodesics with $p_y^0 \in (\frac{1}{2} - \frac{3E_1}{2D_1}, 1]$ lose global optimality during their fifth bang arc, by intersecting with the fourth bang of geodesics of the set Γ_{-g}.

For studying the geodesics of the set Γ_{-f}, we must distinguish the two cases in which $\frac{3E_1}{D_1} \geq 1$ or $\frac{3E_1}{D_1} < 1$. Indeed, in the first case, every geodesic in Γ_{-f} intersects, at (reparameterized) time $\mathcal{T} = 7 + p_y^0 + \mathcal{O}(\rho_0^2)$, the front $\bar{\mathcal{G}}_4$; in the second one, equation (D.2) is satisfied only for $p_y^0 \leq \frac{3E_1}{2D_1} + \frac{1}{2} < 1$.

Then, if $\frac{3E_1}{D_1} \geq 1$, all geodesics in the set Γ_{-f} lose optimality during their fourth bang arc: those with $p_y^0 \in [-1, 1+4C_2\rho_0^2]$ by intersecting $\bar{\mathcal{G}}_4$, those with $p_y^0 \in [1+4C_2\rho_0^2, 1]$ by intersecting $\mathcal{G}_4$. For what concerns the geodesics of the sets $\Gamma_{\pm g}$, we can adapt the demonstration done in Section C.1: more precisely, the geodesics of the set Γ_g lose their global optimality when intersecting the fourth front of geodesics of the sets Γ_{-f} or Γ_{-g}, the suspension of such intersections being respectively provided in equations (D.5) and (31). The geodesic of the set Γ_{-g} lose their global optimality when intersecting the geodesics of the sets Γ_f (equations (D.5) and (D.10)), Γ_g and Γ_{-f} (equation (30)). By direct computation of the tangents to the curves, we see that junction between the intersections $\mathcal{F}_5 \cap \bar{\mathcal{G}}_4$ and $\mathcal{G}_4 \cap \bar{\mathcal{G}}_4$ is C^1.

Let us now assume that $\frac{3E_1}{D_1} < 1$, which implies that equation (D.2) is satisfied only for $p_y^0 \leq \frac{3E_1}{2D_1} + \frac{1}{2} < 1$; in other words, a geodesic with initial adjoint vector $(-1, p_y^0, 1/\rho_0)$ may lose its global optimality before its fourth switching time only if $p_y^0 \leq \frac{3E_1}{2D_1} + \frac{1}{2}$ or $p_y^0 \geq 1 + 4C_2\rho_0^2$: indeed, the front $\bar{\mathcal{F}}_4$ cannot intersect $\mathcal{F}_4$ or $\mathcal{F}_5$, because $A > 0$, and we can neglect eventual intersections with the fronts $\mathcal{G}_5$ and $\bar{\mathcal{G}}_5$, which are not optimal. So, to figure out what happens if $p_y^0 \in [\frac{1}{2} + \frac{3E_1}{2D_1}, 1 + 4C_2\zeta^2]$, we must study the front $\bar{\mathcal{F}}_5$.

Equation (21) shows that the suspension of the front $\bar{\mathcal{F}}_5$ is contained in a horizontal strip of width $\mathcal{O}(\zeta^4)$ centered about $\{y = -4A\zeta^3\}$. This suggests to study its intersection with the fourth bang front of the trajectories Γ_g; from Appendix D-ι), we see that it is an arc of curve of length $\mathcal{O}(\zeta^4)$ that connects the parts of the intersections $\mathcal{G}_4 \cap \bar{\mathcal{G}}_4$ and $\bar{\mathcal{F}}_5 \cap \mathcal{G}_4$.

Computing the slope of the tangent to the curve (D.10), we can see the suspension of the cut locus is at least C^1 (up to the third order in ζ) at the junction between $\bar{\mathcal{F}}_5 \cap \mathcal{G}_4$ and $\mathcal{G}_4 \cap \bar{\mathcal{G}}_4$.

Summing up, differently from the case $\frac{3E_1}{D_1} \geq 1$, the suspension of the cut locus is *disconnected*, with one connected component made by only one branch, and the other one made by three branches, one of which is not C^1.

$A < 0$ In this case, the existence condition for the intersection of the fronts $\mathcal{F}_5$ and $\bar{\mathcal{G}}_4$ is violated; our first concern is then to understand how the geodesics of the set Γ_f with $p_y^0 \geq \frac{1}{2} - \frac{3E_1}{2D_1}$ lose optimality. Inspired by the case $\boldsymbol{A}_-$ with both C_2 and A negative, where a piece of the intersection between the (suspension of the) fronts $\mathcal{F}_4$ and $\bar{\mathcal{F}}_4$ participates to the cut locus, we look at the intersection between the fronts $\mathcal{F}_5$ and $\bar{\mathcal{F}}_4$; from (D.7), we see that this intersection occurs at time $\boldsymbol{T} = 8\rho_0 + \mathcal{O}(\rho_0^2)$, while the self-intersection between the fronts $\mathcal{F}_4$ and $\mathcal{F}_5$ at time $\boldsymbol{T} = (7 - \gamma_0)\rho_0 + \mathcal{O}(\rho_0^2)$ (equation (36)), with $\gamma_0 \geq -1$; then, for $p_y^0 \in [-\frac{E_1}{D_1}, \frac{1}{2} - \frac{3E_1}{2D_1}]$, the intersection with the front $\mathcal{F}_4$ occurs before, and thus belongs to the cut locus.

Summing up, we can distinguish two cases; if $\frac{3E_1}{D_1} \geq 1$, then the cut locus is connected and made of five C^1 branches. More precisely:

- as it occurs in the case A_-, with $C_2 < 0$ and $A < 0$, the geodesics of the set Γ_f with initial adjoint vector $(1, p_y^0, 1/\rho_0)$ and $p_y^0 \in [-1, -1-4(2A+C_2)\zeta^2)$ lose their optimality before the fourth switching time, by intersecting the front $\bar{\mathcal{F}}_4$; if $p_y^0 \in (-1 - (4C_2 + 8A)\zeta^2, \frac{1}{2} - \frac{3E_1}{2D_1})$, then the geodesics lose optimality because of the self intersection $\mathcal{F}_4 \cap \mathcal{F}_5$; finally, if $p_y^0 \in (\frac{1}{2} - \frac{3E_1}{2D_1}, 1]$, they lose optimality after the fourth switching time, intersecting $\bar{\mathcal{F}}_4$.
- the geodesics of the set Γ_{-f} associated with an adjoint vector at time zero equal to $\boldsymbol{\mu}_{-f}(0) = (-1, p_y^0, 1/\rho_0)$ and $p_y^0 \in (1 + 4C_2\zeta^2 + 4(E_2 + D_2/3)\zeta^3, 1]$ lose optimality by intersecting $\mathcal{G}_4$; those with $p_y^0 \in (1 + 4C_2\zeta^2 + 4(E_2 + D_2/3)\zeta^3, 1]$, by intersecting $\mathcal{F}_5$; those with $p_y^0 \in (1 + 4(2A + C_2)\zeta^2, 1 + 4C_2\zeta^2)$, by intersecting $\mathcal{F}_4$; finally, for $p_y^0 \in [-1, 1 + 4(2A + C_2)\zeta^2]$, intersecting the front $\bar{\mathcal{G}}_4$.
- the geodesics of the kind $\Gamma_{\pm g}$ lose optimality during the fourth bang arc, by intersecting, respectively, the front $\bar{\mathcal{F}}_4$ or both fronts $\bar{\mathcal{F}}_4$ and $\mathcal{F}_4$.

If $\frac{3E_1}{D_1} < 1$, the suspension of the cut locus is disconnected and made by two connected components. The main difference with respect to the preceding case ($\frac{3E_1}{D_1} \geq 1$) is that the geodesics of the set Γ_{-f} associated with an initial covector $(-1, p_y^0, 1/\rho_0)$ with $p_y^0 \in (\frac{1}{2} + \frac{3E_1}{2D_1}, 1 + 4(2A + C_2)\zeta^2)$ are not intersecting the front $\bar{\mathcal{G}}_4$. As the intersections of the front $\bar{\mathcal{F}}_4$ with the fronts $\mathcal{G}_4$, $\mathcal{F}_4$ and $\mathcal{F}_5$ occur for p_y^0 close to -1, the only option left is the intersection $\bar{\mathcal{F}}_5 \cap \mathcal{F}_4$, which is studied in Appendix D-ε). In particular, its tangent for $p_y^0 = \frac{1}{2} + \frac{3E_1}{2D_1}$ has slope $-\frac{2D_1}{3(E_1+D_1)}$, which shows that the junction with $\mathcal{F}_4 \cap \bar{\mathcal{F}}_4$ is not C^1.

$C_2 > 0$

To describe the cut locus when $C_1 = 0$, $D_1 > E_1 > 0$ and $C_2 > 0$, we can rely on the analysis carried out up to now; as could be expected, the shape of the cut locus depends on the relative values of the invariants A and C_2 and on the value of $\frac{3E_1}{D_1}$. We are thus studying them separately. The main differences with the cases studied in Section C.1 involve the cut locus of the geodesics of the sets $\Gamma_{\pm f}$.

The suspensions of the cut loci have been illustrated in Figure 13 (cases with $\frac{3E_1}{D_1} \geq 1$) and 14 (cases with $\frac{3E_1}{D_1} < 1$).

$A > C_2$ As already proved, the geodesics of the set Γ_f with initial covector $(1, p_y^0, 1/\rho_0)$ and $p_y^0 \in \big[-1, \frac{1}{2} - \frac{3}{2}\frac{E_1}{D_1}\big]$ lose their optimality because of the intersection of the fronts $\mathcal{F}_4$ and $\mathcal{F}_5$; what happens for the geodesics with $p_y^0 \geq \frac{1}{2} - \frac{3}{2}\frac{E_1}{D_1}$? To answer this question, we recall that the intersection $\bar{\mathcal{G}}_4 \cap \mathcal{F}_4$ does not occur (because $C_2 > 0$), we observe that the front $\bar{\mathcal{G}}_5$ remains "on the left" of the front $\mathcal{G}_5$ (as $A > 0$) and, relying on the computations made in Section C.1, we remark that the intersection $\bar{\mathcal{G}}_5 \cap \mathcal{G}_4$ occurs (and will likely participate to the cut locus). This suggests to investigate the intersection between $\bar{\mathcal{G}}_5$ and $\mathcal{F}_5$. To do it, we can repeat the procedure already carried out for the analysis of the intersections $\mathcal{G}_5 \cap \bar{\mathcal{F}}_5$ and

$\bar{\mathcal{F}}_5 \cap \bar{\mathcal{G}}_5$; we obtain that the suspension of this intersection is the parameterized curve

$$\begin{cases} x = -4(A + C_2)\zeta^3 + 4(1 + p_y^0)C_2\sqrt{\frac{3E_1 - D_1 + 2D_1 p_y^0}{3C_2}}\zeta^{7/2} + \mathcal{O}(\zeta^4) \\ y = 4A\zeta^3 + \mathcal{O}(\zeta^4), \end{cases}$$

for $p_y^0 \in \left(\frac{1}{2} - \frac{3E_1}{2D_1}, 1\right]$. Summing up, we can conclude that the geodesics of the set Γ_f with $p_y^0 \in \left[-1, \frac{1}{2} - \frac{3E_1}{2D_1}\right]$ lose their optimality because of the self-intersection between $\mathcal{F}_4$ and $\mathcal{F}_5$, and those with $p_y^0 \in \left(\frac{1}{2} - \frac{3E_1}{2D_1}, 1\right]$ lose optimality after their fourth switching time, by intersecting with the (fifth front) of the geodesics of the set Γ_{-g}.

For what concerns the cut locus of the geodesics of the set Γ_{-f}, it depends on the value of $\frac{3E_1}{D_1}$; indeed, if $\frac{3E_1}{D_1} \geq 1$, then all Γ_{-f} geodesics lose their optimality before the fourth switching time, by intersecting with (the fourth arc of) the geodesics with of the set Γ_{-g}; if instead $\frac{3E_1}{D_1} < 1$, then only the geodesics with $p_y^0 \in \left[-1, \frac{1}{2} + \frac{3E_1}{2D_1}\right]$ lose their optimality by intersecting with (the fourth arc of) the geodesics of the set Γ_{-g}, whereas those with $p_y^0 \in \left(\frac{1}{2} + \frac{3E_1}{2D_1}, 1\right]$ lose their optimality after the fourth switching time, by intersecting the geodesics of the set Γ_g, as already seen in Section C.2.

The remaining part of the cut locus is completely analogous of the one studied in Section C.1, therefore we do not repeat its description. We can conclude that, if $\frac{3E_1}{D_1} \geq 1$, the suspension of the cut locus is connected and composed by a single branch, whereas if $\frac{3E_1}{D_1} < 1$, the suspension of the cut locus is composed by two connected components. In both cases, they are piecewise C^1.

$0 < A < C_2$ This case is very similar to the precedent one, with the sole exception that, as already remarked in Section C.1, the fronts $\mathcal{G}_4$ and $\bar{\mathcal{G}}_4$ do not intersect, while $\mathcal{G}_5$ and $\bar{\mathcal{G}}_5$ do.

Thus, if $\frac{3E_1}{D_1} \geq 1$, the cut locus is made by the concatenation of pieces of the following intersections

$$\mathcal{F}_4 \cap \mathcal{F}_5 \quad \mathcal{F}_5 \cap \bar{\mathcal{G}}_5 \quad \mathcal{G}_4 \cap \bar{\mathcal{G}}_5 \quad \mathcal{G}_5 \cap \bar{\mathcal{G}}_5 \quad \bar{\mathcal{G}}_4 \cap \mathcal{G}_5 \quad \bar{\mathcal{F}}_4 \cap \bar{\mathcal{G}}_4$$

and it is piecewise C^1.

If $\frac{3E_1}{D_1} < 1$, the suspension of the cut locus is disconnected; one connected component is made by the concatenation of the intersections

$$\mathcal{F}_4 \cap \mathcal{F}_5 \quad \mathcal{F}_5 \cap \bar{\mathcal{G}}_5 \quad \mathcal{G}_4 \cap \bar{\mathcal{G}}_5 \quad \mathcal{G}_5 \cap \bar{\mathcal{G}}_5 \quad \bar{\mathcal{G}}_4 \cap \mathcal{G}_5 \quad \bar{\mathcal{F}}_5 \cap \mathcal{G}_5$$

and is piecewise smooth; the other connected component is the intersection $\bar{\mathcal{F}}_4 \cap \bar{\mathcal{G}}_4$.

$-C_2 < A < 0$ We start by recalling that, for these values of the invariants, the front $\mathcal{F}_4$ is intersecting the front $\mathcal{G}_5$ (see Appendix D-κ)); this intersection involves the geodesics belonging to the set Γ_f with p_y^0 close to -1. On the other hand, the geodesics with $p_y^0 \in [-1, \frac{1}{2} - \frac{3E_1}{2D_1}]$ are involved in the intersection $\mathcal{F}_4 \cap \mathcal{F}_5$, analyzed in the previous sections.

To detect the cut points of the geodesics of the set Γ_f with $p_y^0 \geq \frac{1}{2} - \frac{3E_1}{2D_1}$, we investigate the intersection between the fronts $\mathcal{F}_5$ and $\mathcal{G}_5$. Following the same approach adopted, for instance, when studying the intersection $\bar{\mathcal{F}}_5 \cap \mathcal{G}_5$ (page 21), we can describe the suspension of such intersection as the curve

$$\begin{cases} x = 4(A - C_2)\zeta^3 - 4(1 - p_y^0)\sqrt{\frac{(3E_1 + D_1 + 2D_1 p_y^0)C_2}{3}}\zeta^{7/2} + \mathcal{O}(\zeta^4) \\ y = 4A\zeta^3 + \mathcal{O}(\zeta^4), \end{cases}$$

parameterized by $p_y^0 \in \left[\frac{1}{2} + \frac{3E_1}{2D_1}, 1\right]$.

Concerning the geodesics of the set Γ_{-f}, we still must distinguish the two cases $\frac{3E_1}{D_1} \geq 1$ and $\frac{3E_1}{D_1} < 1$. In the first one, all geodesics lose optimality before the fourth switching time: those with $p_y^0 \in [-1, 1 + 8A\rho_0^2]$ by intersecting $\bar{\mathcal{G}}_4$, the ones with $p_y^0 \in [1 + 8A\rho_0^2, 1]$ by intersecting $\bar{\mathcal{G}}_5$ (see Appendix D-β)).

If $\frac{3E_1}{D_1} < 1$, then only the geodesics with $p_y^0 \leq \frac{1}{2} + \frac{3E_1}{2D_1}$ lose optimality before the fourth switching time, intersecting $\bar{\mathcal{G}}_4$; on the other hand, those with $p_y^0 \in [1 + 8A\rho_0^2, 1]$ still intersect the front $\bar{\mathcal{G}}_5$, before their fourth switching time. The geodesics with $p_y^0 \in \left[\frac{1}{2} + \frac{3E_1}{2D_1}, 1 + 8A\rho_0^2\right]$ lose optimality because of the intersection between the fronts $\bar{\mathcal{F}}_5$ and $\bar{\mathcal{G}}_5$, as already seen in Section C.1.

The rest of the cut locus is, as in the case A_-, $-C_2 < A < 0$, given by the intersection of $\mathcal{G}_4 \cap \bar{\mathcal{G}}_4$.

Summing up, if $\frac{3E_1}{D_1} \geq 1$, the suspension of the cut locus is connected and given by three C^1 branches; if $\frac{3E_1}{D_1} < 1$, the cut locus is composed by two connected components.

$A < -C_2 < 0$ This last case can be deduced by gathering the arguments used to study the precedent cases. In particular, the only difference with the case just analyzed ($-C_2 < A < 0$) involves the "central part" of the (suspension of the) cut locus, which is made by the concatenation of the intersections $\mathcal{F}_4 \cap \mathcal{G}_5$, $\mathcal{F}_4 \cap \bar{\mathcal{F}}_4$ and $\bar{\mathcal{F}}_4 \cap \bar{\mathcal{G}}_5$. More precisely:

- the geodesics of the set Γ_f associated with the adjoint vector $\boldsymbol{\mu}_f(0) = (1, p_y^0, 1/\rho_0)$, with $p_y^0 \in [-1, -1 - 8(A + C_2)\rho_0^2]$, lose optimality by intersection with the fourth bang arc $\bar{\mathcal{F}}_4$; those with $p_y^0 \in [-1 - 8(A + C_2)\rho_0^2, -1 - 8A\rho_0^2]$, by intersection with the fifth bang arc $\mathcal{G}_5$; for $p_y^0 \in \big[-1 - 8A\rho_0^2, \frac{1}{2} - \frac{3E_1}{2D_1}\big]$, because of the self intersection between $\mathcal{F}_4$ and $\mathcal{F}_5$; finally, those with $p_y^0 \in \big[\frac{1}{2} - \frac{3E_1}{2D_1}, 1\big]$ lose optimality after the fourth switching time, by intersection with $\mathcal{G}_5$, as described above.
- analogously, the geodesics of the set Γ_{-f} with initial adjoint vector $\boldsymbol{\mu}_{-f}(0) = (-1, p_y^0, 1/\rho_0)$, with $p_y^0 \in [1 + 8(A + C_2)\rho_0^2, 1]$, lose optimality by intersection with the fourth bang arc $\mathcal{F}_4$, and those with $p_y^0 \in [1 + 8A\rho_0^2, 1 + 8(A + C_2)\rho_0^2]$ by intersection with the fifth bang arc $\bar{\mathcal{G}}_5$. For $p_y^0 \leq 1 + 8A\rho_0^2$, we must distinguish the cases: if $\frac{3E_1}{D_1} \geq 1$, then all geodesics lose optimality by intersecting $\bar{\mathcal{G}}_4$, whereas, if $\frac{3E_1}{D_1} < 1$, only the geodesics with $p_y^0 \leq \frac{1}{2} + \frac{3E_1}{2D_1}$ lose optimality in this way; those with $p_y^0 \in \big[\frac{1}{2} + \frac{3E_1}{2D_1}, 1 + 8A\rho_0^2\big]$ lose optimality after the fifth bang arc, by intersecting $\bar{\mathcal{G}}_5$ (see equation C.2).

C.3 $-D_1 < E_1 < 0$ (case $\boldsymbol{B_-}$)

The last case we consider is the one in which $|D_1| > |E_1|$, but the two invariants have opposite sign; in particular, we assume that D_1 is positive and E_1 negative.

A coarse analysis reveals that the major differences between the case B_- and the case B_+ involve the geodesics of the set Γ_f, as, if $\frac{3E_1}{D_1} < -1$, then a part of the front $\mathcal{F}_4$ intersects the front $\mathcal{G}_4$. Assume indeed that $\frac{3E_1}{D_1} < -1$, and consider the self intersection of the front of the geodesics of the set Γ_f (equation (35)); from the fact that $\gamma_0 \leq \eta$, we see that γ_0 must be greater than or equal to $-\frac{3E_1}{D_1} - 2$ (which is strictly greater than -1): the geodesics with initial covector $p_y^0 \leq -\frac{3E_1}{D_1} - 2$ are not involved in this intersection. On the other hand, (28) states that the intersection between the fourth bang fronts of Γ_f and Γ_g trajectories may occur only if $p_y^0 \leq -\frac{3E_1}{D_1} - 2$, and the suspension of this intersection is a horizontal segment joining the points $\big((\frac{3E_1}{D_1} + 1)\zeta, 4A\zeta^3\big)$ and $\big(-4(A + C_2)\zeta^3, 4A\zeta^3\big)$. This suggests that the only geodesics of the set Γ_f losing optimality after the fourth switching time are those with $p_y^0 \in [-\frac{E_1}{D_1}, \frac{1}{2} - \frac{3E_1}{2D_1}]$, which are involved in the intersection $\mathcal{F}_4 \cap \mathcal{F}_5$ and, to describe the cut locus close to the origin of the plane $\{z = 4\zeta^2\}$ (that is, in a ball of radius $\mathcal{O}(\zeta^3)$), we must concentrate on the front $\mathcal{F}_4$ only.

In instead $\frac{3E_1}{D_1} \geq -1$, then the behavior of the geodesics of the set Γ_f is not much different from the one described in Section C.2.

The other difference with the precedent cases is that $\frac{3E_1}{2D_1} + \frac{1}{2} < 1$, which implies that the intersection of a geodesics of the set Γ_{-f}, with initial covector $(-1, p_y^0, 1/\rho_0)$, with one of the set Γ_{-g} is possible only if $p_y^0 \in \big[-1, \frac{3E_1}{2D_1} + \frac{1}{2}\big]$; as already seen in Section C.2, the suspension of this intersection is, up to higher order terms in ζ, a segment of length $\frac{3}{2}(1 + \frac{E_1}{D_1})\zeta$ and constitutes a connected component of the cut locus. Then, in the case $\boldsymbol{B_-}$ the suspension of the cut locus is always disconnected.

A detailed analysis of the cut locus in the 12 different sub-cases of the case $\boldsymbol{B_-}$ is not necessary, as it can easily be deduced from the preceding ones. For the sake of completeness, we just give, here below, a brief description.

$C_2 < 0$

When C_2 is negative, the cut locus has two connected components, one composed by three piecewise-smooth branches, the other one constituted by one smooth branch. We have four

possible cases, depending on the value of A and $\frac{3E_1}{D_1} \geq -1$. The suspension of the cut locus is plot in Figure 15.

$A > 0$ As already anticipated at the beginning of the section, if $\frac{3E_1}{D_1} \geq -1$ the cut locus is very similar to the one shown in Figure 11 (right). Indeed, all geodesics of the set Γ_f with initial covector $p_y^0 \in [-1, -\frac{3E_1}{2D_1} + \frac{1}{2}]$ lose optimality because of the self-intersection $\mathcal{F}_4 \cap \mathcal{F}_5$, as already seen before; those with $p_y^0 \in [-\frac{3E_1}{2D_1} + \frac{1}{2}, 1]$ intersect the fourth bang arc of the geodesics of the set Γ_{-g}.

The geodesics of the set Γ_{-f} associated with the covector $\boldsymbol{\mu}_{-f}(0) = (-1, p_y^0, 1/\rho_0)$, with $p_y^0 \in [-1, \frac{3E_1}{2D_1} + \frac{1}{2}]$, lose optimality when they intersect the fourth bang front $\bar{\mathcal{G}}_4$ (equation (D.3)); the suspension of this intersection is, up to higher order terms in ζ, a segment of length $\frac{3}{2}(1 + \frac{E_1}{D_1})\zeta$ and constitute one connected component of the cut locus. On the other hand, the geodesics of the set Γ_{-f} with $p_y^0 \geq \frac{3E_1}{2D_1} + \frac{1}{2}$ lose optimality after the fourth switching time, by intersecting the front $\mathcal{G}_4$. Finally, the geodesics of the sets $\Gamma_{\pm g}$ lose optimality during their fourth bang arc.

When $\frac{3E_1}{D_1} < -1$, the geodesics of the set Γ_f involved in the intersection $\mathcal{F}_4 \cap \mathcal{F}_5$ are only those that with initial covector $p_y^0 \in [-\frac{3E_1}{D_1} - 2, 1]$; those with $p_y^0 \in [-1 + 8A\rho_0^2, -\frac{3E_1}{D_1} - 2]$ lose optimality when intersecting the front $\mathcal{G}_4$.

$A < 0$ As when $\frac{3E_1}{D_1} \geq -1$ the cut locus is almost identical to the one shown in Figure 11 (down), we describe in details only the case in which $\frac{3E_1}{D_1} < -1$.

Consider a geodesic of the set Γ_f, associated with the adjoint vector $\boldsymbol{\mu}_f(0) = (1, p_y^0, 1/\rho_0)$, and assume that $\frac{3E_1}{D_1} < -1$; we have that

- if $p_y^0 \in \big[-\frac{3E_1}{2D_1} + \frac{1}{2}, 1\big]$, then the geodesic loses optimality during its fifth bang arc, by intersection with the front $\bar{\mathcal{F}}_4$ (see Appendix D-ε));
- if $p_y^0 \in \big(-1, \frac{3E_1}{2D_1} + \frac{1}{2}\big]$, the geodesics loses optimality because of the self intersection of the fronts $\mathcal{F}_4$ and $\bar{\mathcal{F}}_5$.

For what concerns the geodesics of the set Γ_{-f}, they lose optimality in the following way, according to the value of the initial covector $(-1, p_y^0, 1/\rho_0)$:

- if $p_y^0 \in \big[-1, \frac{3E_1}{2D_1} + \frac{1}{2}\big]$, during their fifth bang arc, by intersection with the front $\bar{\mathcal{G}}_4$;
- for $p_y^0 \in \big[\frac{3E_1}{2D_1} + \frac{1}{2}, 1 + 4(2A + C_2)\rho_0^2\big]$, during their fifth arc, by intersection with the front $\mathcal{F}_4$;
- for $p_y^0 \geq 1 + 4(2A + C_2)\rho_0^2$, again by intersection with the front $\mathcal{F}_4$, but before their fourth switching time.

$C_2 > 0$

If $\frac{3E_1}{D_1} \geq -1$, the suspension of the cut locus is very similar to the one, corresponding to the same relative values of A and C_2, shown in Figure 14. More difference with the precedent cases arise when $\frac{3E_1}{D_1} < -1$; these last cases are described in more details and shown in Figure 17.

$A > C_2$ If $\frac{3E_1}{D_1} \geq -1$ the suspension of the cut locus is given by the concatenation of (pieces of) the following intersections:

$$\mathcal{F}_4 \cap \mathcal{F}_5, \quad \mathcal{F}_5 \cap \bar{\mathcal{G}}_5, \quad \mathcal{G}_4 \cap \bar{\mathcal{G}}_5, \quad \mathcal{G}_4 \cap \bar{\mathcal{G}}_4, \quad \bar{\mathcal{G}}_4 \cap \bar{\mathcal{G}}_5, \quad \bar{\mathcal{F}}_5 \cap \mathcal{G}_5$$

plus the connected component $\bar{\mathcal{F}}_4 \cap \bar{\mathcal{G}}_4$.

On the other hand, if $\frac{3E_1}{D_1} < -1$, then the intersection between the fronts $\mathcal{F}_5$ and $\bar{\mathcal{G}}_5$ does not occur; then, the geodesics of the set Γ_f associated with $p_y^0 \in [-\frac{3E_1}{D_1} - 2, 1]$ lose their optimality at the self intersection $\mathcal{F}_4 \cap \mathcal{F}_5$, while those associated with $p_y^0 \in [-1, -\frac{3E_1}{D_1} - 2]$ lose optimality when intersecting the front $\mathcal{G}_4$. The cut locus is thus given by the concatenation

$$\mathcal{F}_4 \cap \bar{\mathcal{F}}_5, \quad \mathcal{F}_4 \cap \mathcal{G}_4, \quad \mathcal{G}_4 \cap \bar{\mathcal{G}}_5, \quad \mathcal{G}_4 \cap \bar{\mathcal{G}}_4, \quad \bar{\mathcal{G}}_4 \cap \mathcal{G}_5, \quad \bar{\mathcal{F}}_5 \cap \mathcal{G}_5,$$

plus the connected component $\bar{\mathcal{F}}_4 \cap \bar{\mathcal{G}}_4$.

$0 < A < C_2$ The only difference between this case and the precedent one is that the intersection $\mathcal{G}_4 \cap \bar{\mathcal{G}}_4$ does not participate to the cut locus, and that the intersection of the fronts $\mathcal{G}_4$

and $\bar{\mathcal{G}}_5$ is optimal only if the first component p_x^0 of the initial covector $\boldsymbol{\mu}_g(0)$ associated with the geodesic belonging to the set Γ_g satisfies $p_x^0 \leq \frac{2A}{C_2} - 1$ (as already discussed at page 43).

Then, if $\frac{3E_1}{D_1} \geq -1$, the suspension of the cut locus is given by the concatenation of (pieces of) the intersections

$$\mathcal{F}_4 \cap \mathcal{F}_5, \quad \mathcal{F}_5 \cap \bar{\mathcal{G}}_5, \quad \mathcal{G}_4 \cap \bar{\mathcal{G}}_5, \quad \mathcal{G}_5 \cap \bar{\mathcal{G}}_5, \quad \bar{\mathcal{G}}_4 \cap \mathcal{G}_5, \qquad \mathcal{G}_5 \cap \bar{\mathcal{F}}_5$$

plus the connected component $\bar{\mathcal{F}}_4 \cap \bar{\mathcal{G}}_4$.

If instead $\frac{3E_1}{D_1} < -1$, the geodesics of the set Γ_f with initial momentum $p_y^0 \in [-\frac{3E_1}{D_1} - 2, 1]$ lose their optimality at the self intersection $\mathcal{F}_4 \cap \mathcal{F}_5$, while those with $p_y^0 \in [-1, -\frac{3E_1}{D_1} - 2]$ lose optimality when intersecting the front $\mathcal{G}_4$. The cut locus is thus given by the concatenation of (pieces of) the intersections

$$\mathcal{F}_4 \cap \mathcal{F}_5, \quad \mathcal{F}_4 \cap \mathcal{G}_4, \quad \mathcal{G}_4 \cap \bar{\mathcal{G}}_5, \quad \mathcal{G}_5 \cap \bar{\mathcal{G}}_5, \quad \bar{\mathcal{G}}_4 \cap \mathcal{G}_5, \quad \bar{\mathcal{F}}_5 \cap \mathcal{G}_5,$$

and the connected component $\bar{\mathcal{F}}_4 \cap \bar{\mathcal{G}}_4$.

$-C_2 < A < 0$ If $\frac{3E_1}{D_1} \geq -1$ the suspension of the cut locus is disconnected: one connected component is made by the intersection of the geodesics of the set Γ_{-f} with initial momentum $p_y^0 \in \big[-1, -\frac{1}{2} - \frac{3E_1}{2D_1}\big]$ with the front $\bar{\mathcal{G}}_4$; the other connected component is made by 3 branches, meeting (in the plane $\{z = 4\zeta^2\}$) at the point $(4(A-C_2)\zeta^3, 4A\zeta^3)$: the self intersection $\mathcal{F}_4 \cap \mathcal{F}_5$, the intersection $\mathcal{F}_5 \cap \mathcal{G}_5$ and the concatenation of the intersections

$$\mathcal{F}_4 \cap \mathcal{G}_5, \quad \mathcal{G}_5 \cap \bar{\mathcal{G}}_5, \quad \bar{\mathcal{F}}_5 \cap \bar{\mathcal{G}}_5.$$

If $\frac{3E_1}{D_1} < -1$, as seen above, then the self intersection $\mathcal{F}_4 \cap \mathcal{F}_5$ involves only the geodesics with initial momentum $p_y^0 \in \big[-\frac{3E_1}{D_1} - 2, 1\big]$; moreover, the intersection between the fifth front of the geodesics of the sets Γ_f and Γ_g does not occur. The cut locus is thus made by two connected components: one is the intersection $\bar{\mathcal{F}}_4 \cap \bar{\mathcal{G}}_4$; the other one, the concatenation of the intersections

$$\mathcal{F}_4 \cap \bar{\mathcal{F}}_5, \quad \mathcal{F}_4 \cap \mathcal{G}_4, \quad \mathcal{F}_4 \cap \mathcal{G}_5, \quad \mathcal{G}_5 \cap \bar{\mathcal{G}}_5, \quad \bar{\mathcal{F}}_4 \cap \bar{\mathcal{G}}_5 \quad \bar{\mathcal{F}}_5 \cap \bar{\mathcal{G}}_5.$$

$-A < -C_2 < 0$ If $\frac{3E_1}{D_1} \geq -1$ the cut locus is completely analogous to the corresponding one depicted in Figure 14.

If instead $\frac{3E_1}{D_1} < -1$, then the cut locus is thus made by two connected components: the intersection $\bar{\mathcal{F}}_4 \cap \bar{\mathcal{G}}_4$ and the concatenation of the intersections

$$\mathcal{F}_4 \cap \bar{\mathcal{F}}_5, \quad \mathcal{F}_4 \cap \mathcal{G}_4, \quad \mathcal{F}_4 \cap \mathcal{G}_5, \quad \mathcal{F}_4 \cap \bar{\mathcal{F}}_4, \quad \bar{\mathcal{F}}_4 \cap \bar{\mathcal{G}}_5 \quad \bar{\mathcal{F}}_5 \cap \bar{\mathcal{G}}_5.$$

D Intersections between regular bang-bang geodesics with different initial control

In this Section, we provide the existence conditions, the intersection times and the expression of the suspensions on the plane $\{z = 4\zeta^2\}$ of the intersections between bang-bang geodesics. These results are obtained following the same procedure described in Section 4.1.

α) $\bar{\mathcal{F}}_4 \cap \bar{\mathcal{G}}_4$ may be easily recovered from the computation at page 20, by applying suitably Lemmas 4-5. In particular, we deduce that such intersections may occur only if $C_1 \leq 0$ and, if $C_1 = 0$, if

$$E_1 + \frac{2 - p_y^0}{3} D_1 \geq 0 \tag{D.1}$$

$$E_1 + \frac{1 - 2p_y^0}{3} D_1 \geq 0, \tag{D.2}$$

where the geodesics belonging to the set Γ_{-f} is associated with the initial adjoint vector $\boldsymbol{\mu}_{-f}(0) = (-1, p_y^0, 1/\rho_0)$. The intersection occurs at (reparameterized) time $\mathcal{T}$ such that

$$\mathscr{T}_4 - \mathcal{T} = -2(1 + p_y^0)C_1\rho_0^2 - 2(1 + p_y^0)\Big(E_1 + \frac{1 - 2p_y^0}{3} D_1\Big)\rho_0^3 \mathcal{O}(\rho_0^4),$$

and the suspension of the intersection at $z = 4\zeta^2$ is given by

$$\begin{cases} x = (1-p_y^0)\zeta - \big((1-12p_y^0-5(p_y^0)^2)\frac{A}{4} - (p_y^0+3)C_2\big)\zeta^3 + \mathcal{O}(\zeta^4) \\ y = -4A\zeta^3 - \frac{2}{3}\big(D_1(p_y^0)^2 + (3E_1+D_1)(1-p_y^0) - c_1\big)\zeta^4 + \mathcal{O}(\zeta^5). \end{cases} \tag{D.3}$$

β) $\mathcal{G}_4 \cap \bar{\mathcal{F}}_4$ This case can be obtained from the precedent one, by a rotation of $\pi/2$ around the $z-$axis and the permutation $\clubsuit$. We consider a Γ_g geodesic with initial covector $(\beta, 1, 1/\rho_0)$, and a Γ_{-f} geodesic with initial covector $(-1, \nu, 1/\widetilde{\rho}_0)$, where ν and $\widetilde{\rho}_0$ are power series in ρ_0. We fix $\boldsymbol{T} = (7+\beta)\rho_0 + \mathcal{O}(\rho_0^2)$ and look at the intersection of the two geodesics at time $\boldsymbol{T}$. As we find

$$\nu = 1 + 2(\beta+1)C_2\rho_0^2 + \mathcal{O}(\rho_0^3), \tag{D.4}$$

this intersection occurs only if $C_2 \leq 0$. The intersection occurs at (reparameterized) time $\mathcal{T} = \mathscr{T}_4 + 2(1-\beta)C_2\rho_0^2 + \mathcal{O}(\rho_0^3)$ and its suspension is the curve, parameterized by $\beta \in [-1,1]$,

$$\begin{cases} x = (4A + 2(1-\beta)C_2)\zeta^3 + \mathcal{O}(\zeta^4) \\ y = (\beta-1)\zeta - \big((1-12\beta-5\beta^2)\frac{A}{4} - \frac{1}{24}(5+9\beta-9\beta^2-5\beta^3)C_2\big)\zeta^3 + \mathcal{O}(\zeta^4). \end{cases} \tag{D.5}$$

γ) $\bar{\mathcal{G}}_4 \cap \mathcal{F}_4$ We describe here the last intersection between fourth bang front, that is, the one between the fronts $\bar{\mathcal{G}}_4$ and $\mathcal{F}_4$. This one too yields from the computation at page 20, after a suitable application of Lemmas 4-5.

In particular, we find that this intersections occur only for $C_2 \leq 0$ at time

$$\mathcal{T} = \mathscr{T}_4 + 2(1-\eta)C_2\rho_0^2 + \mathcal{O}(\rho_0^3),$$

where $\mathscr{T}_4$ is the fourth switching time of the geodesic of the set Γ_{-g} with initial momentum $\boldsymbol{\mu}_{-g}(0) = (\eta, -1, 1/\rho_0)$. The suspension of such intersection is described by the following curve, parameterized by $\eta \in [-1,1]$:

$$\begin{cases} x = -(4A + 2(1+\eta)C_2)\zeta^3 + \mathcal{O}(\zeta^4) \\ y = (1+\eta)\zeta + \big((1+12\eta-5\eta^2)\frac{A}{4} - \frac{1}{24}(5-9\eta-9\eta^2+5\eta^3)C_2\big)\zeta^3 \\ \qquad +\mathcal{O}(\zeta^4). \end{cases} \tag{D.6}$$

Up to third order terms in ζ, this curve is a segment of length $\sim 2\zeta$.

δ) $\mathcal{F}_4 \cap \bar{\mathcal{F}}_4$ In general, the intersections among geodesics with opposite initial velocity occur only close to the the vertical axis, that is, at a time $\boldsymbol{T} \sim 8/p_z(0)$; since we are considering fourth arcs, this means that the second component of the initial momentum must be close to ± 1. We then set $p_y^0 = -1 + \sum_{k\geq 1}\gamma_k\rho_0^k$ for the second component of the adjoint covector (at time zero) associated with any trajectory of the set Γ_f, and $p_y^0 = 1 + \sum_{k\geq 1}\nu_k\rho_0^k$ for the second component of the adjoint covector (at time zero) associated with any trajectory of the set Γ_{-f}. Equating the jets as usual, we find that the intersection occurs if $\nu_1 = \gamma_1 = 0$ and $\gamma_2 - \nu_2 = -8(A+C_2)$, which is admissible only if $A + C_2 \leq 0$.

The suspension of the intersection is given by the curve, parameterized by $\gamma_2 \in [0, -8(A+C_2)]$, is given by

$$\begin{cases} x = -(4A + 4C_2 + \gamma_2)\zeta^3 + \mathcal{O}(\zeta^4) \\ y = -(4A + 4C_2 + \gamma_2)\zeta^3 + \mathcal{O}(\zeta^4). \end{cases}$$

ε) $\bar{\mathcal{F}}_5 \cap \mathcal{F}_4$ For ρ_0 and $\boldsymbol{T}$ fixed, we consider a trajectory of the set Γ_{-f} with initial covector $(-1, p_y^0, 1/\rho_0)$ and a trajectory of the set Γ_f with initial covector $(1, \gamma, 1/\widetilde{\rho}_0)$, with $\gamma = \sum_{k\geq 0}\gamma_k\rho_0^k$ and $\widetilde{\rho}_0 = \rho_0 + \sum_{k\geq 2}\alpha_k\rho_0^k$. We assume that $\boldsymbol{T}$ is greater than the fourth switching time of the first geodesics, but smaller than the fourth switching time of the second one.

Imposing the equality of the jets at each order, we find that

$$\gamma_0 = -1, \quad \gamma_1 = 0, \quad \gamma_2 = -4C_2 + (p_y^0+1)^2C_1,$$
$$\mathbb{T}_4 - \boldsymbol{T} = -\big(4(p_y^0+1)C_1 + 8A\big)\rho_0^3 + \mathcal{O}(\rho_0^4),$$

where $\mathbb{T}_4$ denotes the fourth switching time of the trajectory belonging to the set Γ_f. This implies that, if $C_1 = 0$, the intersection occurs only if $C_2 \leq 0$ and $A \leq 0$.

If $C_1 = 0$, the suspension of the intersections to the plane $\{z = 4\zeta^2\}$ is given by the curve

$$\begin{cases} x = -4A\zeta^3 + \big(-\frac{2}{3}D_1(p_y^0)^3 + (E_1 - D_1)(p_y^0)^2 + 2E_1 p_y^0 \\ \qquad +\frac{1}{3}(D_1 - 5E_1 - 4\mathcal{d}_1)\big)\zeta^4 + \mathcal{O}(\zeta^5) \\ y = -4A\zeta^3 - \big(2D_1(p_y^0)^2 - 4E_1 p_y^0 - \frac{2}{3}\mathcal{c}_1\big)\zeta^4 + \mathcal{O}(\zeta^5). \end{cases}$$

Applying a rotation of π around the axis z (and p_z in the adjoint space) and the transformation $\blacklozenge$, we obtain the expression of the suspension of the intersection $\mathcal{F}_5 \cap \bar{\mathcal{F}}_4$:

$$\begin{cases} x = 4A\zeta^3 + \big(\frac{2}{3}D_1(p_y^0)^3 + (E_1 - D_1)(p_y^0)^2 - 2E_1 p_y^0 \\ \qquad +\frac{1}{3}(D_1 - 5E_1 - 4\mathcal{d}_1)\big)\zeta^4 + \mathcal{O}(\zeta^5) \\ y = 4A\zeta^3 - \big(2D_1(p_y^0)^2 + 4E_1 p_y^0 - \frac{2}{3}\mathcal{c}_1\big)\zeta^4 + \mathcal{O}(\zeta^5), \end{cases}$$

where p_y^0 denotes the second component of the initial momentum of the geodesic belonging to the set Γ_f. The existence conditions for such intersection are the same, and the intersection time is

$$\mathbb{T}_4 - \boldsymbol{T} = -\big(4(1 - p_y^0)C + 8A\big)\rho_0^3 + \mathcal{O}(\rho_0^4), \tag{D.7}$$

where $\mathbb{T}_4$ denotes the fourth switching time of the trajectory belonging to the set Γ_{-f}.

ζ) $\mathcal{G}_4 \cap \bar{\mathcal{G}}_5$ For ρ_0 and $\boldsymbol{T}$ fixed, we consider a trajectory of the set Γ_{-g} with initial covector $\boldsymbol{\mu}_{-g}(0) = (p_x^0, -1, 1/\rho_0)$ and a trajectory of the set Γ_g with initial covector $(\beta, 1, 1/\widehat{\rho}_0)$, with $\beta = \sum_{k\geq 0} \beta_k \rho_0^k$. We assume that $\boldsymbol{T}$ is greater than the fourth switching time of the first geodesics, but smaller than the fourth switching time of the second one (denoted with $\mathbb{T}_4$ in the following).

Imposing the equality of the jets at each order, we find the constraints

$$\beta_0 = 1, \quad \beta_1 = 0, \quad \beta_2 = 4C_1 - (1 - p_x^0)^2 C_2, \tag{D.8}$$

so that, for $C_1 = 0$, this intersection occurs only if $C_2 \geq 0$. As $\mathbb{T}_4 - \boldsymbol{T} = \big(8A + 4(p_x^0 - 1)C_2\big)\rho_0^3 + \mathcal{O}(\rho_0^4)$, then this intersections occurs only for

$$p_x^0 \geq 1 - \frac{2A}{C_2},$$

which also imposes $A \geq 0$.

When $C_1 = 0$, the suspension of the intersections to the plane $\{z = 4\zeta^2\}$ is given by the following parameterized curve

$$\begin{cases} x = -4(A + p_x^0 C_2)\zeta^3 + \big(2D_2(p_x^0)^2 + 4E_2 p_x^0 + \frac{2}{3}\mathcal{c}_2\big)\zeta^4 + \mathcal{O}(\zeta^5) \\ y = (4A - (1 - p_x^0)^2 C_2)\zeta^3 + \big(\frac{2}{3}D_2(p_x^0)^3 + (E_2 - D_2)(p_x^0)^2 \\ \quad -2E_2 p_x^0 + \frac{1}{3}D_2 + \frac{5}{12}\mathcal{c}_1 - \frac{1}{2}\mathcal{d}_2 - \frac{5}{12}D_1\big)\zeta^4 + \mathcal{O}(\zeta^5), \end{cases} \tag{D.9}$$

The third order term describes is an arc of parabola with vertex for $p_x^0 = 1$. The slope of the tangent to the curve is given by

$$\frac{y\prime(p_x^0)}{x\prime(p_x^0)} = \frac{p_x^0 - 1}{2} + \mathcal{O}(\rho_0).$$

The intersection $\bar{\mathcal{G}}_4 \cap \mathcal{G}_5$ can be easily recovered from the one just studied, by changing all signs in the suspension and applying a suitable permutation of the invariants. As, under such permutations, A and C_2 are unchanged, at the third order term the suspension is the symmetric of (D.9) with respect to the origin.

η) $\mathcal{G}_5 \cap \bar{\mathcal{G}}_5$ For ρ_0 and $\boldsymbol{T}$ fixed, we consider a trajectory of the set Γ_g with initial covector $\boldsymbol{\mu}_g(0) = (\beta, 1, 1/\rho_0)$ and a trajectory of the set Γ_{-g} with initial covector $\boldsymbol{\mu}_{-g}(0) = (\eta, -1, 1/\widehat{\rho}_0)$.

These two trajectories intersects only if $\beta - \eta = \frac{2A}{C_2}$; in particular, this imposes $|A| < C_2$. The intersection occurs at time $\boldsymbol{T} = 8\rho_0 + \frac{4}{C_2}\Big(C_2^2\beta^2 - 2AC_2\beta - A^2 + \frac{2}{3}C_2^2\Big)\rho_0^3 + \mathcal{O}(\rho_0^4)$. The suspension of the intersections to the plane $\{z = 4\zeta^2\}$ is given by

$$\begin{cases} x = 4(A - C_2\beta)\zeta^3 + \mathcal{O}(\zeta^4) \\ y = -4\frac{A}{C_2}\big(A - C_2\beta\big)\zeta^3 + \mathcal{O}(\zeta^4), \end{cases}$$

where $\beta \in \big[\max\{-1, \frac{2A}{C_2} - 1\}, \min\{1 - \frac{2A}{C_1}, 1\}\big]$. The leading term is a segment of slope $-A/C_2$.

θ) $\mathcal{F}_5 \cap \bar{\mathcal{G}}_4$ For ρ_0 and $\boldsymbol{T}$ fixed, we consider a trajectory of the set Γ_f with initial covector $(1, p_y^0, 1/\rho_0)$ and a trajectory of the set Γ_{-g} with initial covector $(\beta, -1, 1/\widetilde{\rho}_0)$, with $\beta = \sum_{k\geq 0} \beta_k \rho_0^k$ and $\widetilde{\rho}_0 = \rho_0 + \sum_{k\geq 2} \alpha_k \rho_0^k$. We assume that $\boldsymbol{T}$ is greater than the fourth switching time of the first geodesics, but smaller than the fourth switching time of the second one. Equating as usual the jets of the two geodesics, we find

$$\beta_0 = -1, \quad \beta_1 = 0, \quad \beta_2 = 8A - 4(1+p_y^0)C_1,$$
$$\mathbb{T}_4 - \boldsymbol{T} = \big(2A(1+p_y^0) + (1+p_y^0)C_1 + ((p_y^0)^2 + 2p_y^0 - 3)C_2\big)\rho_0^3 + \mathcal{O}(\rho_0^4),$$

where $\mathbb{T}_4$ denotes the fourth switching time of the geodesics belonging the set Γ_{-g}. We can verify that, for $C_1 = 0$, $A > 0$ and $C_2 < 0$, this expression is always negative. Indeed, it is a concave parabola in p_y^0, which is positive for $p_y^0 = 1$ and $p_y^0 = -1$, so positive on the whole interval. This implies that, for $C_1 = 0$, the intersection occurs only if $C_2 \leq 0$ and $A \geq 0$.

For $C_1 = 0$, the suspension of the intersections to the plane $\{z = 4\zeta^2\}$ is the curve

$$\begin{cases} x = -4A\zeta^3 + \big(\frac{2}{3}D_1(p_y^0)^3 + (E_1+D_1)(p_y^0)^2 + 2E_1p_y^0 \\ \quad -\frac{1}{3}(D_1 + 5E_1 + 4d_1)\big)\zeta^4 + \mathcal{O}(\zeta^5) \\ y = 4A\zeta^3 - \big(2D_1(p_y^0)^2 + 4E_1p_y^0 - \frac{2}{3}c_1\big)\zeta^4 + \mathcal{O}(\zeta^5). \end{cases} \tag{D.10}$$

ι) $\bar{\mathcal{F}}_5 \cap \mathcal{G}_4$ The analysis of this intersection can be derived from the precedent one, just by applying the suitable permutations of invariants and rotations. In particular, we get that, when $C_1 = 0$, this intersection may occur only if $A > 0$ and $C_2 < 0$. The suspension of this intersection is given by the curve

$$\begin{cases} x = 4A\zeta^3 + \big(-\frac{2}{3}D_1(p_y^0)^3 + (E_1+D_1)(p_y^0)^2 - 2E_1p_y^0 \\ \quad -\frac{1}{3}(D_1 + 5E_1 + 4d_1)\big)\zeta^4 + \mathcal{O}(\zeta^5) \\ y = -4A\zeta^3 - \big(2D_1(p_y^0)^2 - 4E_1p_y^0 - \frac{2}{3}c_1\big)\zeta^4 + \mathcal{O}(\zeta^5), \end{cases}$$

where $p_y^0 \in [-1, 1]$ denotes the second component of the initial covector of the geodesics belonging to the set Γ_{-f}.

κ) $\mathcal{F}_4 \cap \mathcal{G}_5$ These case can be recovered by applying to the results of θ) a rotation of $\pi/2$ around the z and the p_z axes and the permutation of the invariants ♣.

We consider a trajectory of the set Γ_g with initial covector $(p_x^0, 1, 1/\rho_0)$ and we intersect it with a geodesic of the set Γ_f. We obtain that such intersections occur only for $p_x^0 \geq 1 + \frac{2A}{C_2}$.

If $C_1 = 0$, the suspension on the plane $\{z = 4\zeta^2\}$ reads

$$\begin{cases} x = 4(A - p_x^0C_2)\zeta^3 + \big(2D_2(p_x^0)^2 - 4E_2p_x^0 - \frac{2}{3}d_2\big)\zeta^4 + \mathcal{O}(\zeta^5) \\ y = (4A + (1-p_x^0)^2C_2)\zeta^3 + \big(-\frac{2}{3}D_2(p_x^0)^3 + (E_2 - D_2)(p_x^0)^2 \\ \quad -2E_2p_x^0 + \frac{1}{3}(D_2 + 5E_2 + 4d_2)\big)\zeta^4 + \mathcal{O}(\zeta^5) \end{cases} \tag{D.11}$$

References

[1] A. Agrachev, G. Stefani, and P. Zezza. Strong optimality for a bang-bang trajectory. *SIAM J. Control Optim.*, 41(4):991–1014, 2002.

[2] A. A. Agrachev, El-H. Chakir EL-Alaoui, J.-P. Gauthier, and I. Kupka. Generic singularities of sub-Riemannian metrics on R3. *Comptes-Rendus de l'Académie Sci., Paris*, pages 377–384, 1996.

[3] A. A. Agrachev and Yu. L. Sachkov. *Control Theory from the Geometric Viewpoint.* Springer-Verlag, 2004.

[4] A.A. Agrachev, D. Barilari, and U. Boscain. *A Comprehensive Introduction to Sub-Riemannian Geometry.* Studies in Advanced Mathematics. Cambridge University Press, 2019.

[5] A.A. Agrachev and J.P. Gauthier. On the Dido Problem and plane isoperimetric problems. *Acta Appl. Math.*, 57:287–338, 1999.

[6] E. A.L. Ali and G. Charlot. Local (sub)-Finslerian geometry for the maximum norms in dimension 2. *J. Dyn. Control Syst.*, (25):457–490, 2019.

[7] E. A.L. Ali and G. Charlot. Local contact sub-Finslerian geometry for maximum norms in dimension 3. *Math. Control Relat. Fields*, 0, 2020.

[8] A.A. Ardentov, E. Le Donne, and Y.L. Sachkov. A sub-Finsler problem on the Cartan group. *Proc. Steklov Inst. Math.*, 304:42–59, 2019.

[9] D. Barilari, U. Boscain, E. Le Donne, and M. Sigalotti. Sub-Finsler geometry from the time-optimal control viewpoint for some nilpotent distributions. *J. Dyn. Control Syst.*, 3(3):547–575, 2017.

[10] B. Bonnet, J.-P. Gauthier, and F. Rossi. Generic singularities of the 3D-contact sub-Riemannian conjugate locus. *C.R. Math.*, 357(6):520–527, 2019.

[11] E. Breuillard and E. Le Donne. On the rate of convergence to the asymptotic cone for nilpotent groups and subfinsler geometry. *Proc. Natl. Acad. Sci. USA*, 110(48):19220–19226, 2013.

[12] El-H. Chakir E-Alaoui, J.-P. Gauthier, and I. Kupka. Small sub-Riemannian balls on R3. *J. Dyn. Control Syst.*, 2(3):359–421, 1996.

[13] J. N. Clelland and C. G. Moseley. Sub-Finsler geometry in dimension three. *Differ. Geom. Appl.*, 24(6):628 – 651, 2006.

[14] J. N. Clelland, C. G. Moseley, and G. R. Wilkens. Geometry of sub-Finsler Engel manifolds. *Asian J. Math.*, 11(4):699 – 726, 2007.

[15] M. Golubitsky and V. Guillemin. *Stable Mappings and Their Singularities*. Graduate texts in mathematics. Springer, 1974.

[16] F. Harrache. *Les métriques sous-Finslériennes en dimension 3*. PhD thesis, Ecole doctorale 548. `https://hal.science/tel-03723279v1`.

[17] Wolfram Research, Inc. Mathematica, Version 11.3. Champaign, IL, 2018.

[18] F. Jean. *Control of Nonholonomic Systems: from Sub-Riemannian Geometry to Motion Planning*. SpringerBriefs in Mathematics. Springer, 2014.

[19] L. V. Lokutsievskiy. Convex trigonometry with applications to sub-Finsler geometry. *Sbornik: Math.*, 210(8):1179–1205, 2019.

[20] R. Montgomery. *A Tour of Subriemannian Geometries, Their Geodesics and Applications*. American Mathematical Society, 2006.

[21] L. Poggiolini and G. Stefani. State-local optimality of a bang-bang trajectory: a Hamiltonian approach. *Syst. Control. Lett.*, 53, 2004.

[22] J.W. Rutter. *Geometry of Curves*. Chapman Hall/CRC Mathematics Series. CRC Press, 2018.

[23] L. Sacchelli. Short geodesics losing optimality in contact sub-Riemannian manifolds and stability of the 5-dimensional caustic. *SIAM J. Control Optim.*, 57(4):2362–2391, 2019.

[24] M. Sigalotti. Bounds on time-optimal concatenations of arcs for two-input driftless 3D systems. In *Proceedings of the 21st IFAC Control Conference*, 2020.

[25] E. D. Sontag *Mathematical Control Theory: Deterministic Finite Dimensional Systems* Springer Science & Business Media, 2013.